UNCLASSIFIED

AFOSR-TR-97

0136

SECURITY CLASSIFICATION OF THIS PAGE

REPORT DOCUMENTATION PAGE

0188

1a. REPORT SECURITY CLASSIFICATION UNCLASSIFIED	1b. RESTRICTIVE MARKINGS None
2a. SECURITY CLASSIFICATION AUTHORITY	3. DISTRIBUTION/AVAILABILITY OF REPORT Unrestricted
2b. DECLASSIFICATION/DOWNGRADING SCHEDULE	
4. PERFORMING ORGANIZATION REPORT NUMBER(S) GITAER-EAD 97-1	5. MONITORING ORGANIZATION REPORT NUMBER(S)
6a. NAME OF PERFORMING ORGANIZATION Georgia Tech Research Corporation 6b. OFFICE SYMBOL (If applicable)	7a. NAME OF MONITORING ORGANIZATION AFOSR
6c. ADDRESS (City, State, and ZIP Code) Georgia Institute of Technology School of Aerospace Engineering, Atlanta, GA 30332-0150	7b. ADDRESS (City, State, and ZIP Code) Same CO 8C
8a. NAME OF FUNDING/SPONSORING ORGANIZATION AFOSR 8b. OFFICE SYMBOL (If applicable)	9. PROCUREMENT INSTRUMENT IDENTIFICATION NUMBER F49620-93-1-0342
8c. ADDRESS (City, State, and ZIP Code) AFOSR/NA, 110 Duncan Avenue, Suite B115, Bolling AFB, DC20332-0001 (NA)	10. SOURCE OF FUNDING NUMBERS PROGRAM ELEMENT NO. 61102F PROJECT NO. 2307 TASK NO. A5 WORK UNIT ACCESSION NO.

11. TITLE (Include Security Classification)

AASERT: Adaptive Control for Diagnosis of Transient Vortex Interactions (U)

12. PERSONAL AUTHOR(S) Komerath, N.M., Magill, J.C., Darden, L.-A., Dishman, D., Peterson, K.G., Ames, R.G.

13a. TYPE OF REPORT	13b. TIME COVERED	14. DATE OF REPORT (Year, Month, Day)	15. PAGE COUNT
FINAL TECHNICAL	FROM 1/93 TO 11/96	1997, January, 29.	130

16. SUPPLEMENTARY NOTATION

17. COSATI CODES			18. SUBJECT TERMS (Continue on reverse if necessary and identify by block number)
FIELD	GROUP	SUB-GROUP	Dynamic Manipulator, vortex control, Wind-Driven Manipulator, Stagnation Point Actuator, unsteady aerodynamics, flight control, maneuvers

19. ABSTRACT (Continue on reverse if necessary and identify by block number)

Two inventions enabled substantial progress on related problems. The Wind-Driven Dynamic Manipulator enables high-rate, arbitrary-trajectory simulation of aircraft maneuvers in the wind tunnel. Adaptive control has been used to converge accurately to specified pitch histories using this light and flexible robotic device, powered by wind energy. Active stabilization has been used to develop a pitch-roll-yaw manipulator. Laser sheet imaging during pitch-yaw maneuvers of a YF-22 model showed transient vortex interactions even during quasi-static motions. Dynamic pitch derivatives were measured using system identification and periodic excitation. Static and transient force measurement are feasible. The Stagnation Point Actuator (SPA) enables suppression and amplification of forebody vortex asymmetry, providing effective roll-yaw control at high angle of attack. The SPA produces roll and yaw coefficients similar to those of blowing and strakes, with continuous, high-rate control of the asymmetry. Wing rock has been induced and suppressed with high repeatability. Piecewise-linear frequency-domain transfer functions have been used to model the response of the pressure and the roll moment to SPA deflection. Various time scales are identified.

20. DISTRIBUTION/AVAILABILITY OF ABSTRACT	21. ABSTRACT SECURITY CLASSIFICATION
☒ UNCLASSIFIED/UNLIMITED ☐ SAME AS RPT. ☐ DTIC USERS	(U)
22a. NAME OF RESPONSIBLE INDIVIDUAL DR L. SAKELL	22b. TELEPHONE (Include Area Code) 202-767-4933 22c. OFFICE SYMBOL NA

DD Form 1473, JUN 86 *Previous editions are obsolete.* SECURITY CLASSIFICATION OF THIS PAGE

UNCLASSIFIED

Final Technical Report

AFOSR Grant No. F49620-93-1-0342

AASERT: ADAPTIVE CONTROL FOR DIAGNOSIS OF TRANSIENT VORTEX INTERACTIONS

Research Team:
Narayanan M. Komerath
John C. Magill
Leigh-Ann Darden
David Dishman
Kevin G. Peterson
Richard Ames

SCHOOL OF AEROSPACE ENGINEERING
GEORGIA INSTITUTE OF TECHNOLOGY
ATLANTA, GEORGIA 30332-0150

Air Force Technical Monitors:
Maj. Dan Fant and Dr. Len Sakell
Air Force Office of Scientific Research

January 1997

Effort sponsored by the Air Force Office of Scientific Research, Air Force Materiel Command, USAF, under grant number F49620-93-1-0342. The U.S. Government is authorized to reproduce and distribute reprints for Governmental purposes notwithstanding any copyright notation thereon."

ADAPTIVE CONTROL FOR DIAGNOSIS OF TRANSIENT VORTEX INTERACTIONS

Narayanan Komerath , School of AE, Georgia Tech, Atlanta, GA 30332-0150
narayanan.komerath@aerospace.gatech.edu 404-894-3017

SUMMARY

This grant enabled two inventions and substantial advances on two related problems. The Wind-Driven Dynamic Manipulator enables high-rate, arbitrary-trajectory simulation of aircraft maneuvers in the wind tunnel. Adaptive control has been used to converge accurately to specified pitch histories using this light and flexible robotic device, powered by the wind energy downstream of the model in a wind tunnel. Active stabilization has been used to develop a pitch-roll-yaw manipulator for a large low-speed tunnel. Quantitative laser sheet flow imaging during pitch-yaw maneuvers of a YF-22 model showed transient vortex interaction phenomena occurring even during quasi-static motions. Measurement of dynamic pitch derivatives was demonstrated using system identification and periodic excitation of a model. Static force measurement and force measurement during maneuvers are being explored for miniaturized versions of this device, for micro-UAV applications.

The second invention is the Stagnation Point Actuator (SPA) for forebody vortex control. This device enables suppression and amplification of forebody vortex asymmetry, thereby providing effective roll-yaw control on wing-bodies at high angle of attack. The apparatus is much simpler than competing solutions which use blowing or strakes, while producing the same magnitudes of roll and yaw coefficients. In addition, it offers continuous and high-rate control of the amplitude of the asymmetry. Wing rock has been induced and suppressed with high repeatability. The device has opened the door to resolving the various fluid dynamic, aerodynamic and inertial time scales involved in the dynamics of maneuvering aircraft. Piecewise-linear frequency-domain transfer functions have been shown to be successful in modeling the response of the lateral pressure difference and the roll moment to the lateral displacement of the stagnation point from the plane of lateral symmetry. Research is continuing on developing effective control systems which include the functional form of each of the various phenomena which are encountered.

CONTENTS

LIST OF FIGURES

I. INTRODUCTION

This AASERT Grant funded student research to enable the exploration of the flight regime where vehicles go through arbitrary, rapid, multiple-axis maneuvers. Progress came along two major avenues, both developed during the course of this project:

1. Research on an Adaptive Wind-Driven Dynamic Manipulator, learning to compensate in real time for deflections, vibrations and other trajectory errors of light, flexible and fast-responding manipulators.
2. Research on the control and utilization of time-varying forebody vortex asymmetry to produce desired yawing and rolling moments on aircraft models at high incidence, using a Stagnation Point Actuator.

The unique nature of the AASERT grant provided the freedom to experiment with new ideas of higher technical risk than the parent grant. The work reported here is a combination of device invention, system design and fabrication, and exploration of problems at the frontiers of vortex aerodynamics and nonlinear control, using quantitative techniques. In each case, the device was invented to address a pressing need, but then was taken through proof-of-concept through several demonstrations of effective use in aerodynamics and controls research. The student research was leveraged with research instrumentation and other resources from various sources, the aeromodeling and flying skills of several students, and the enthusiastic assistance of faculty and researchers in other disciplines. In the process, one PhD and three M.S. degrees have been earned, and a second PhD and a fourth M.S. are in progress.

The invention of these devices enables progress in better understanding of the regime of high-rate, multiple-axis maneuvers and their associated vortex dynamics, and in our ability to develop control systems for future aircraft, incorporating rate-dependent aerodynamic interaction phenomena. Both of these are unique devices, where we have had to create the design criteria and the application domains, because they break through several traditional constraints in aerodynamics and flight dynamics.

The technical summary is divided into Parts A and B, and the References and figures are numbered sequentially within each part. The project team, the inventors and publications are listed in the final section.

II. TECHNICAL SUMMARY, PART A: WIND-DRIVEN DYNAMIC MANIPULATOR

Concept

This is a solution to the problem of developing a high-rate, multiple degree-of-freedom robotic manipulator to simulate high-acceleration aircraft maneuvers in the wind tunnel, and to measure forces and moments during these maneuvers. Applications are now seen in the development of micro-UAVs, both bird-sized and insect-sized.

The Wind-Driven Dynamic Manipulator (WDM, see Figure A1) is a robotic device which executes arbitrary, multidimensional maneuvers of vehicle models in a wind tunnel at high rates. Tunnel freestream kinetic energy is used to power the device. Transmission of reactions to the tunnel structure is thus minimized, and power consumption is negligible compared to conventional devices. Support interference is minimized by using slender and flexible supports and correcting for deflection errors. The device can also be used to measure aerodynamic forces and moments on the test model during the maneuver. The concept and results achieved with the device are summarized, and a new 3 degree-of-freedom device is described in this report. Five example applications are summarized. Transient vortex interactions are visualized quantitatively in coupled pitch-yaw maneuvers. Force and moment measurement in quasi-steady testing is described. Dynamic stability parameters are measured using a second-order dynamic model of the system. An adaptive algorithm improves the simulation of the model, and enables new dynamic characteristics to be learned. The development of flight control laws for new aircraft is discussed. Design parameters are discussed. The performance equations of the device show maneuvering rates increasing faster than the reduced frequency as tunnel speed increases.

The WDM gets its high-rate maneuverability from the fact that it uses the kinetic energy available in the tunnel freestream to drive the lifting surfaces which, in turn, drive the model through the maneuvers. The bandwidth of the WDM is limited primarily by the bandwidth of the motors used to drive the controlling surfaces. Since each controlling surface is a symmetrical airfoil and the motor produces a torque about the quarter-chord (where there is a very small, nearly zero pitching moment), the motors need only overcome the inertia of the wings as they move through calculated trajectories. This enables designs wherein the WDM is capable of performing high frequency repetitive motions, such as might be used to measure unsteady effects. Transient maneuvers are studied by repeating them many times precisely so that phase-resolved measurement techniques can be used.

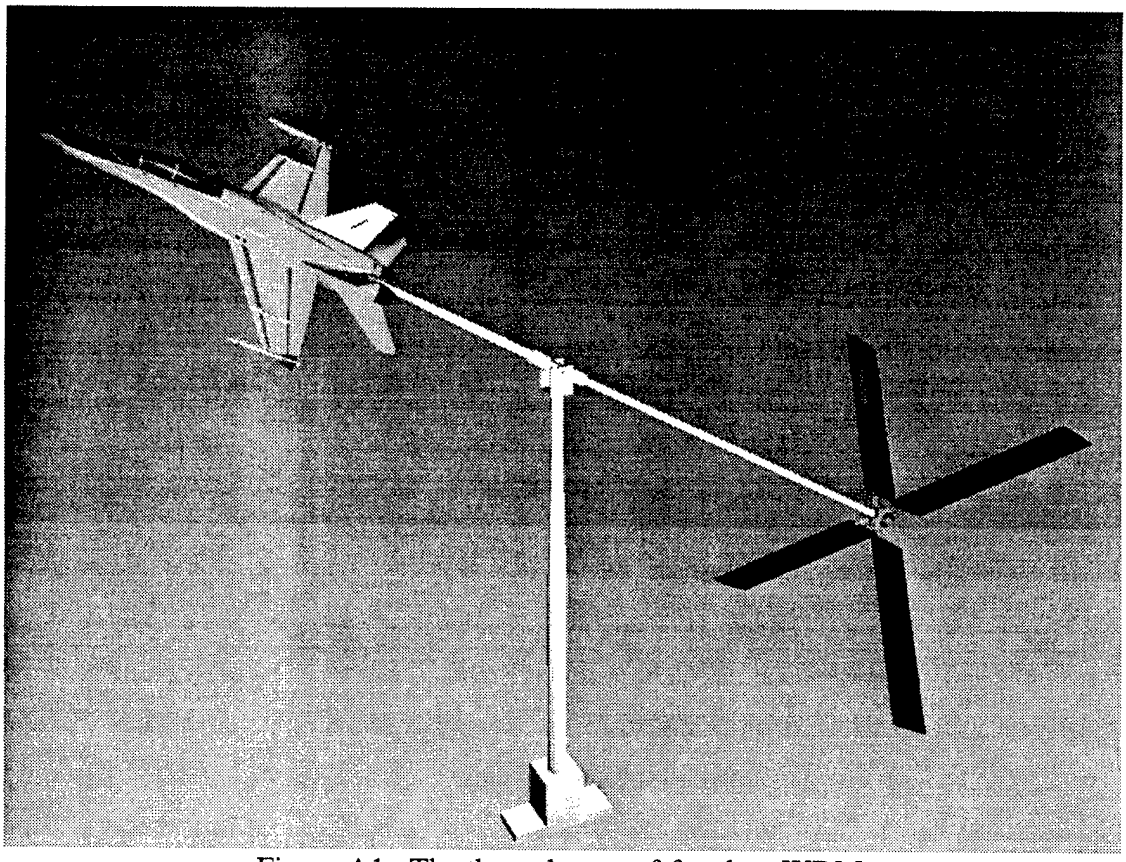

Figure A1: The three-degree-of-freedom WDM.

Conventional Methods

Conventional methods are inadequate to simulate and study such flows and their effects, for several reasons. Let us assume that every maneuver can be broken down into different segments to satisfy the constraints of the support systems and measuring instruments, and the accelerations in each phase simulated separately, as a first step. There is some evidence that scaling based on the reduced-frequency concept may yield useful results. Thus, for example, a full-scale aircraft yaw rate of 50 deg. s^{-1} at a flight speed of 100 m/s translates to a scaled rate of 160 deg. s^{-1} of a 1/32-scale model at a tunnel speed of 10 m/s. The problem now reduces to that of moving a model through such motions simultaneously about multiple degrees of freedom. The most obvious approach is to mount the model on a manipulator arm and drive it through the required motions under computer control. Mechanisms with multiple degrees of freedom usually have some of the motors mounted away from the base; i.e., they must be moved too. Wind loads during the maneuver will cause some deflection and thus the trajectory must be corrected for these errors, which become bigger with wind speed and maneuver rate. Designs using stiff-armed robots become too heavy and bulky. Besides the obvious cost and engineering constraints, the resulting device usually becomes larger than the model, causing significant levels of flow interference. A simpler approach is to use cam-driven mechanisms to simulate one aspect of one maneuver precisely and repetitively. The mechanism must then be specific to each maneuver. In contrast, a precise, slender robotic arm would enable us to repeat, exactly, each segment of the complex maneuver as many times as desired. Thus the transient interaction phenomena, however, complex, can be converted into periodic phenomena and measured using phase-synchronized diagnostic techniques.

A survey of current approaches A4-A21 demonstrates the complexity and sophistication used to achieve multi-axis motions. Hydraulic systems, high-torque motors, concentric arms, and even total redesign of the wind tunnel facility to accomodate the reactions of these huge systems are all observed. In contrast, the 3DWDM system is a device that can be set up in a couple of hours, consumes little power, and does not transmit reactions to the supports. Below we examine each of five applications in turn.

Wind-Driven Manipulator Designs

After several student projects examining this problem, we set out in 1993 to study the basic problem of correcting for deflection errors encountered with a lightweight robotic manipulator. This led to the invention of the WDM. Several versions of the device are shown in Fig. A2, ranging from a pitch-only device to a full 3-d.o.f. device. It should be noted that the rotational degrees of freedom pose greater challenges than the linear ones: All

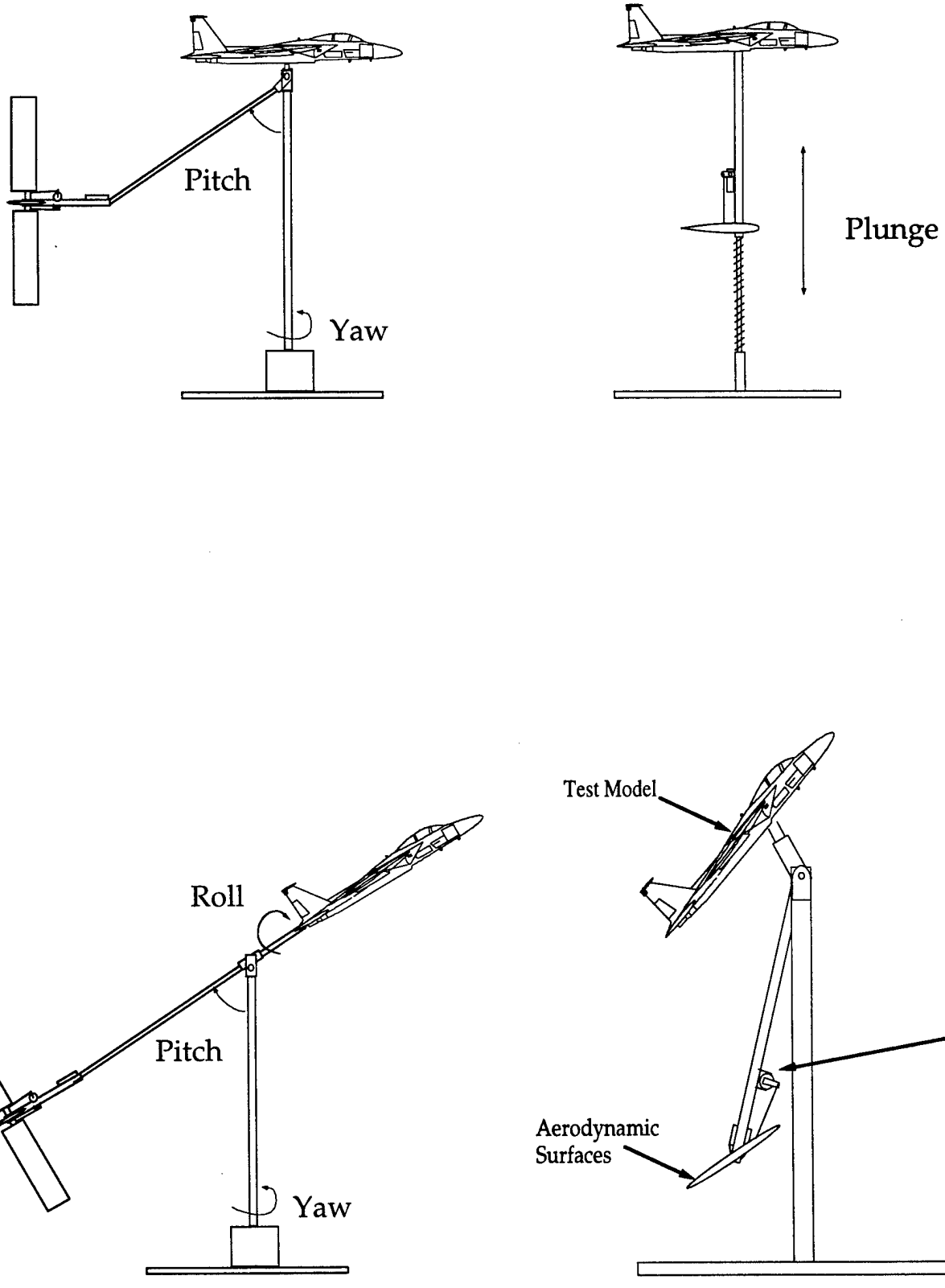

Figure A2: Several versions of the WDM.

motors needed for the 3 linear degrees of freedom (x, y, and z translation) can be mounted close to the floor, so that their weight does not affect the manipulator design.

The one-DOF manipulator (pictured in Fig. A2) was designed and built during 1993 and consists of a boom/lifting surface combination providing pitch-only motion. The lifting surface is actuated by a small, high-bandwidth motor, enabling the device to perform high-rate maneuvers. The device was constructed for use with 1/32-scale plastic models. The constant-chord, NACA 0012-section wing was constructed of balsa spars and lite-ply ribs and sheeting. An aluminum block was used to connect each wing half to an aluminum axle. The wings were attached to the axle at their quarter-chord and were actuated by a single commercially-available model airplane servo. A pulse code generator provided an interface between a D/A converter on the control computer and the controller inside the servo. Wing and pitch angle measurements were acquired using optical encoders. The encoder signals were counted by a 4-axis encoder interface which was mounted in an 80386 PC. The PC also generated the position command signals to the servo via an analog I/O board.

Dynamic Pitch Variation

To make the WDM useful for aerodynamic experiments, it is necessary to design a controller which moves the test model through a predetermined trajectory repeatedly. Performance of the controller varies with controller complexity. In this section a simple PID controller and a more complex adaptive controller are described and their tracking performances compared. Figure A3 shows the structure of a controller for a WDM. Wing and model angles are measured using encoders and fed back to the control computer. The computer compares these measurements with the desired trajectory and adjusts the wing angles to match the trajectories.

The first WDM control experiments were with a PID controller applied to the pitch manipulator (A1). The tests were conducted in the Low Turbulence Wind Tunnel at Georgia Tech at a speed of 40fps. Fig. A4 shows tracking of a square wave and a more complex trajectory. The PID gains were chosen empirically. Though this type of control is simple, a set of gains yields good performance for only a small range of maneuvers, and the controller must be tuned when the prescribed maneuver is changed greatly.

Adaptive Pitch Variation Algorithm

A number of more complex controllers have been tested on the pitch manipulator[A22, A23]. The most successful has been an adaptive controller. The controller assumes a form for the equations of motion of the manipulator which include several

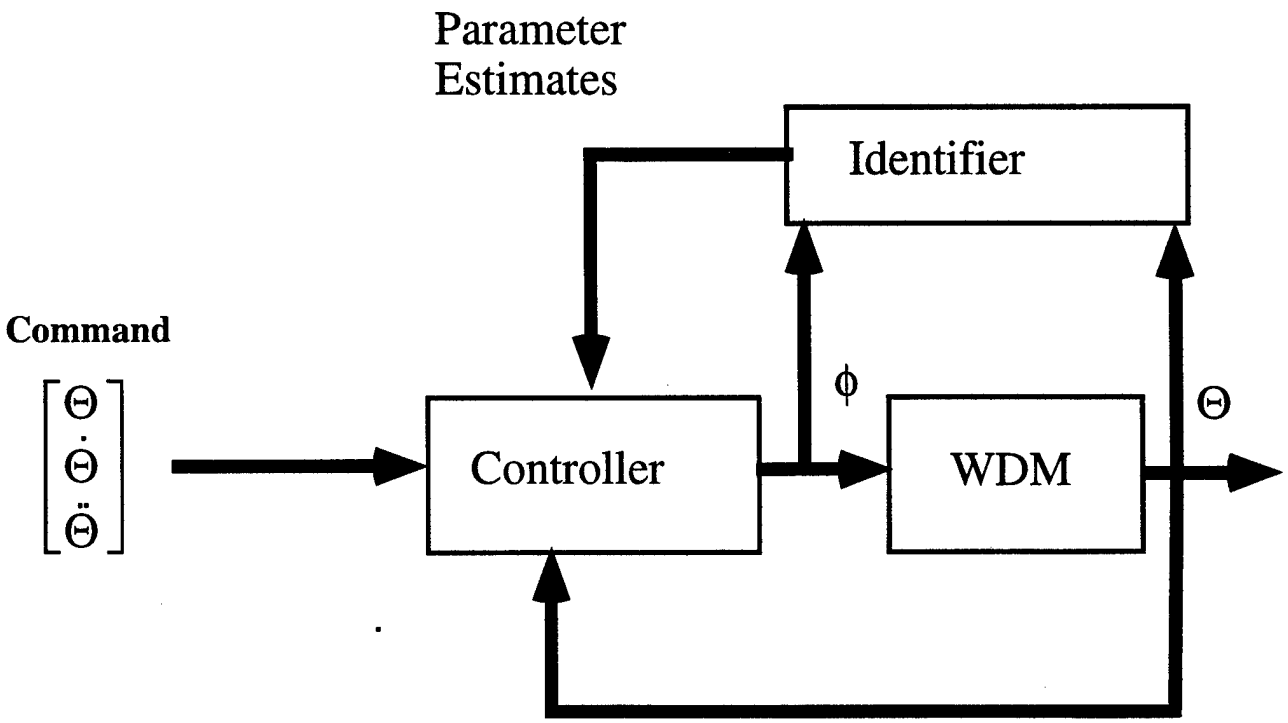

Figure A3: A controller for a one-degree-of-freedom WDM,

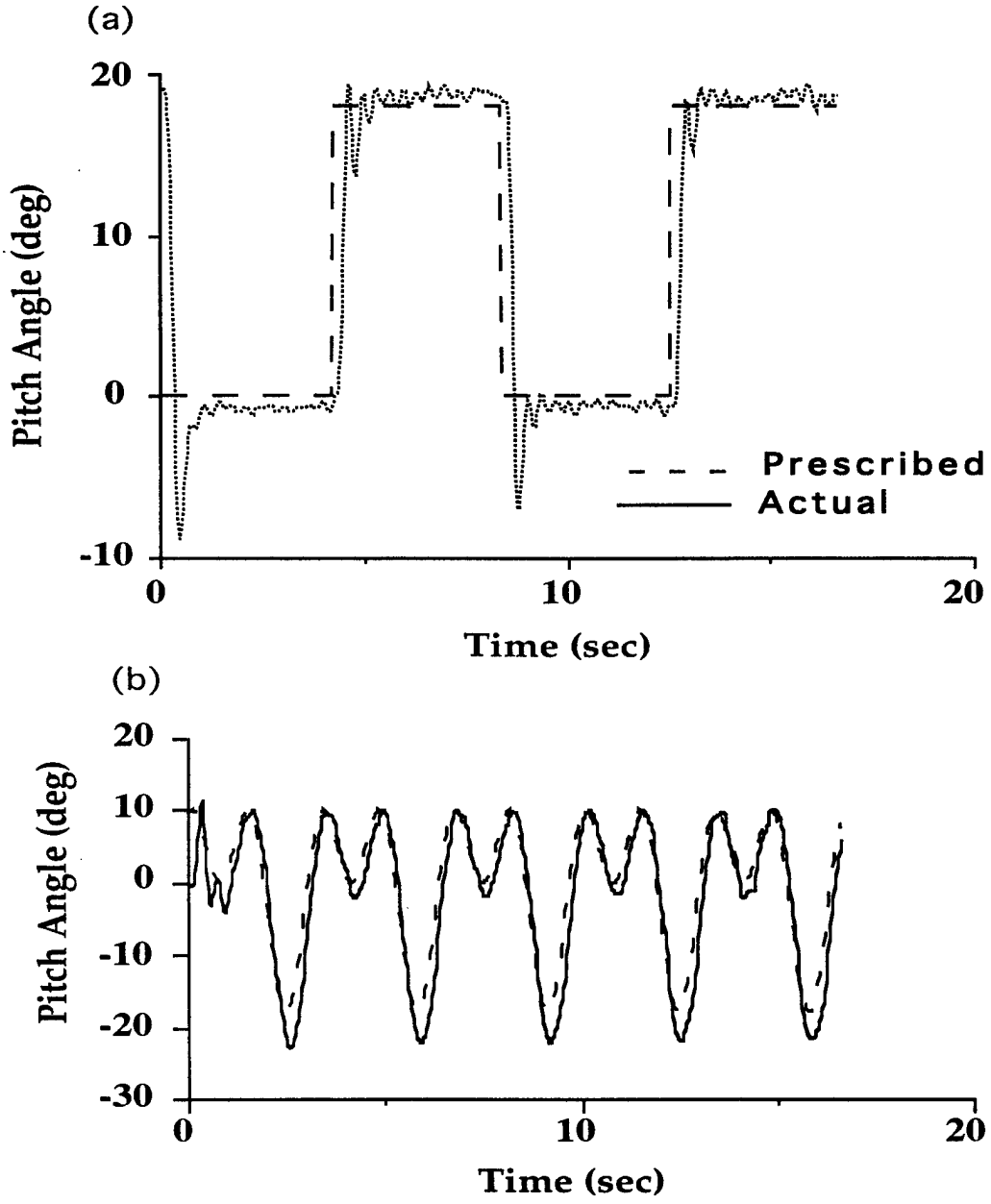

Figure A4: Response to two types of inputs.

unknown parameters in the aerodynamic and inertial functions. This controller uses the tracking error signal to adjust its estimate of the aerodynamic and inertial parameters. This model knowledge is used in turn to improve the controller. The first two parts of Fig. A5 show tracking response with a delta wing model attached. The controller learns the aerodynamic functions of the test model and improves the tracking, as can be seen between Figures A5a and A5b. Figure A5c displays adaptive controller performance with a 1/32-scale F/A-18 model in a low-speed wind tunnel.

Accommodating Unsteady Aerodynamics and Servo Dynamics

Unsteady aerodynamics of the control wings introduce actuator dynamics that compound the servo dynamics. Control design has been successful under the assumption that these dynamics are fast. The control wing lift transients have a time constant approximately equal to the time required for a particle to traverse the chord. For a 15cm wing in a 15m/s flow, the time constant is 10ms. A linear model of the pitch manipulator has a pair of complex poles near 7 rad/sec., more than an order of magnitude slower than the wings.

In the future, control design for high-rate maneuvers may need to accomodate actuator dynamics. Since servo dynamics are slower than the wing aerodynamics, their effects will be the first to require attention.

Multiple degree-of-freedom maneuvers

Figure A2b shows a 2-d.o.f. manipulator. The device was constructed primarily of aluminum tubing with a 1/2" steel shaft fitted into the lower end of the mast and pressed into the bearings in the base to provide yaw rotation. An aluminum fork, which housed the pitch bearings, was mounted at the top of the mast. The 2-DWDM was designed for use with 1/32-scale plastic models. The four wings were made using a moldless foam core fiberglass construction wherein a foam wing form with a balsa trailing edge is coated with glass fiber and epoxy resin. This type of thin-walled construction allowed for very light, low-inertia wings that would respond quickly to control inputs. The wing cross section was NACA 0012. Each pair of opposing wings was gauged so that no differential deflection was possible, and each pair was driven by a single radio control servo. The pulse modulator used to interface the one-DOF WDM servo was also used for the pitch/yaw servos. The pitch and yaw angular measurements were provided by potentiometers. The 2D WDM was controlled both by a radio control unit and, later, a PID tracking controller. All feedback control was accomplished using a combination A/D IO board. This device has been used to execute simultaneous pitch and yaw maneuvers of a

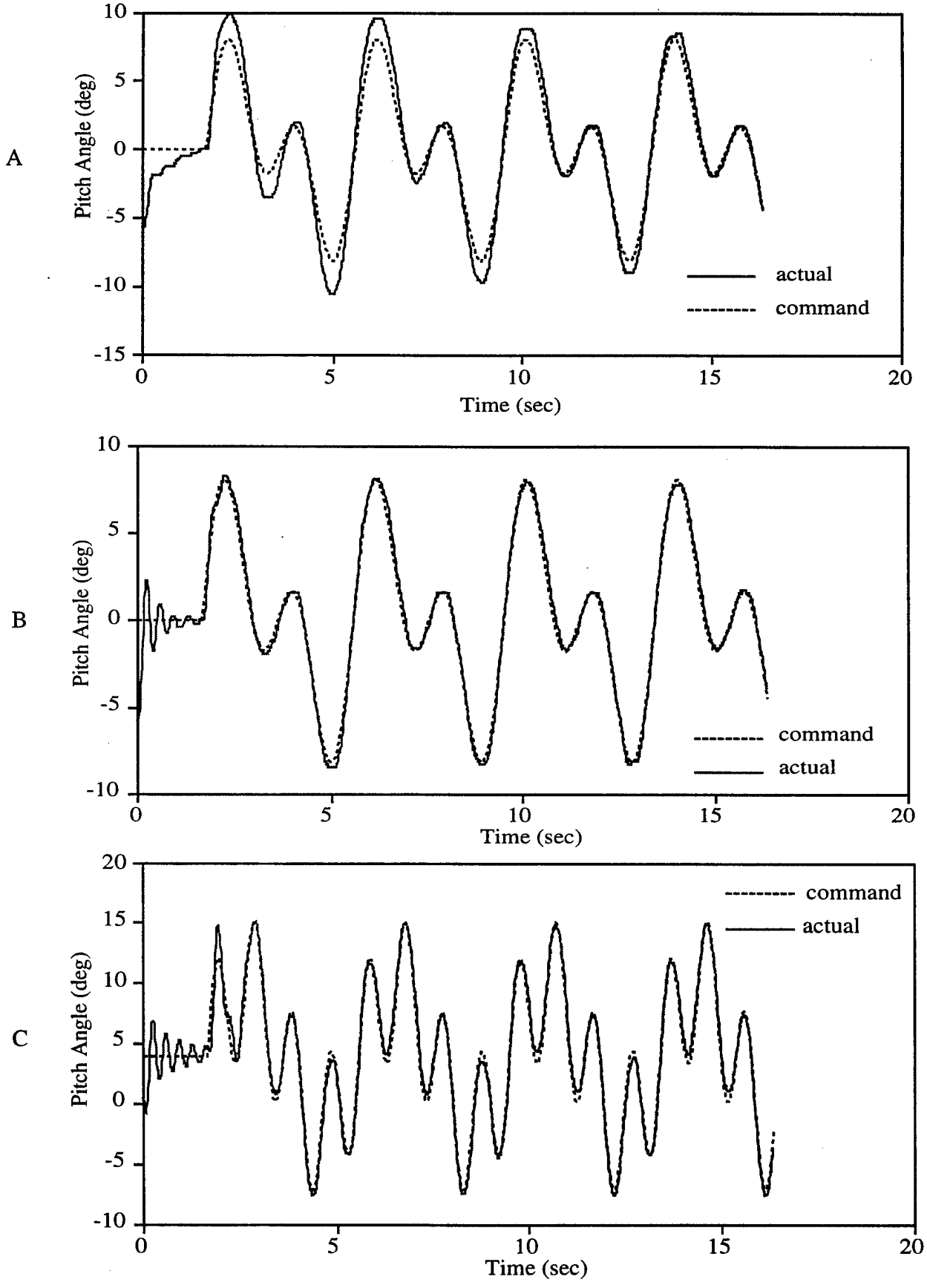

Figure A5: (a) Beginning response to specified pitch trajectory of a delta wing. (b) Steady-state trajectory delta wing. (c) Steady-state response with 1/32 scale F-18 model.

1/32-scale YF-22 model in the 7' x 9' wind tunnel at Georgia Tech using a PID controller[A24,A25]. Again, good tracking is obtained on both axes, despite the existence of cross-coupling (the control wings, when yawed, will have different aerodynamic characteristics and thus pitch differently, for example).

Exploration of Vortex Interactions

Figure A6 shows several video frames of flow visualization over a 1/32-scale YF-22 executing a simultaneous pitch-yaw maneuver. Smoke sheets, initially horizontal, are drawn into the vortex system over the model, and a vertical section is illuminated using a copper vapor laser sheet, just upstream of the vertical fins in the nominal zero-yaw, zero-pitch position [A25]. The interaction of the wing vortex system with the fins is clearly seen, as well as the generation of vortices from the fins themselves.

Measurement of Rate Effects

The rate of maneuvers such as that in Fig. A6 can be varied, and rate effects on the flow can be studied. Transient interactions between vortices and surfaces can also be studied as periodic phenomena by repeating the maneuver precisely, many times. In Fig. A7, trajectories of the leading edge vortices in a plane near the tails are plotted for the same pitch/yaw maneuver at two rates. As expected at these relatively low rates, the trajectories are nearly identical. However, severe and sudden vortex bursting phenomena can be induced by these interactions, as shown in Ref. A25: these are not anticipated by quasi-steady theory, and bring new time scales into the dynamics.

Measurement of Forces, Moments and Dynamic Stability Parameters

In addition to its uses for flow visualization and measurement, the WDM offers a means of measuring dynamic stability parameters for aircraft, both for linear and nonlinear mathematical models. While traditional force measurement devices such as load cells and strain gages can be mounted to a model undergoing such maneuvers, a more elegant way of force measurement is to extract it from the input required to drive the manipulator. This can be done at two levels. Firstly, the force measurement can be directly calibrated against a number of known forces. With some more care and effort, the forces can be derived from a simulation model of the manipulator. Typically, the experimenter will know the structure of the aerodynamic functions and will seek to measure a finite set of unknown coefficients.

Consider first the linear case of the pitch manipulator (Ref. A26). The manipulator is assumed to be a second order linear system for small amplitude motions, with the control wing incidence ϕ as the input and the manipulator / model pitch angle Θ as the output:

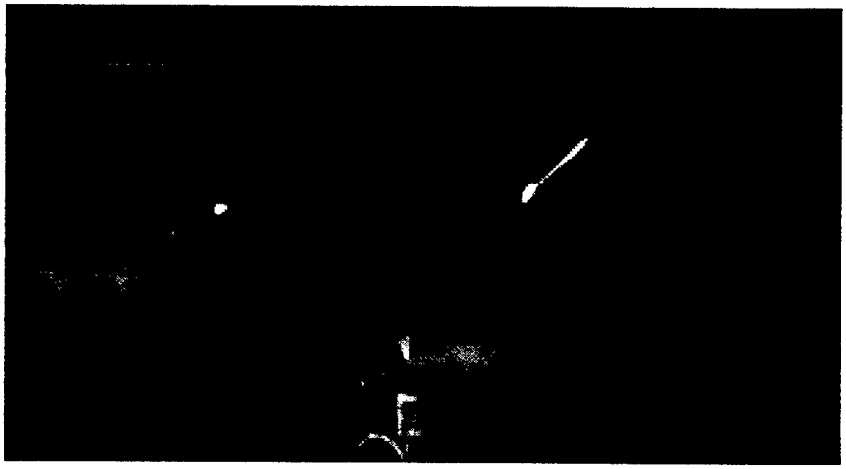

Pitch Angle: 19.61 deg
Yaw Angle: 15.4 deg L
Pitch Rate: 17.2 deg/s U
Yaw Rate: 12.9 deg/s R

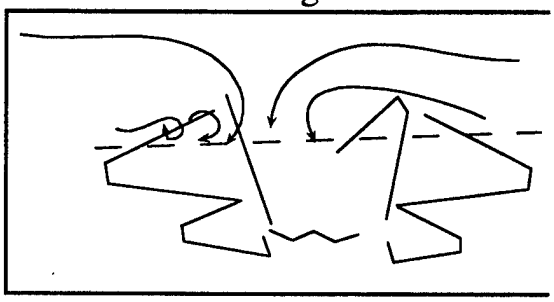

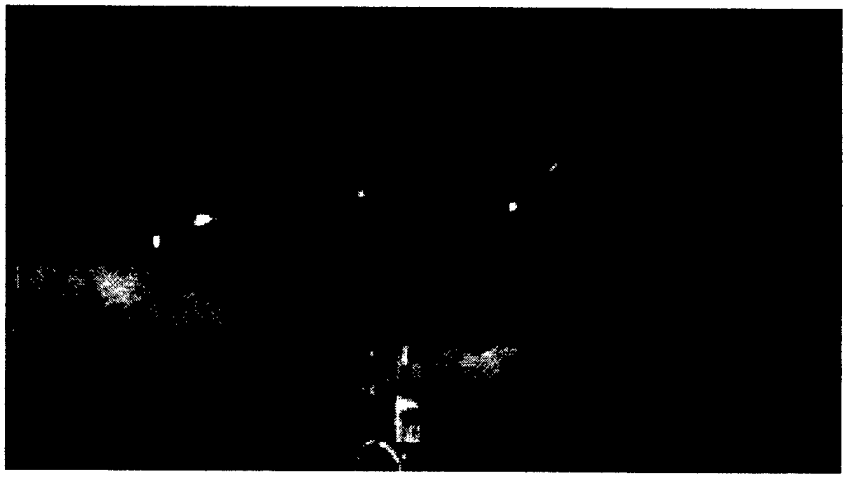

Pitch Angle: 20.59 deg
Yaw Angle: 10.5 deg L
Pitch Rate: 4.3 deg/s U
Yaw Rate: 40.9 deg/s R

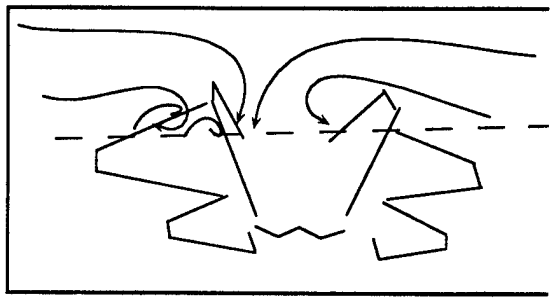

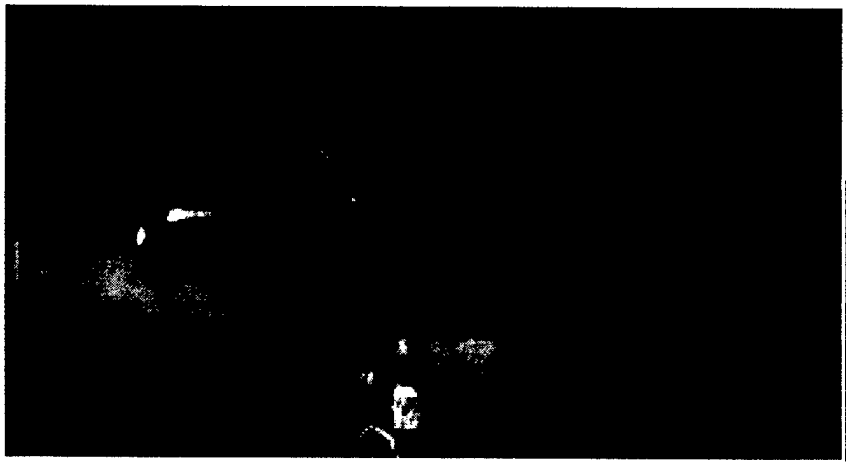

Pitch Angle: 21.4 deg
Yaw Angle: 6.0 deg L
Pitch Rate: 2.15 deg/s U
Yaw Rate: 23.7 deg/s R

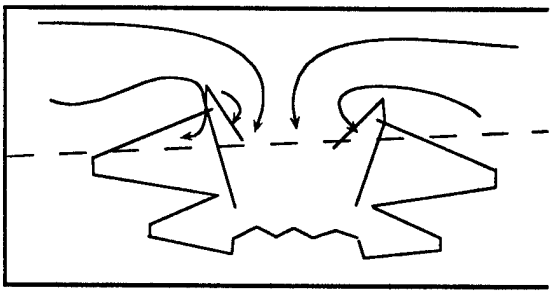

Figure A6: YF-22 in Pitch-Yaw Using WDM: Planar Images of Flow at Mid-Chord during Left Yaw-Pitch Down.

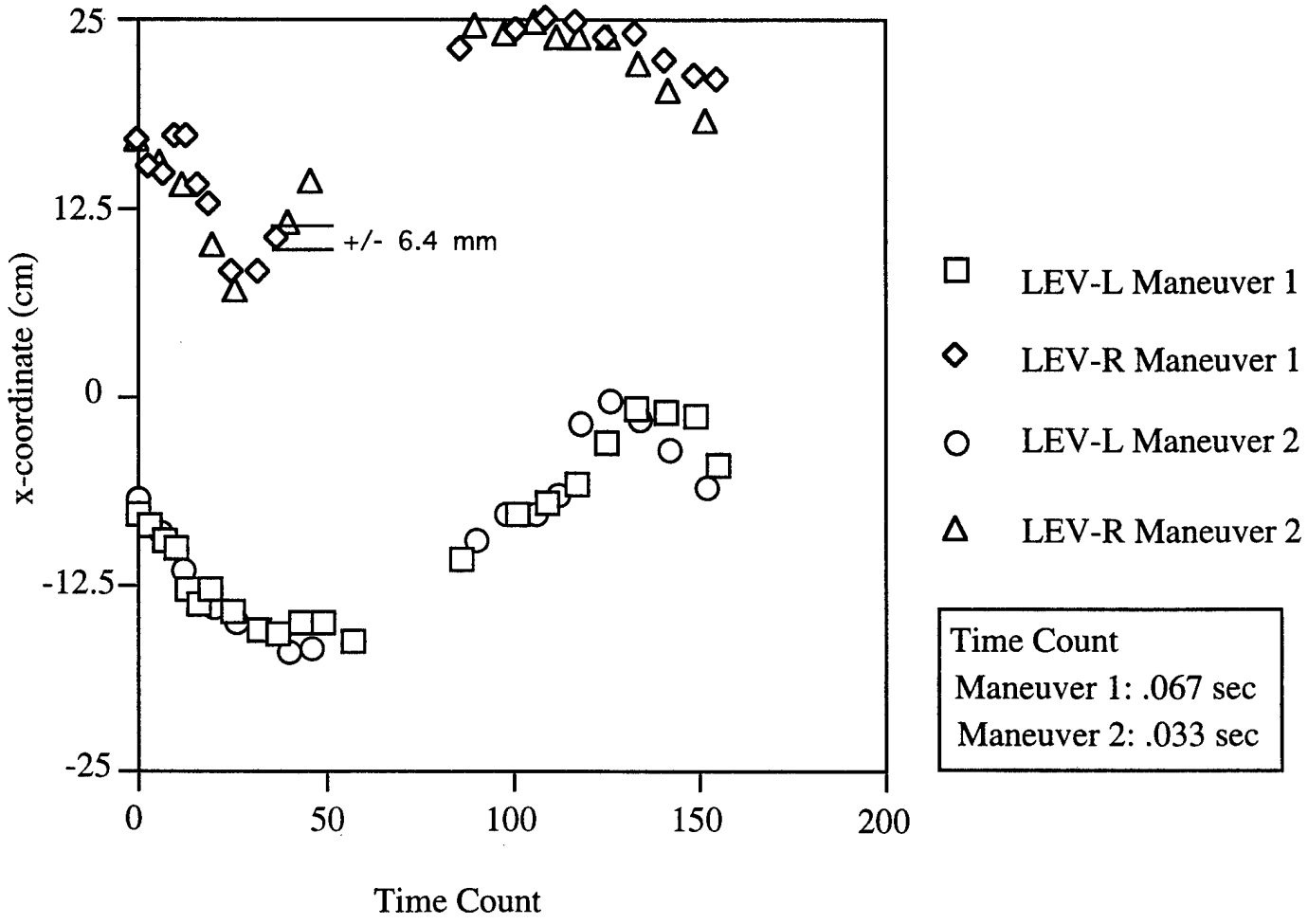

Figure A7: Comparison of left and right leading edge vortex trajectories behind a 1/32nd scale YF-22 during identical pitch-yaw maneuvers at different rates.

$$J\ddot{\Theta}'' = -M_{\dot{\Theta}'}\dot{\Theta}' - M_{\Theta}\Theta + M_{\phi}\phi$$

Four parameters are needed to describe the system: the inertia J of the rotating assembly, the pitch stiffness M_θ (the slope of the pitching moment vs. pitch angle curve), the pitch damping $M_{\dot{\theta}}$ (the slope of the pitching moment vs. pitch rate curve), and the input sensitivity M_ϕ. The inertias are measured outside the tunnel using a torsion pendulum or other appropriate means. Two experiments are then conducted using the WDM (see Fig. A8). In the first experiment, the WDM is placed alone in the wind tunnel. With the wind on, the control wing is excited with a small amplitude broadband signal, and the pitch angle is recorded. From control wing angle and pitch angle time histories, the transfer function for the manipulator, and hence its stiffness and damping, can be determined. This experiment is then repeated with the model attached to the manipulator. A difference between the two parameter sets yields the parameters for the aircraft model.

Similar algorithms can be used to measure nonlinear aerodynamic function parameters for the test model if appropriate function parameters for the test model and appropriate identification schemes are employed. Nonlinear identification requires larger amplitude motion than do the small-perturbation linear models. Linear identification experiments have been performed. A test model consisting of a wing on the end of a rod is used because its damping and stiffness can be easily predicted and compared with the measured results. The stiffness varies linearly with the length of the rod, and the damping varies with the square of the rod length. So far, these relationships are observed qualitatively, but good accuracy in stability parameter measurement has yet to be obtained.

Development of New Aircraft Control Schemes

Many new aircraft control strategies are emerging, including thrust vectoring, moving noses (see Part B of this report), and other means of vortex control. Most of these are intended for use in the high-α regime. The WDM provides a means for measuring the effectiveness of these techniques. Forces produced by these actuators can be measured as the aircraft executes a maneuver under WDM control. Thus the actuator effectiveness can be studied completely without a free-flight model and a full stabilizing control system. Likewise, design of actuation force and moment controllers can be designed and evaulated using the WDM.

The 3-Degree-Of-Freedom, Roll-Pitch-Yaw Manipulator

A roll-pitch-yaw wind-driven manipulator has been developed and demonstrated in the 7' x 9' low speed tunnel at Georgia Tech. The 3DWDM provided all of the benefits of

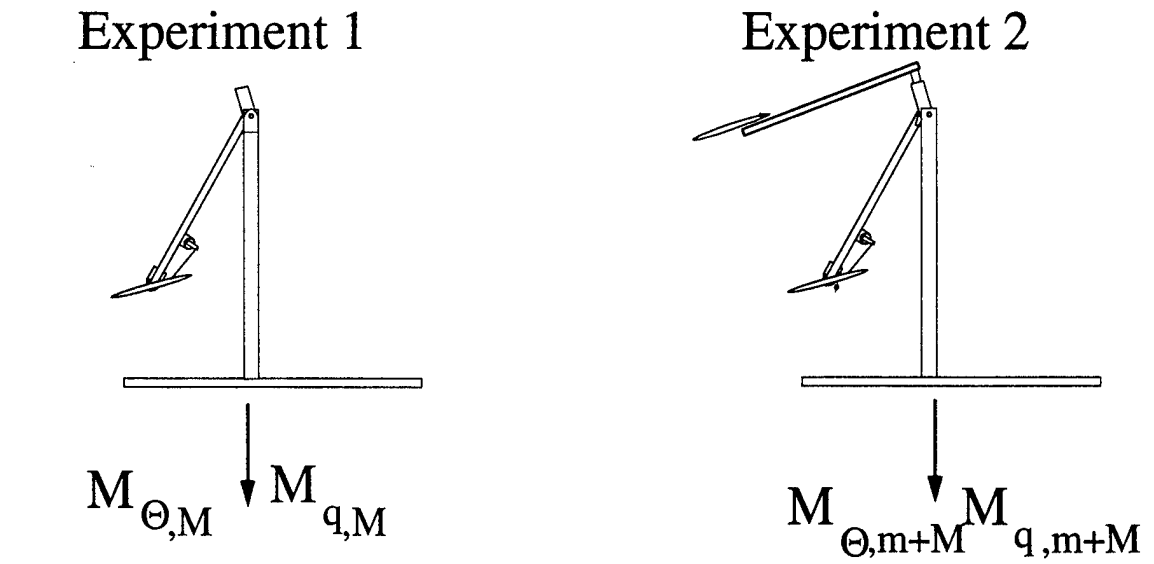

Arithmetic

$$M_{\Theta,m} = M_{\Theta,m+M} - M_{\Theta,M} \qquad M_{q,m} = M_{q,m+M} - M_{q,M}$$

Subscripts: M - Manipulator m - model

Figure A8: Parameter measurement setup for the 1DOF WDM.

its WDM predecessors but also provided the ability to prescribe combined motions about the pitch, yaw, and roll axes. The device was designed using computer-aided design, and tested in the computer using an animated rendering of the assembly drawings. A frame from the animation is shown in Fig. A1. Detailed dimensions are shown in Fig. A9.

The four wings were articulated independently; each wing had its own controlling servo motor. Common mode deflection of the horizontal and vertical wings resulted in pitch and yaw respectively, while differential deflection produced roll. The motors used to control the wings were small, high-speed motors with an integrated 76:1 gearbox and integrated magnetic encoders that were used as feedbacks to the motor control circuitry.

The wings again used a rectangular-planform and NACA 0012 section, as with both previous WDM designs. The wings were constructed of a foam core with carbon-fiber skins and a layed-up carbon-fiber spar. All composite parts were vacuum-bagged and cured in an autoclave to provide maximum strength with minimum weight. The carbon-fiber spars included integrated steel axles that attached to the pivots at the rear of the booms. As before, the wings were pivoted about their quarter-chord.

The rest of the 3DWDM was machined from aluminum and steel. Link 1 was solid aluminum. The rear section of Link 3 was made of thin-walled aluminum tubing. Link 2, the sting section of Link 3, and all of the axles were made of steel. Measurements of the roll, pitch, and yaw angles were provided by optical encoders equipped with index markers so that absolute positioning was possible. All data acquisition and control functions were accomplished on a 33MHz 80486 PC. Two interface boards were required. A 4-axis encoder interface was used to count the encoder signals and provide position measurements and a servo motor position control controller board was used to transmit commands to the motors and receive feedback from the motor encoders.

Manipulator Design Considerations

WDM design for maneuver tracking is a task of balancing four concerns: minimizing interference between the control wings and the test model, maximizing the available driving moment, minimizing inertias, and minimizing response time of the wings. Control wing interference can be quantified by examining the velocity perturbations at a reference point on the test model due to the control wings. A lifting line analysis applied to the finite wings serves as a good tool. It is easily seen that the interference is negligible, primarily because of the large distances, and the fact that the control wings seldom operate at highly-loaded conditions. The disturbances decrease with increasing arm length and increase with wing chord. For the 3 d.o.f. device, the upper bound on velocity perturbation at the model is 0.2% of the freestream velocity.

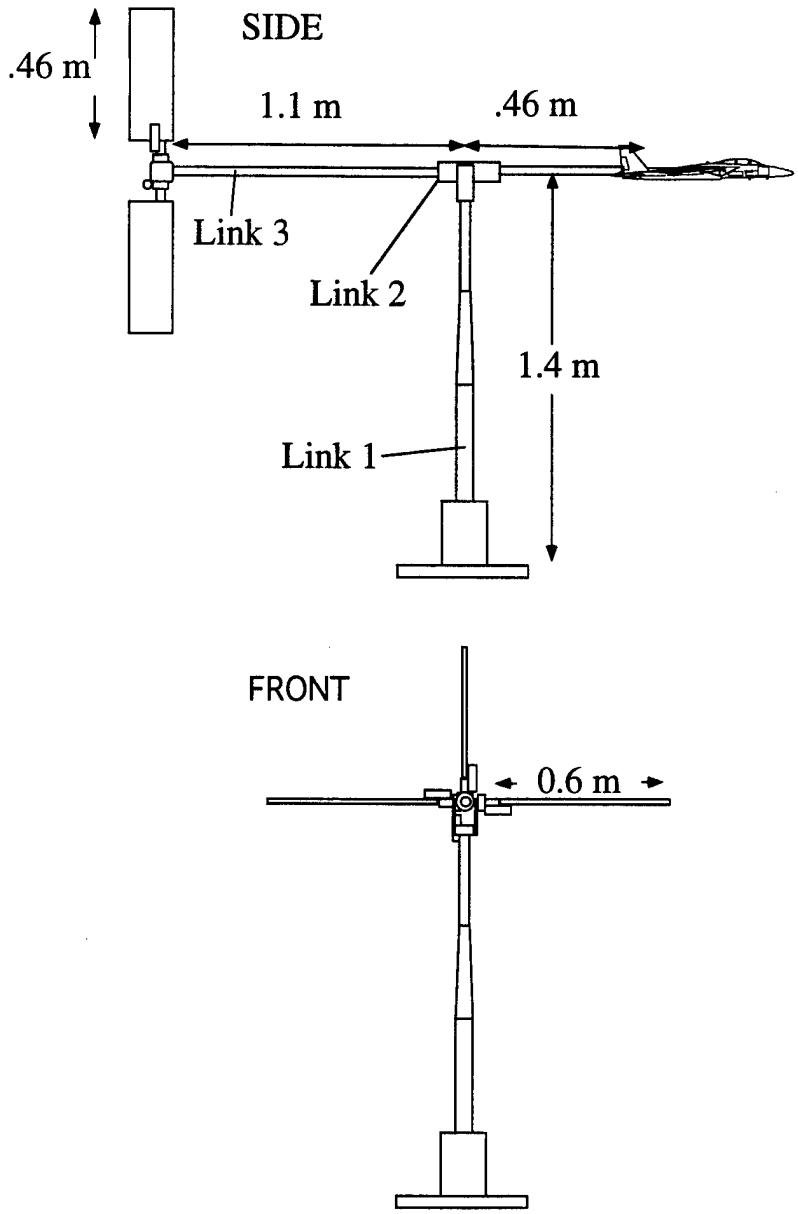

Figure A9: Dimensions of 3D WDM

The available driving moment is determined by the wing area and lifting characteristics and by the length of the manipulator arm. Both of these may have detrimental effects on inertia, interference, and response time of the wings, and a long arm also results in restricted motion in a closed test section. Inertia is dominated by the mass of the wings and the servo motors. Thus a long arm results in large inertias. The mass of the wing and servo assembly must be minimized by careful design. The time constant of the wing is roughly related to the time it takes a particle to traverse the wing chord. It is best then to use wings with a high aspect ratio. In Fig. A10, three performance plots are used to size the 3 DWDM. They are based on estimates of moments and intertias. The first shows how the time to complete a 90 degree maximum effort roll varies as the chord to freestream velocity ratio (c/v) is varied. In Fig. A10b, the maximum pitch rate achievable in a 60-degree sinusoidal pitch oscillation is shown, also as a function of c/v. Finally, Fig. A10c depicts the pitch rate at the end of a -30 deg. to +30deg. maximum pitch-up. All of these are for a given arm length, but results for three different freestream velocities are shown. They are useful in determining the wing aspect ratio. Other design tradeoff plots are used to select arm length, servo motors, wing sections and other characteristics. Note that the available moments and hence the available rates, follow a speed-squared scaling. Most rate phenomena are reduced by a linear function of velocity, making the WDM viable as a device for use in high-speed subsonic tunnels.

The WDM configuration for parameter measurement is different from that for maneuver tracking. Maneuver tracking requires a manipulator which dominates the test model, making the model aerodynamics easy to overcome. Parameter measurement requires that the test model contribute significantly to the system dynamics so that the model properties can be distinguished from those of the manipulator. A manipulator with interchangeable wings, adjustable arm lengths, and rate-augmenting geared model attachment would allow the same device to be used for all types of experiments.

Initial Experiments with the 3 d.o.f. Manipulator

Figure A11 (from Ref. A27) shows the response of the 3 DWDM to step inputs in pitch. This experiment was run with a sting-mounted F-16 model. There was strong dynamic coupling between the pitch, yaw and roll, but the device stabilized and was able to hold the model steady at desired angle of attack, as shown by the flat zones where pitch, yaw and roll are all held constant. It should be noted that the model was free of the vibration associated with conventional mounts, partly because no reactions are transmitted to the walls. This capability is especially useful for quasi-static testing. Fig. A12 shows the WDM response to a high-rate input. Note the strong coupling between the yaw and roll,

A

B

C

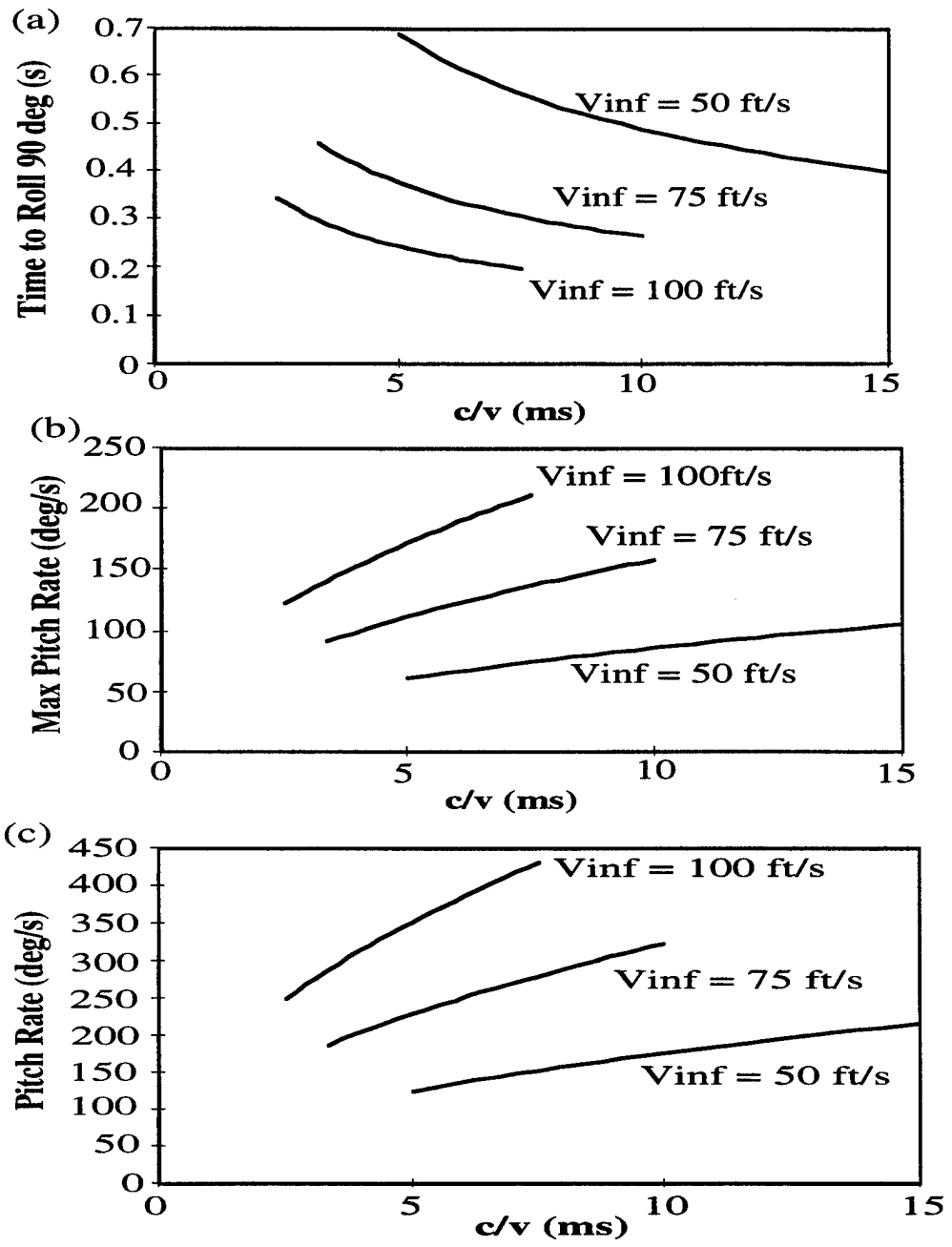

Figure A10: WDM design parameter tradeoffs. (a) time to roll vs. c/v; (b) maximum pitch rate during 60 deg. sinusoidal oscillation; (c) pitch rate at end of -30 deg. to 30 deg. pitch up.

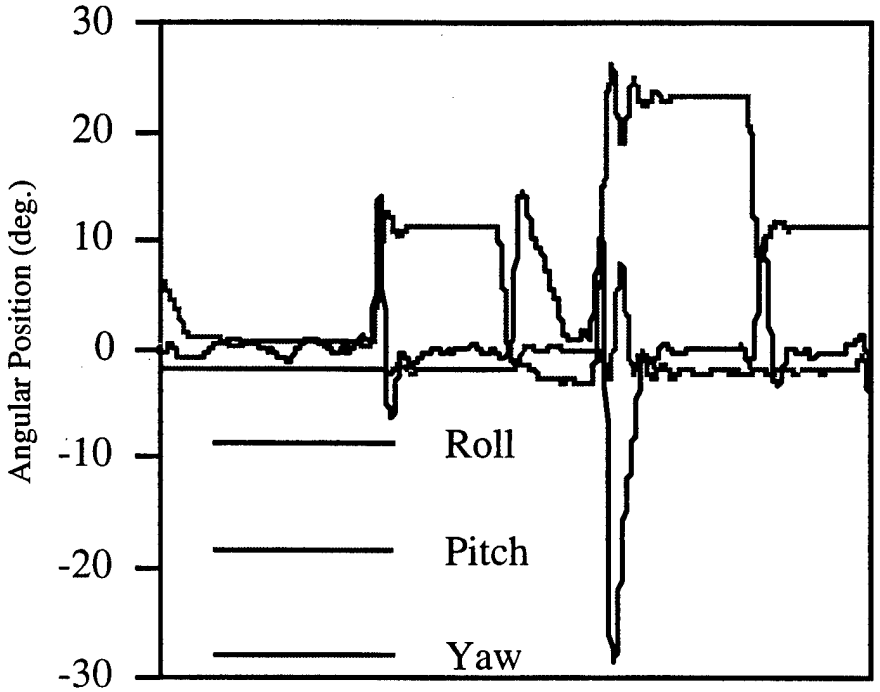

Figure A11: 3DWDM response to step pitch inputs.

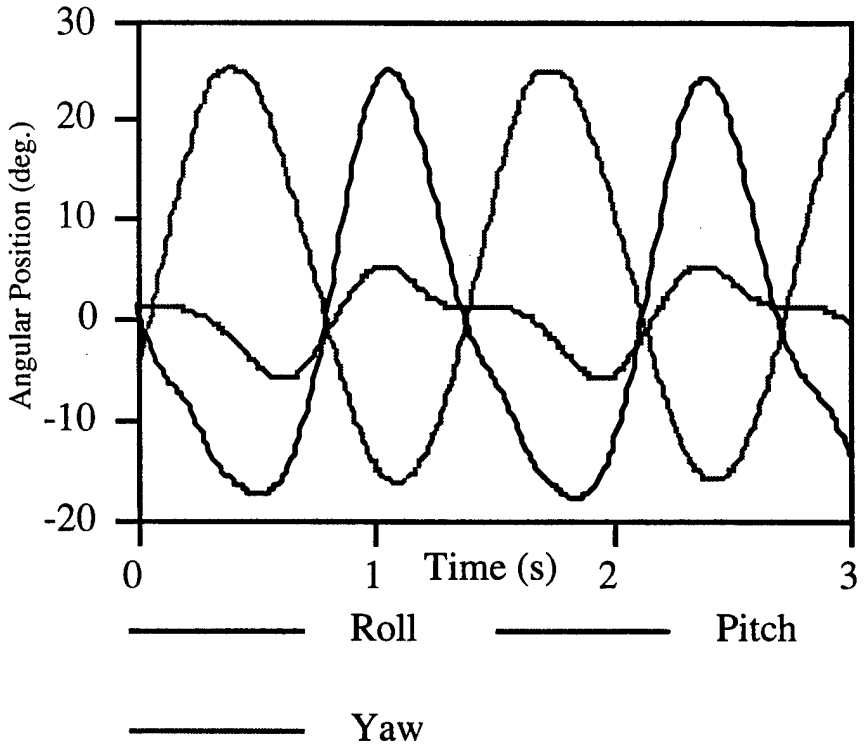

Figure A12: 3DWDM response to high yaw rate input.

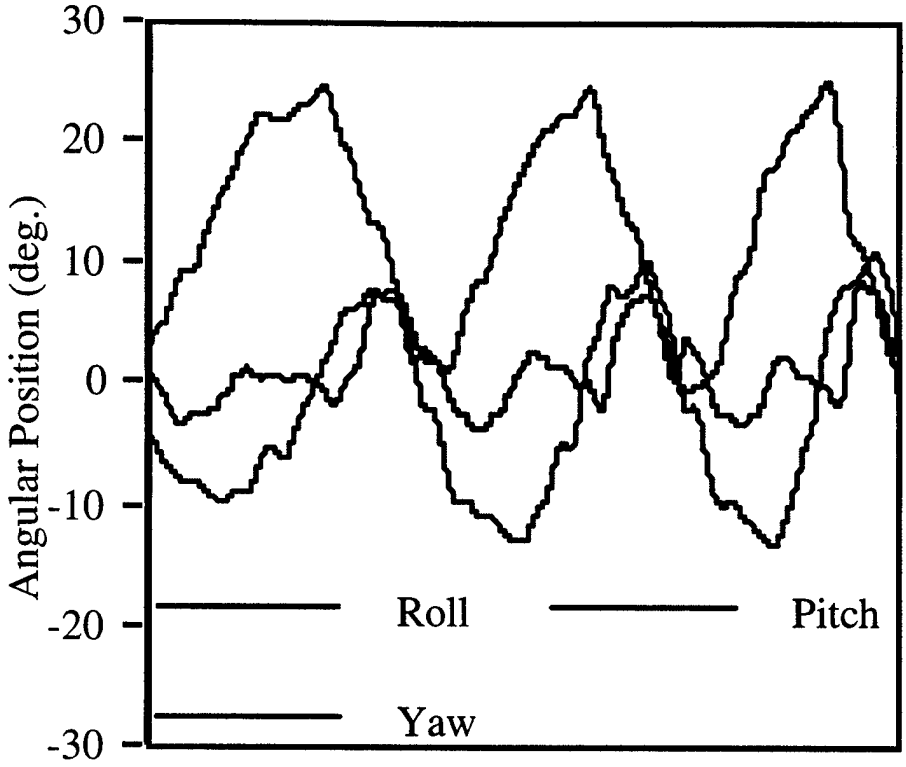

Figure A13: 3DWDM response to combined pitch/yaw input.

and the 90-deg. phase lag. During testing, the WDM was taken to a transient roll rate of 2100 deg. /sec. with no damage. Fig. A13 shows the WDM response to a joystick-commanded, combined pitch-yaw input. This is a large amplitude, low rate input over a total sampling time of approximately 10 seconds.

Expansion to Six Degrees-of-Freedom

Figure A14 shows the 3 d.o.f. WDM installed in the 7' x 9' wind tunnel (the engineer in the picture is Kevin Peterson). Translational degrees of freedom are easily incorporated using floor - or roof-based linear traverses with conventional electric drives. Transient speeds as high as 40fps are achievable with a linear actuator being assembled at the 7' x 9' tunnel in Winter '97.

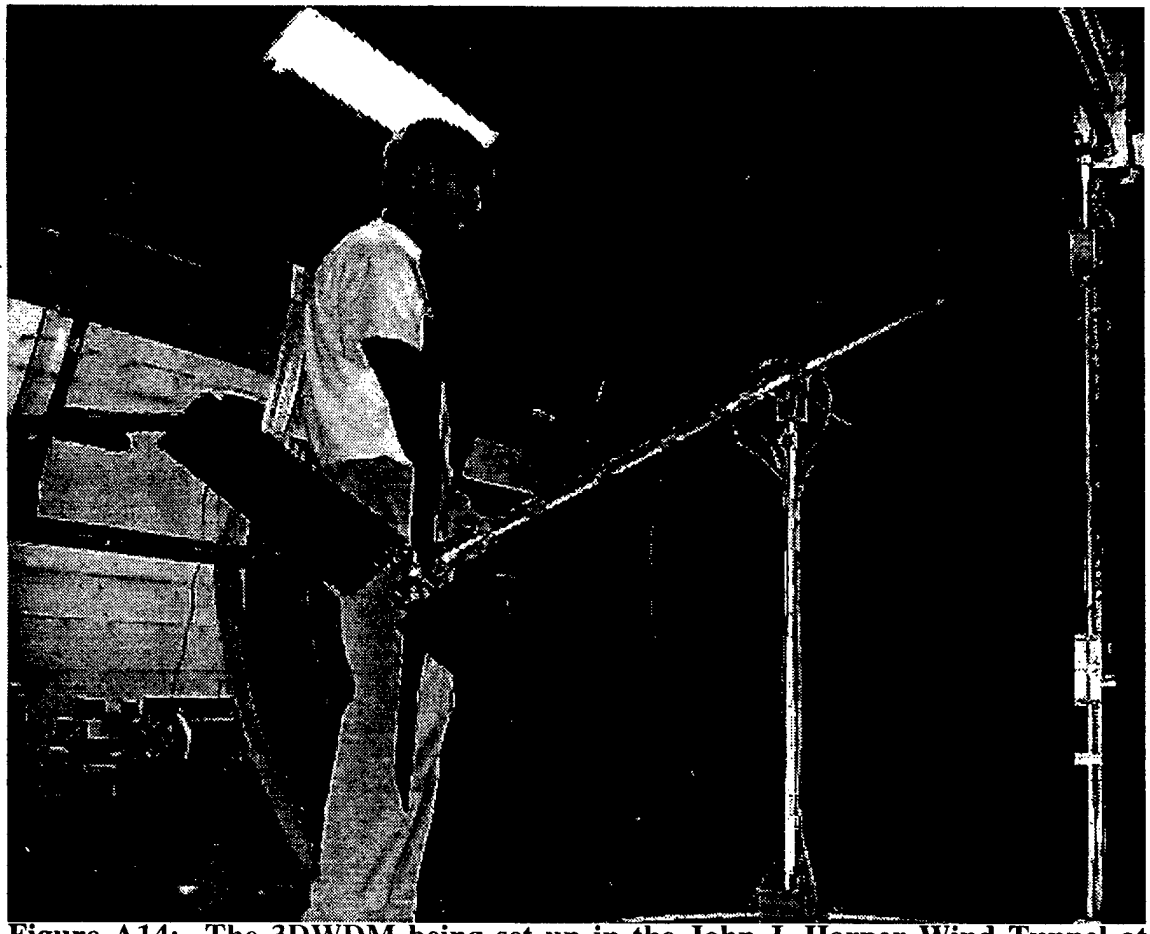

Figure A14: The 3DWDM being set up in the John J. Harper Wind Tunnel at Georiga Tech.

III. TECHNICAL SUMMARY, PART B: STAGNATION POINT ACTUATOR FOR VORTEX CONTROL

Concept

This study started by asking the following: *"Since forebody vortex asymmetry appears to originate in the stagnation region at the very nosetip, can we control the forebody vortices in a continuous, deterministic and rapid manner by moving the stagnation point?"* We have shown that this is not only possible, but that:

a) linear relationships describe the response of the yawing moment as well as the wing rolling moment to the motion of the stagnation point,

b) the Stagnation Point Actuator (SPA) is as effective as blowing, suction, strakes and other forebody symmetry control devices, while being extremely simple by comparison, and

c) the SPA response being clean, we are able to use it to study the various time scales involved in the vortex aerodynamics of a maneuvering aircraft.

This research program sought to uncover the causes and effects of asymmetric forebody vortex loading on vehicles at high angle of attack. This problem has become increasingly important as the flight envelope of highly maneuverable aircraft has expanded. At angles of attack above about 20 deg., the vortices over the forebody of the aircraft are usually asymmetric[B1-B5], *even when great care is taken to hold a symmetric flight condition and the forebody geometry is as cleanly symmetric as wind tunnel models, free-flight scale models, and flight test aircraft can be made.* This asymmetry induces a pressure differential across the forebody which creates a side force and yaw moment on the vehicle (Fig. B1). The source of these asymmetric vortices has been argued in the literature for quite some time. However, the initial belief in the hydrodynamic instability theory seems to have been replaced by the theory that small geometric asymmetries in the forebody create the asymmetries in vortex patterns[B1,B6,B7].

In addition to the asymmetric forebody vortices, the existence of vortex burst becomes an issue[B5,B7]. This process can be influenced by the asymmetry of the forebody vortices, with the burst location moving asymmetrically over the wings (Fig. B2). Of course, vortex bursting over the wings will decrease the lift on the wings. So asymmetric bursting can result in roll moments. Predicting these roll moments can be very difficult because of the existence of multiple states of roll behavior, dependent on the roll angle and the angle of attack[B8-B10].

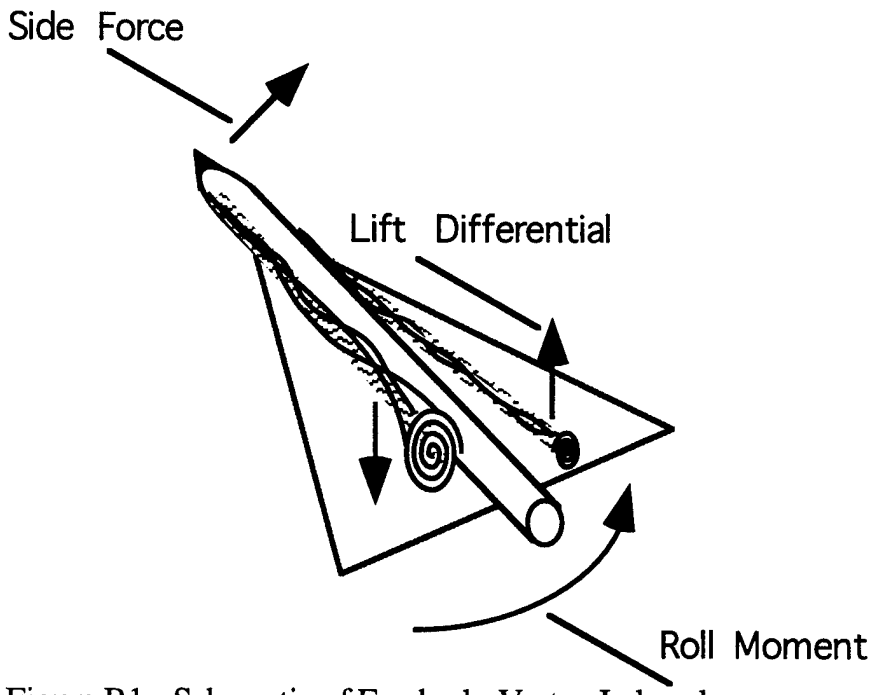

Figure B1: Schematic of Forebody Vortex Induced Forces and Moments on a Delta-Wing Model

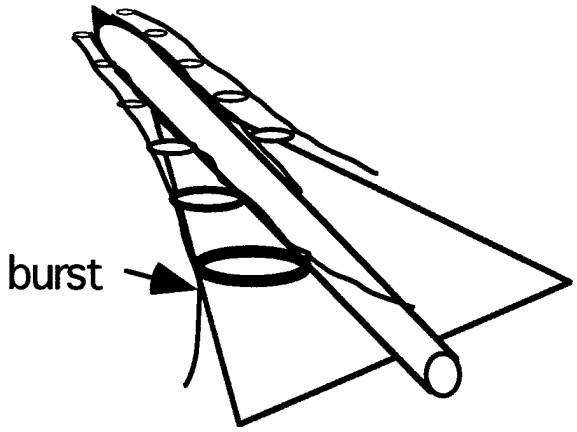

Figure B2: Schematic of Asymmetric Vortex Burst on a Delta-Wing Model

While the asymmetric forebody vortices and wing vortex burst are creating unwanted lateral loads on the aircraft, the empennage also begins to lose its effectiveness[B11]. At high angle of attack the flow around the tail section is dominated by sporadic wake flow conditions, which lower the forces created by the tail section. As a result, and because of the interest in tailless stealthy aircraft, it has become increasingly important to find new sources of control action, which can take advantage of the relatively smooth flow at the forebody.

Previous Work

Several forebody vortex actuators have been proposed and examined in the literature. Forebody blowing and suction to manipulate the vortices have been documented in refs. B12 - B16. Ng and Malcolm[B12] performed water tunnel flow visualization tests on F/A-18 models to compare blowing from a localized jet, blowing from a slot, and surface suction. Cornelius et al.[B13] have compared several nozzle geometries and blowing angles for an X-29 aircraft model. Miller and Gile[B14] have compared jet strengths and blowing directions in a water tunnel over models of differing leading edge sweep angles for static conditions and dynamic pitch maneuvers. Alexander and Meyn[B15] have investigated outward, downward, and tangential blowing with different mass flows, slot lengths, and positions. Wing rock suppression by forebody blowing has even been reported by Celik et.al[B16].

The use of rotatable nose strakes to control vortex asymmetry is described in refs. B2, B3, and B17 - B2l. Malcolm[B20] summarizes these and points out that the strakes simply provide a bias to the flow rather than produce substantial vorticity. One strake produced no vorticity, but when two were present, they tended to alleviate the net asymmetry. In addition, ref. B20 argues that the strake size must be related to the range of flow conditions over which the device would be effective. It has thus been argued[B20] that the deflectable strakes used by Malcolm and Skow[B17] and Murri and Rao[B18] would be potentially effective over a wider range of operating conditions than the techniques which rely on adding vorticity. Ng and Malcolm[B19] have found that a pair of nose tip strakes rotated about the roll axis can be effective in controlling the yaw moment. Suarez et al.[B21] compared a single strake to a pair on the nose boom of an X-29 configuration. They found that rotating these strakes varied the degree of asymmetry. Finally, Moskovitz et al.[B3] have used a rotating nosetip with varying ellipticity to create a discontinuity in the surface contour and hence to modify the surface pressure gradient.

Stagnation Point Actuator Hypothesis

The device used here is a stagnation point actuator (SPA) which consists of a nose-tip cone which rotates in the yaw plane, thus deflecting the stagnation point from the axis of lateral symmetry. This actuator was inspired by the experiments in Ref. B22 in which a double-delta wing model was being tested using flow visualization techniques in the Georgia Tech Low Speed Wind Tunnel. A stable, repeatable asymmetry was noticed under symmetric mounting conditions. The asymmetry was traced to the very tip of the nose, where a minor dent was found. This dent effectively shifted the stagnation point laterally from the vertical plane of symmetry. The asymmetry was eliminated by gradually correcting the geometric imperfection. Therefore, it is hypothesized that continuous variations in asymmetry can be achieved by continuous, quasi-steady motion of the nose stagnation point.

The Stagnation Point Actuator triggers varying degrees of asymmetry at the very origin of the shear layers which roll up into the forebody vortices: the stagnation point at the nosetip. By displacing the stagnation point from the plane of lateral symmetry, the boundary layer development in the stagnation point flowfield is biased. The precise means of displacing the stagnation point is a matter of detailed design preference: the most convenient means we have found in a small-scale wind tunnel experiment is a nose cone which can be yawed using a push-rod connected to a servo motor[B23]. As shown in Fig. B1, the net result of displacing the stagnation point to the right is that the boundary layer profile on the right side is more favorable, and the vortex is stronger and closer to the surface. The suction on the favored side is thus stronger, and a side force (and hence a yawing moment) develops towards the right side.

At first sight, such an approach would seem to have little hope of controlling vortex asymmetry precisely: we just bias the stagnation point flow and let the vortices develop unhindered thereafter. Soon after the first test of the SPA[B24], however, it became obvious that the issue of interest had changed from merely *suppressing* forebody vortex asymmetry, which happened quite easily, to that of *inducing desired directions and levels* of yawing and rolling moments, *at desired rates.* Clearly, the stagnation point flow held the key to controlling the entire vortex system.

Chronology of Objectives

This study has been guided by the search for answers to a number of related questions. It began by asking the question: Is there a cause and effect relationship between the stagnation point deflection and the forebody vortex asymmetry? Having answered this question in the affirmative, the study moved on to determining the nature of this

relationship. It was found that the vortex response to stagnation point deflection exhibited a linear relationship with a time lag superimposed over most of the forebody. The relationship changes downstream of the wing leading edge to one which is nonlinear and perhaps indeterminate. To determine the origin of the time lag, a causal relationship was sought between the stagnation point deflection and the wing rolling moment. Although the analysis of the nature of this relationship is still ongoing, it has become clear that there are multiple types of roll moment responses and multiple time scales related to that response. This problem became very complex; so we asked if we could induce a desired rolling motion of a free-to-roll aircraft by moving the nose actuator. This was successfully achieved. Indeed the SPA is successful in inducing and stopping wing rock. In the study then, the nose stagnation point actuator has been used to achieve five goals. We have:

1.) proven the effectiveness of the nose actuator in altering vortex flow conditions,

2.) proven the effectiveness of the nose actuator in creating roll moments,

3.) proven the effectiveness of the nose actuator in creating pressure gradients across the forebody,

4.) studied the time scales of the flow phenomena, and

5.) begun to model the vortex flow through the use of control law theory.

Experiments on the Relation Between Vortex Asymmetry and SPA Deflection

Two series of experiments have been performed. The first series of tests was devoted to determining the response of the vortex flow to changes in the stagnation point location[B25]. The second group of experiments concentrated on the roll moment and pressure differential responses to stagnation point excitation[B9,B26]. Both sets of experiments yielded information related to the time scales of the physical phenomena involved.

In order to determine the effectiveness of the stagnation point actuator in altering the forebody vortex flow, a series of laser sheet videography experiments were performed in the 1.07 m square test section Low Speed Wind Tunnel at the Georgia Institute of Technology School of Aerospace Engineering. The model used in all of the experiments related to this project is a delta-wing (of aspect ratio 2.0) aircraft with body-of-revolution fuselage and pointed nose and aft body (Fig. B3). The delta wing has sharp edges beveled at 18 deg. on the lower surface and leading edge sweep of 63.47 deg. The conical nosetip is rotated in the yaw plane through deflection angles of up to ±10 deg. using a series of push rods attached to a remote controlled servo motor (Fig. B4). For these flow visualization experiments the model was mounted at zero bank and sideslip and 30 deg.

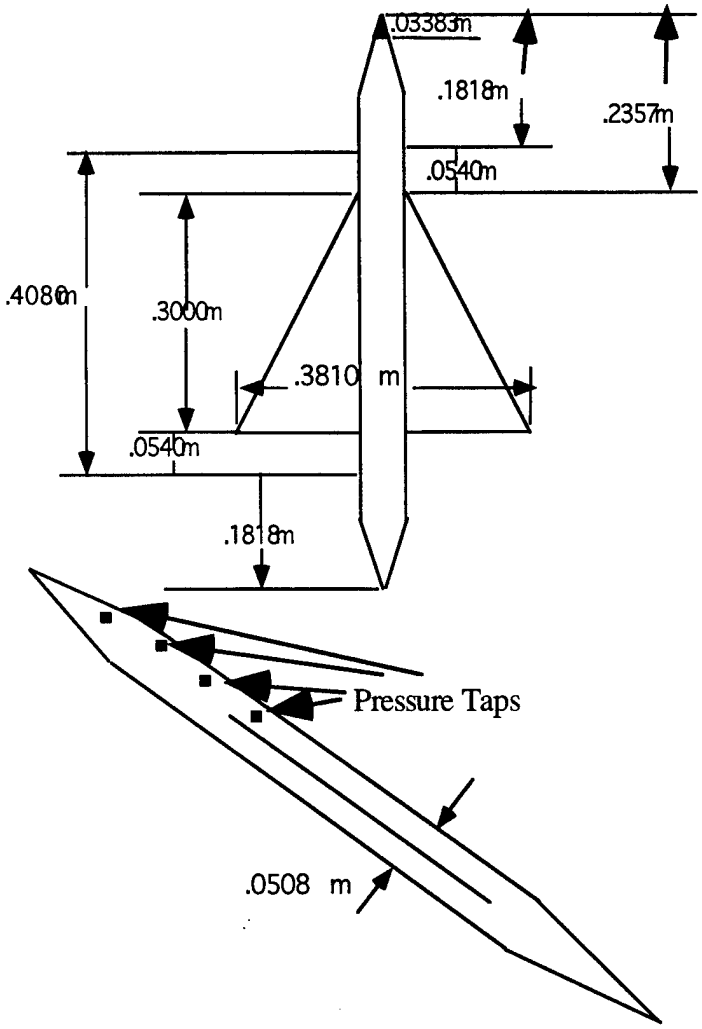

Figure B3: Aspect Ratio 2.0 Delta Wing Model with Body of Revolution Fuselage and Moveable Nose Cone

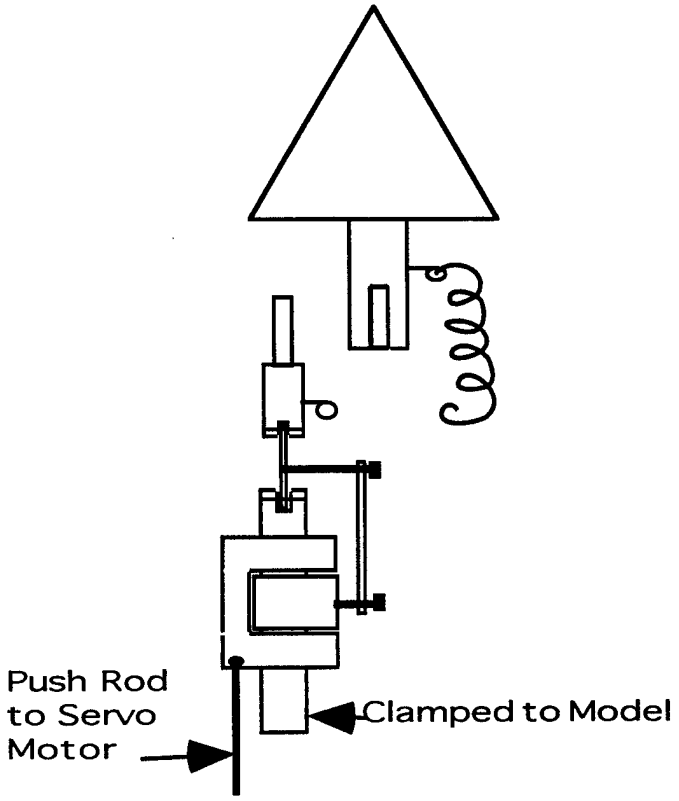

Figure B4: Schematic Diagram of Nose Mechanism

angle of attack. A laser sheet was projected onto the top surface of the model and illuminated smoke particles emitted from a set of smoke wires mounted upstream of the model (Fig. B5). In this way, the vortices over the top portion of the model could be visualized and captured with a video camera mounted downstream of the model. The instantaneous nose deflection angle was measured simultaneously.

When considering asymmetric vortices, two features need to be contemplated. The strengths and relative sizes of the two vortices will differ, and the trajectories of the two vortices will differ. To determine the causal relationship between nosetip motion and responding vortex behavior, a single metric relating the effect of both these features is needed. We use the point at which the line of zero vorticity, or Zero Vorticity Contour (ZVC), intersects the model fuselage. The ZVC separates the two vortices and rotates with them, always pointing toward the stronger vortex core. If the pair of vortices are symmetric, then the ZVC will intersect the fuselage at its point of symmetry. If the pair of vortices are asymmetric, then the azimuth angle of the intersection point indicates the relative strength and position of the two vortices. This concept is illustrated in Fig. B6. It should be noted, however, that over the wings the forebody vortices and wing leading edge vortices interact with each other so that the ZVC may not be a monotonic indicator over all ranges of the aircraft body. Evidence of this behavior will be shown later in the results from this experiment.

Table 1: Test Conditions, Measurement Planes, and Uncertainties

Freestream Velocity	2.1 m/s
Angle of Attack	30 deg. ± 0.5 deg.
Yaw Angle	0. deg. ± 0.1 deg.
X-coordinate of Plane A	0.259 m ± 0.001 m
X-coordinate of Plane B	0.314 m ± 0.001 m
X-coordinate of Plane C	0.369 m ± 0.001 m

Table 2: Sampling Parameters

Data Plane	A	B
Number of Data Points	256	256
Time Increment	1/30 sec.	1/10 sec.
Frequency Increment	0.117 Hz	0.0391 Hz
Period	8.5 sec.	25.6 sec.
X-coordinate	0.259 m	0.314 m

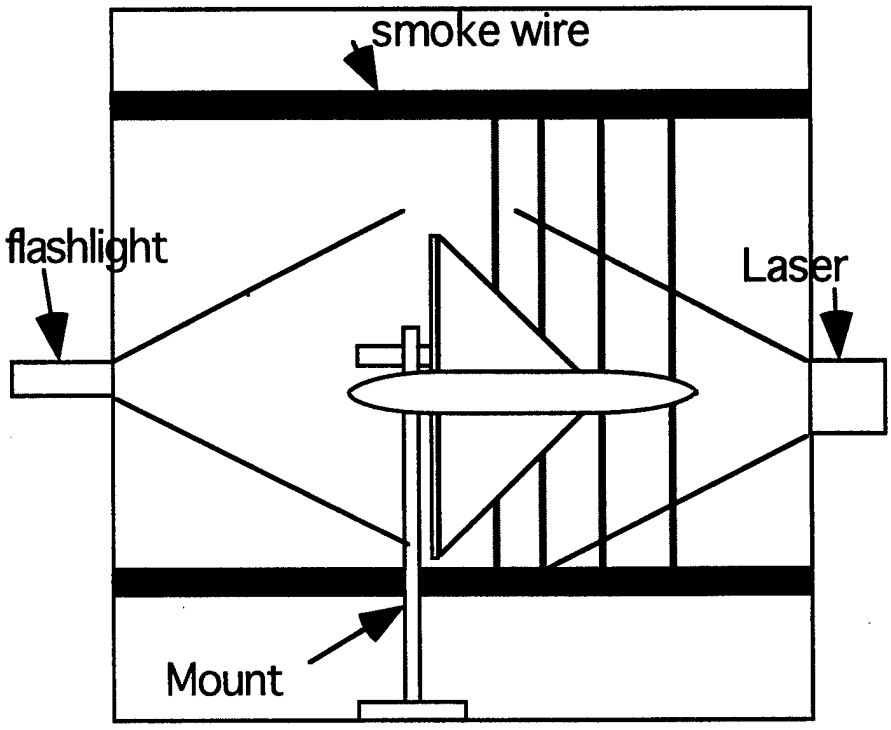

Figure B5a: Rear View of Wind Tunnel Setup

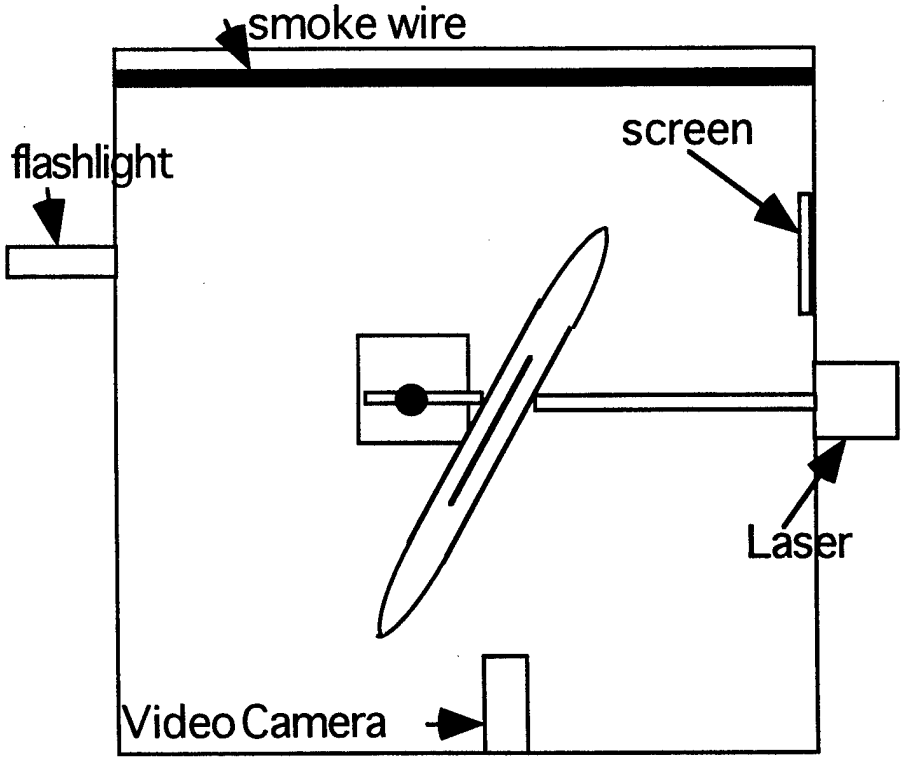

Figure B5b: Top View of Wind Tunnel Setup

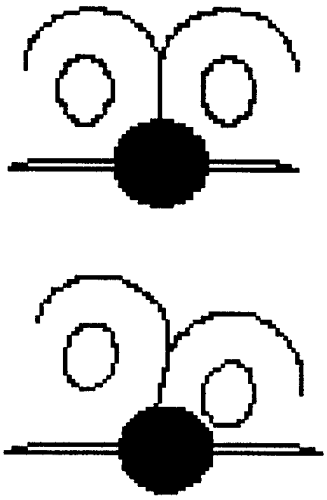

Figure B6: Illustration of the Zero Vorticity Contour as a metric of asymmetry.

Time series data relating the nosetip deflection to the subsequent dynamic vortex behavior were obtained for three laser sheet planes oriented perpendicular to the freestream flow. It turns out that vortex burst dominates the flow features at the aftmost data plane, which prevents the use of the ZVC. The low velocity of the tests was dictated by the need to capture good flow images. The test conditions and sampling parameters are outlined in Tables 1 and 2.

Experiments on the Relation Between Roll Moment, Side Force, and SPA Deflection

A second series of experiments was performed to determine the effect of stagnation point motion on the roll moment and pressure differential across the forebody. The model was sting mounted through its roll axis to a strain gage balance in the Low Speed Wind Tunnel (Fig. B7). In addition, four sets of static pressure taps were installed in the forebody of the model. The pairs of taps were positioned 70 deg. from the vertical axis of symmetry at stations 140, 160, 190, and 240 mm aft of the nose stagnation point (Fig. B3).

Roll moment and pressure data were measured at 0 deg. bank and yaw angle for sting angles ranging from 20 deg. to 45 deg. The freestream velocity for these tests was increased to 45 ft/s to 65 ft/s. Static nose deflections as well as sine wave and square wave nose deflections were examined. The test conditions and sampling parameters are summarized in Tables 3 and 4.

Table 3: Zero Bank Test Conditions

Parameter	Range Tested	Incremented by
Sting Angle	20 deg. - 45 deg.	5 deg.
Freestream Speed	45 ft/s - 65 ft/s	5 ft/s
Static Nose Deflection	-10 deg. - 10 deg.	1 deg.

Table 4: Sampling Parameters for the Sine and Square Wave Nose Deflections

Wave Frequency	Sampling Rate	Sampling Time
1.0 Hz	100 Hz	20 seconds
0.5 Hz	100 Hz	30 seconds
0.1 Hz	100 Hz	60 seconds

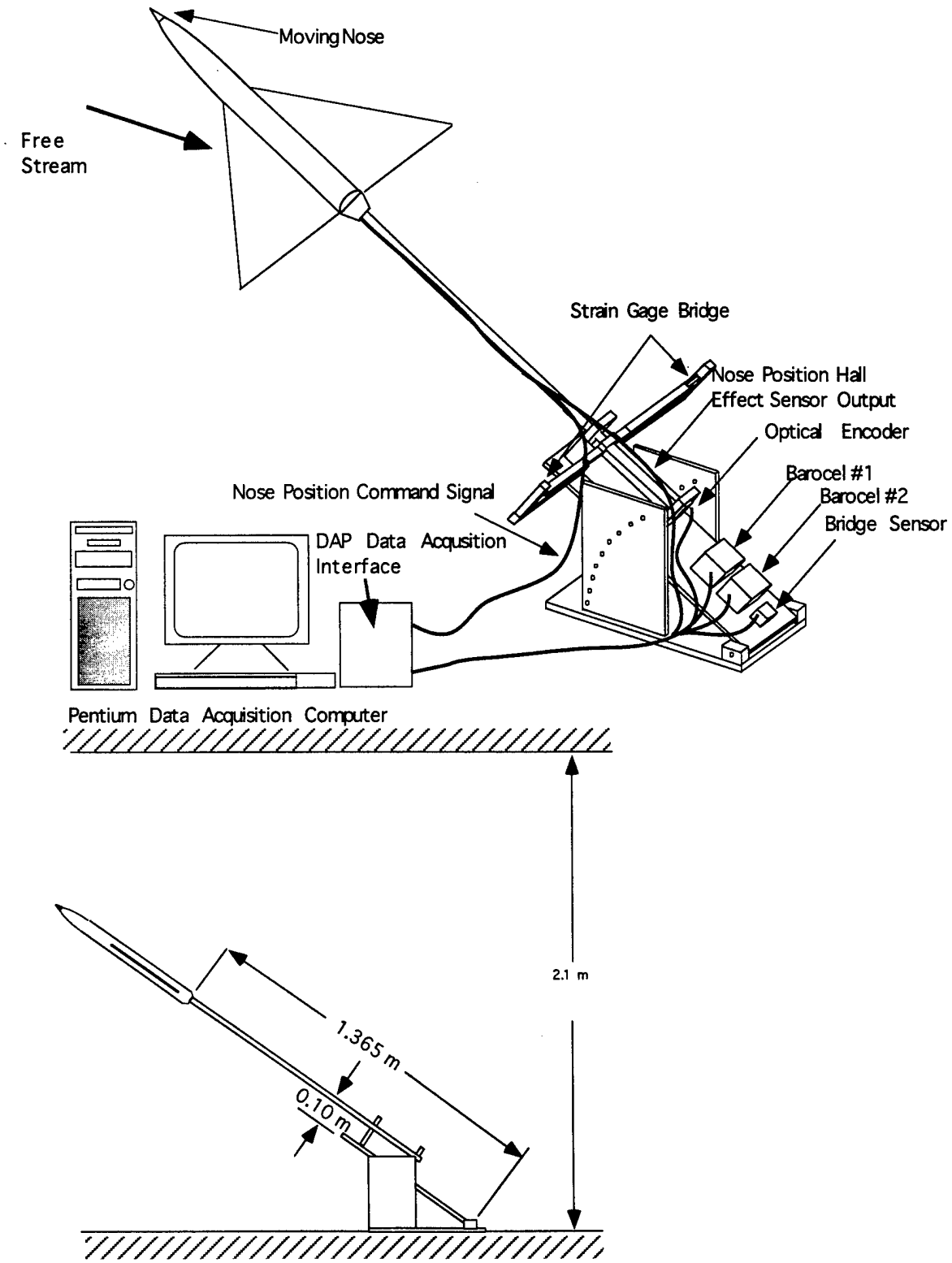

Fig. B7: Aspect Ratio 2.0 Delta Wing-Body Model on Roll Balance

In the second round of roll moment and pressure differential experiments, the test conditions were expanded to determine the effects that finite bank angles would introduce. The model was mounted in the John J. Harper Wind Tunnel using the same roll balance used for the earlier roll moment tests. The Harper Tunnel has a test section area 4.56 times that of the Low Speed Wind Tunnel. Although it was not expected that the area change would create a difference in results, it was found that the tunnel blockage effects in the Low Speed Tunnel were significant enough to induce a wall effect induced angle of attack change from the tunnel ceiling. In other words, the data from the tests in the Low Speed Tunnel correspond to angles of attack 2 to 5 deg. lower than the sting angle. In this series of experiments we again measured the roll moment and pressure differential created by static, sine wave, and square wave nose deflections.

In addition to the constrained model attitude test conditions, some initial studies into the dynamic effects of roll attitude were performed. The model was allowed freedom to roll about its axis and even allowed to initiate wing rock. The test conditions and sampling parameters used in these experiments are outlined in Tables 5 and 6.

Table 5a: Constrained Model Test Conditions

Parameter	Test Range	Incremented by:
Sting Angle	35 deg. - 45 deg.	5 deg.
Freestream Speed	55 ft/s - 75 ft/s	10 ft/s
Bank Angle	-5 deg. - 5 deg.	1 deg.

Table 5b: Free-to-Roll Model Test Conditions

Parameter	Test Range	Incremented by:
Sting Angle	35 deg. - 45 deg.	5 deg.
Freestream Speed	55 ft/s - 75 ft/s	10 ft/s

Table 6: Sampling Parameters for Sine and Square Wave Nose Deflections

Wave Frequency	Sampling Rate	Sampling Time
1.0 Hz	50 Hz	15 seconds
0.5 Hz	50 Hz	20 seconds
0.1 Hz	50 Hz	30 seconds

Effectiveness in Altering Vortex Flow

To begin the analysis of the stagnation point actuator's effectiveness, steady correction of vortex asymmetry was attempted. The moving nosetip was deflected to small finite angles using a remote controller. Time was allowed for the vortex system to respond to the motion, and the effect was recorded. Through a series of stagnation point adjustments, static correction of flow asymmetry was achieved for angles of attack of 20, 30, and 40 deg. Complete symmetry was not achieved for 50 deg. incidence, although some correction was possible. This result is shown in Fig. B8 from Ref. B25.

In order to determine the unsteady effects of moving the stagnation point, the nosetip was placed through fairly random oscillations and the resultant vortex behavior was recorded. Through extensive computer post processing, time history plots relating the instantaneous nosetip angle and matching ZVC azimuth angle were created. The time response data for planes A and B are shown in Fig. B9 and B10. Dynamic vortex behavior was recorded for plane C, but the effects of vortex bursting and interaction caused non-monotonic behavior in the ZVC. For this reason, the data at plane C is omitted. The plots relate an indisputable cause and effect relationship between nose motion and vortex rotation.

For the purposes of our initial study into the form of the nose - vortex relationship, it was decided to concentrate on a linear response approximation using a transfer function analysis. The time traces for the nose motion and ZVC rotation were sampled with random starting points and Fourier transformed. Autospectra of the nose and ZVC motion and their cross-spectrum were computed. The process was repeated with new starting points in the data series 1000 times and the ensemble average of the iterations was computed. The resultant autospectra for the data at plane A are shown in Fig. B11. Notice that the spectral energy of the ZVC deflection is higher than that of the nose deflection. One will also notice a peak frequency of 0.4 Hz, which is the frequency at which the nose was deflected.

The coherence plot and transfer function magnitude and phase for the data at plane A are shown in Fig. B12 - B14. Examining the transfer function magnitude plot indicates that the sensitivity of vortex response increases with rate of nose motion. The transfer function phase plot shows that the phase shift between nose motion and resultant vortex motion decreases with increasing nosetip frequency. In addition, extrapolating the curve back to zero frequency indicates a 180 deg. steady state phase shift. In other words, a nosetip motion to the right will create a ZVC motion to the left for the flight conditions tested.

The linear slope of the phase plot in the low frequency range allowed the time delay between nose motion and ZVC rotation to be computed. The delay is on the order of 5

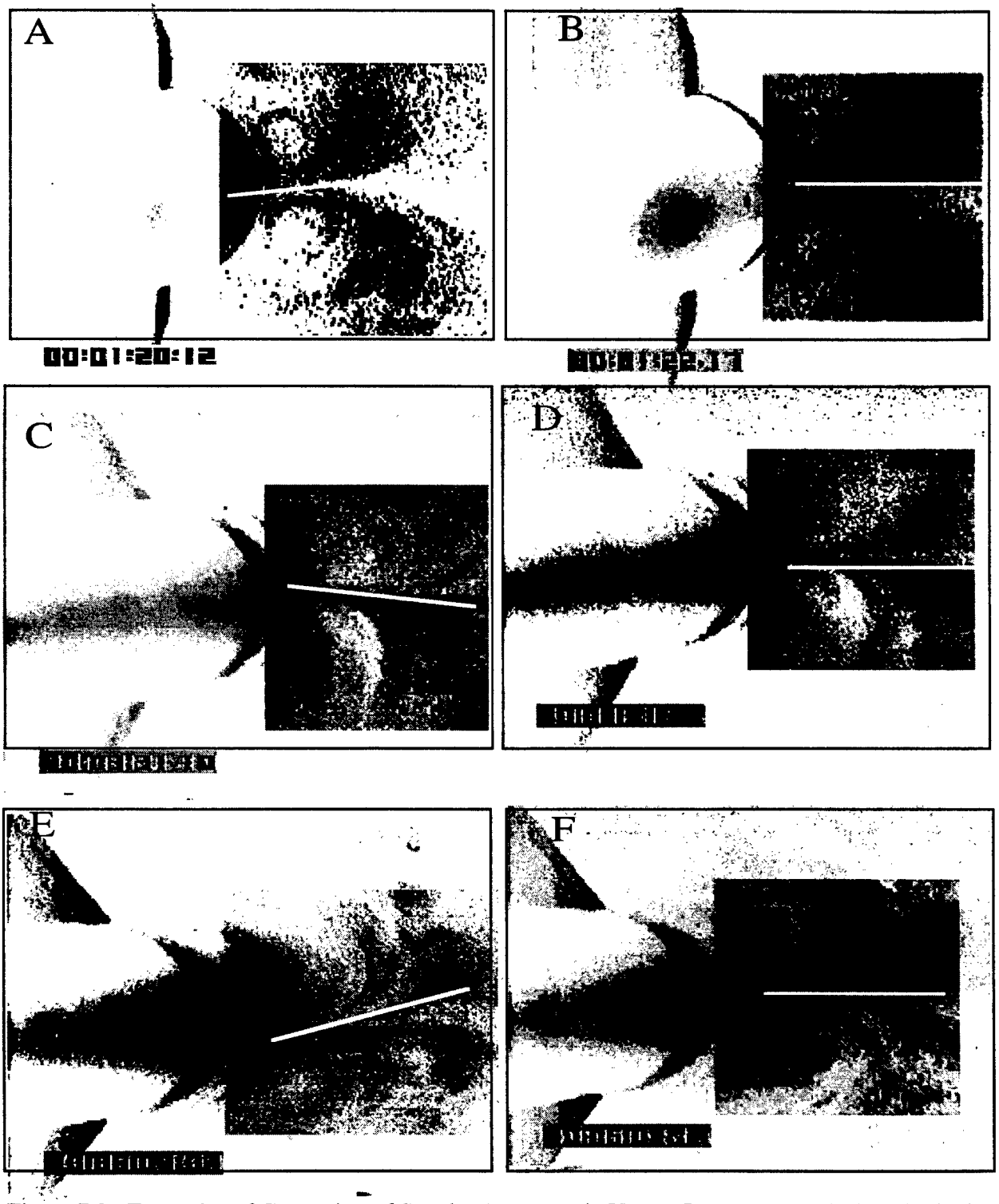

Figure B8: Examples of Correction of Steady Asymmetric Vortex Patterns over the Forebody by Motion of the Nose Tip. (A) Asymmetric at 20 deg. angle of attack, (B) Symmetric at 20 deg., (C) Asymmetric at 30 deg., (D) Symmetric at 30 deg., (E) Asymmetric at 40 deg., and (F) Symmetric at 40 deg. Image enhanced for gray-scale paper printing.

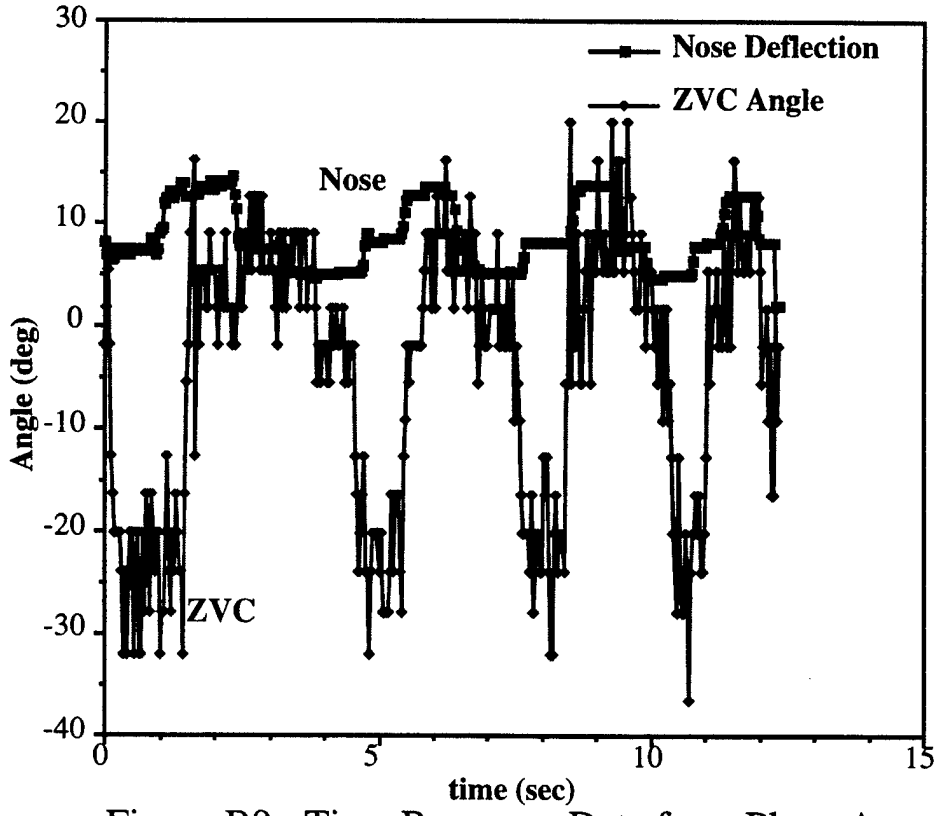

Figure B9: Time Response Data from Plane A

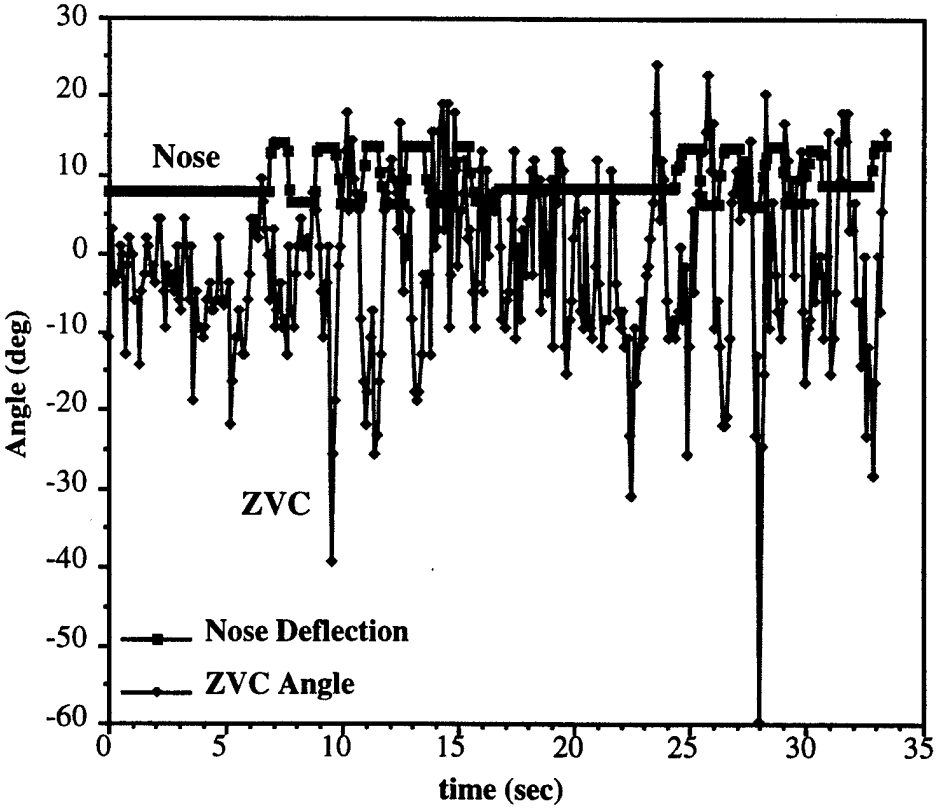

Figure B10: Time Response Data from Plane B

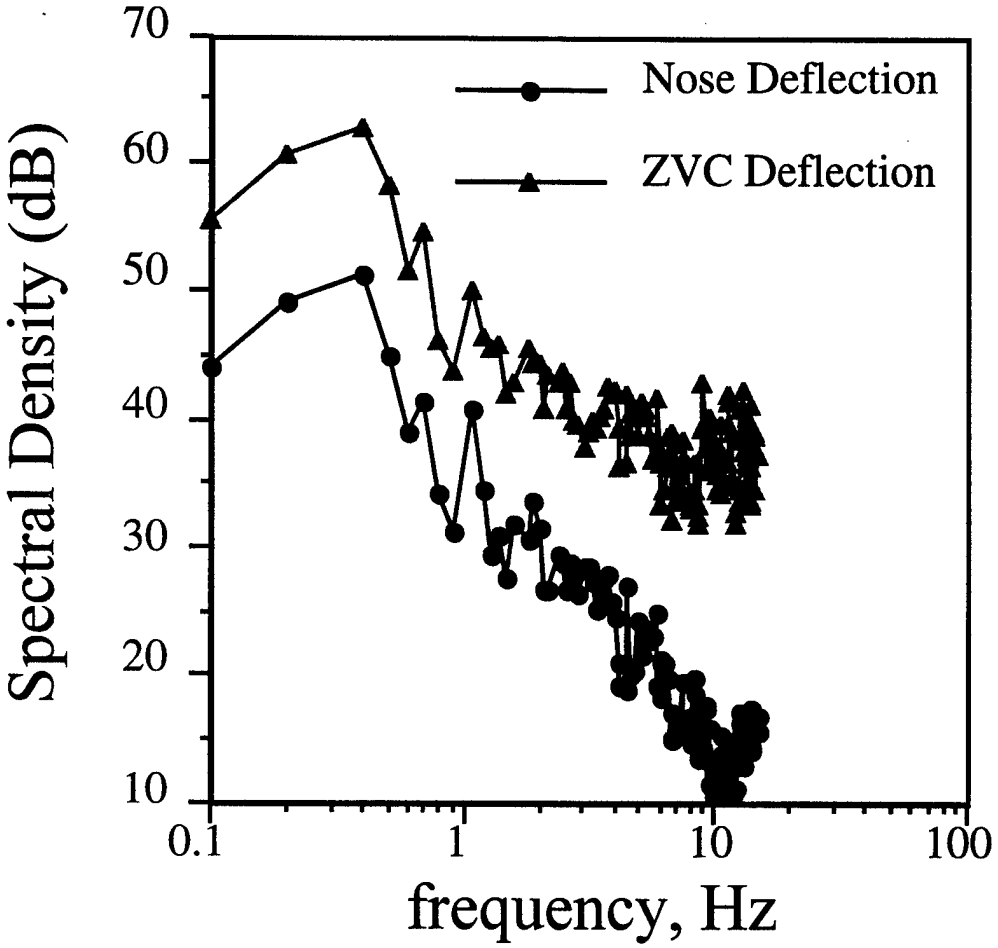

Figure B11: Auto-spectra of Nose Deflection and ZVC Deflection at Plane A

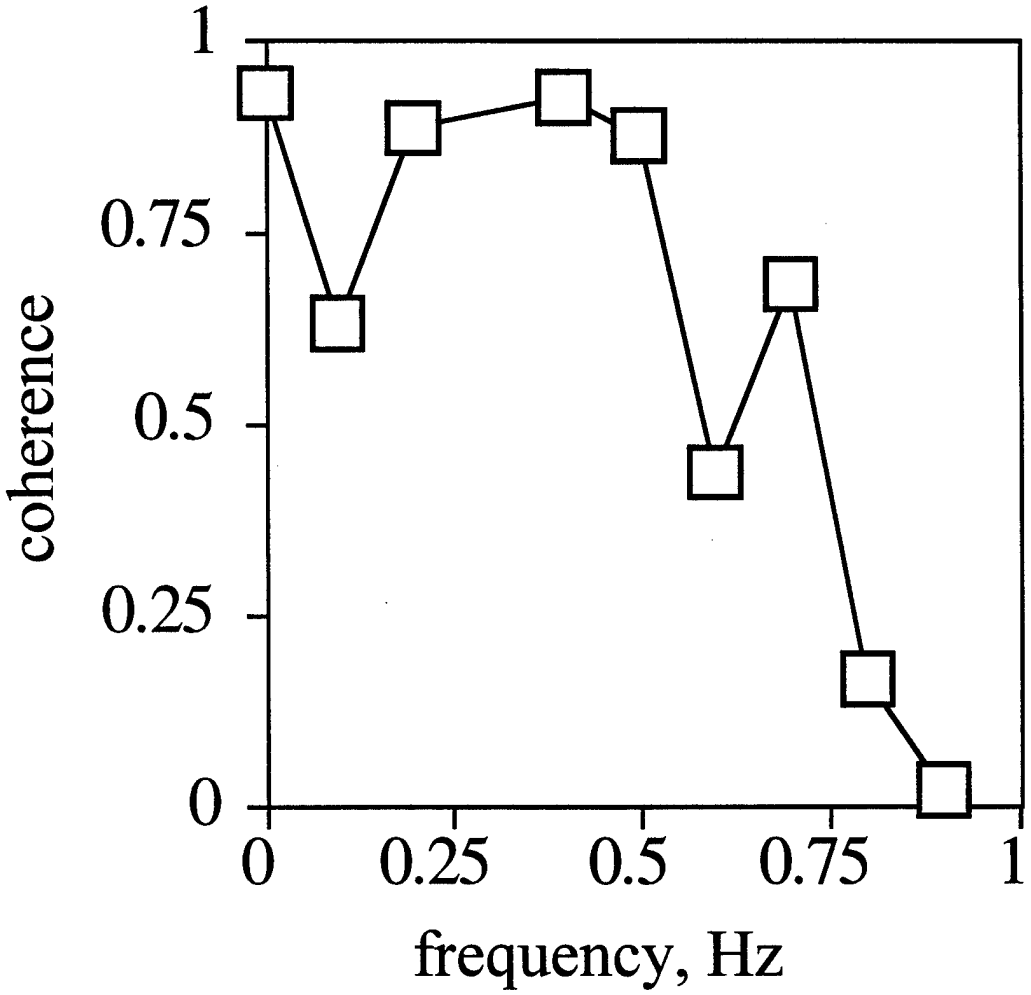

Figure B12: Coherence of Transfer Function at Plane A

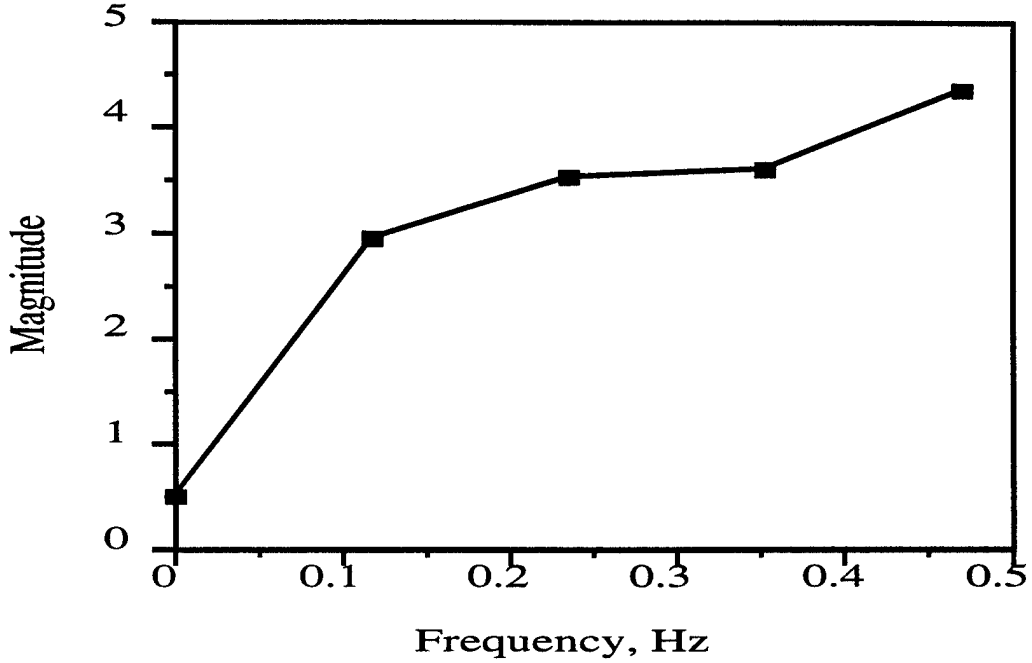

Figure B13: Transfer Function Magnitude for Data at Plane A

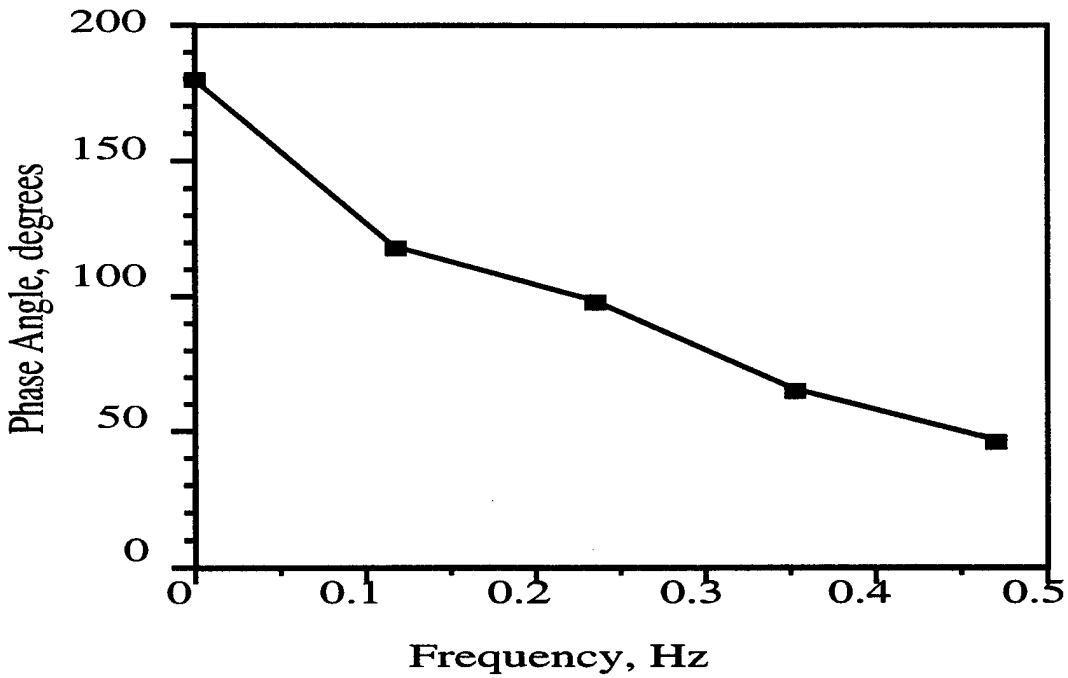

Figure B14: Transfer Function Phase Angle for Data at Plane A

seconds, a rather surprising result that was verified through comparison with the videotape data. This time delay is on the order of ten times the convection lag. This phenomenon is attributed to the non-linear effects of vortex interaction and flow separation. The time lags for planes A, B, and C are compared in Table 7.

Table 7: Time Lag Comparison

Plane	A	B	C
From Transfer Function	5.4 sec.	7.2 sec.	N/A
From Videotape	3.8 sec.	4.2 sec.	5.8 sec.
Convection at Freestream Speed	0.125 sec.	0.155 sec.	0.185 sec.

Effectiveness in Creating Roll Moments

In determining the effectiveness of the stagnation point actuator, the model was tested under constrained bank angles to isolate the flow phenomena from the inertia and dynamic attitude features. When constrained, the model experiences dynamic roll moments from two physical phenomena. First, the motion of the stagnation point causes a pressure differential across the forebody. This creates a side force at the forebody, which when multiplied by the rather sizable moment arm, produces a yawing moment. This side force induced yawing moment will establish a component of cross flow capable of changing the attitude of freestream flow. The second source of roll moment on a constrained model occurs when the asymmetric vortices created at the forebody reach the wing leading edge and interact with the wing vortices. Free-to-roll tests were also performed in order to introduce the inertia effects and the effects of the dynamic attitude of the model.

Examining the dynamic data of the roll moment tests performed in the Low Speed Wind Tunnel and in the Harper Wind Tunnel reveals that three distinct angle of attack states exist, each with unique behavior in the nosetip induced roll moment response. Figures B15 - B17 show the roll moment time history obtained for the model at 45, 35, and 40 deg. sting angle in the Harper Wind Tunnel. Figure B18 presents the time history of the roll moment created on the model at 35 deg. sting angle in the Low Speed Wind Tunnel.

High Angle of Attack Behavior:

At high angles of attack, such as for the 45 deg. sting angle case shown in Fig. B15, the roll moment behavior is characterized by a small roll moment in phase with the nose motion.

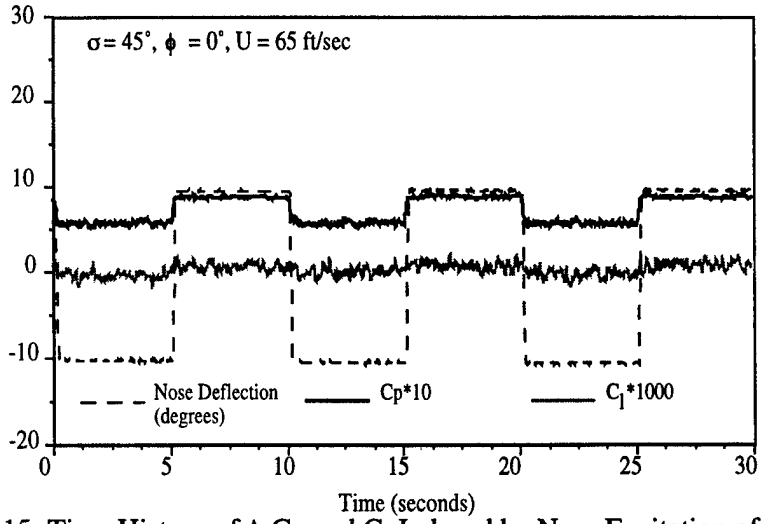

Figure B15: Time History of Δ C_p and C_l Induced by Nose Excitation of 0.1 Hz at σ=45°

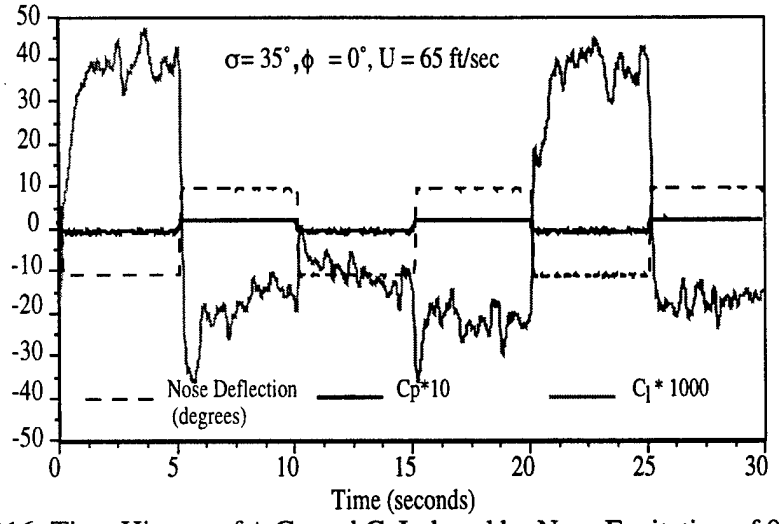

Figure B16: Time History of Δ C_p and C_l Induced by Nose Excitation of 0.1 Hz at σ=35°

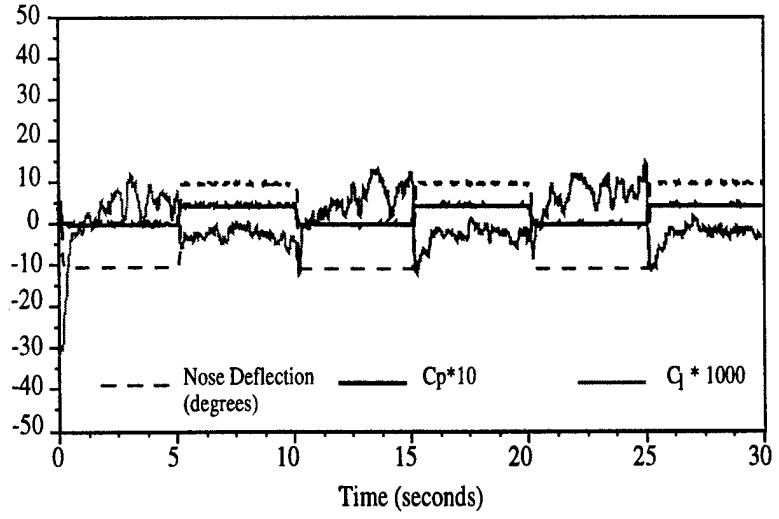

Figure B17: Time History of Δ C_p and C_l Induced by Nose Excitation of 0.1 Hz at σ=40°

Moderate Angle of Attack Behavior:

For moderate angles of attack, like the 35 deg. sting angle shown in Fig. B16, moving the nose stagnation point creates a fairly sizable roll moment 180 deg. out of phase with the nose motion. If we compare the results of Fig. B16 from the Harper Wind Tunnel for 35 deg. sting angle to the results for 40 deg. sting angle (Fig. B19) in the Low Speed Wind Tunnel, we see that the moderate angle of attack features still hold. Keep in mind that due to wall interference effects, the effective angle of attack for 40 deg. sting angle in the Low Speed Wind Tunnel is close to 35 deg. In this example case of a sine wave nose deflection, we see that 0.1 Hz excitation frequency will yield an average roll moment coefficient of 0.075. Increasing the frequency changes the phase shift in the response and lowers the resultant roll moment magnitude.

Close examination of Fig. B18 and B20 for 35 deg. sting angle tests in the Low Speed Tunnel reveal some rather interesting results that might be characterized as belonging to a sub-moderate classification. Notice that in both the sine and square wave excitations, the higher rate nose motions result in the characteristic 180 deg. phase shift seen to exist at moderate angles of attack. However, at the lower frequency nose motion a complex behavior is noticed. Scrutiny of the 0.1 Hz square wave nose motion shows that the initial response is 180 deg. out of phase, but that a second response follows with a return of the roll moment to near zero conditions. Also, the data obtained show that the amplitude of the roll moment is lower than for slightly higher angles of attack. The exact mechanism by which this behavior occurs is as yet not completely understood.

Intermediate Angle of Attack Behavior:

The third angle of attack state discovered to date can be characterized by the data of Fig. B17 for 40 deg. sting angle in the Harper Tunnel. From this data one will find an initial roll moment spike that is followed by a return to steady state that is out of phase with the nose motion. This seems to be a combination of the high and moderate angle of attack states.

In addition to the discovery of the angle of attack states, the roll moment experiments yielded a number of other interesting results. Fig. B19 shows the response of the roll moment to square wave nose oscillations at 40 deg. sting angle in the Low Speed Tunnel. These results are interesting because one can see that the roll moment responds well to square wave nose deflection input, i.e. the roll moment response has a sharp wave front in response to a sharp nose motion. This makes the nosetip actuator very useful in studying basic vortex dynamics since a square wave contains spectral energy at an infinite number of frequencies. Also notice that increasing the nose excitation frequency results in an increase in the response lag and a decrease in the response amplitude.

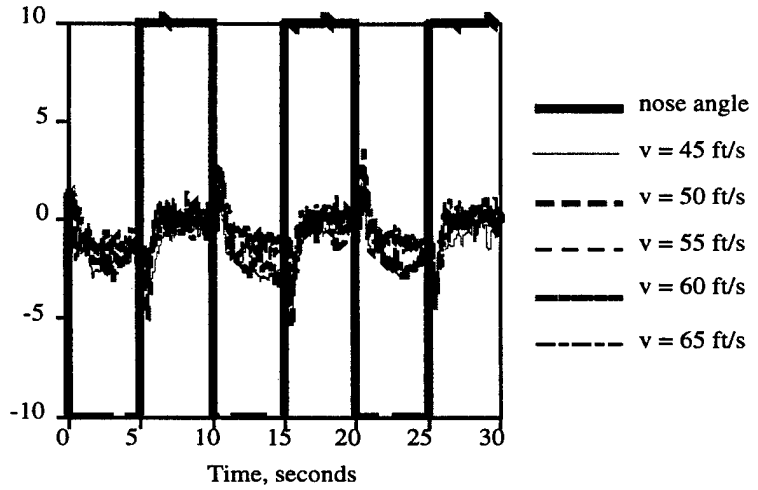

Figure B18: Rolling Moment Coefficient Response to Square Wave Motion at 0.1 Hz at 35 deg. angle of attack. Axis is nose angle in deg. and Cm * 100

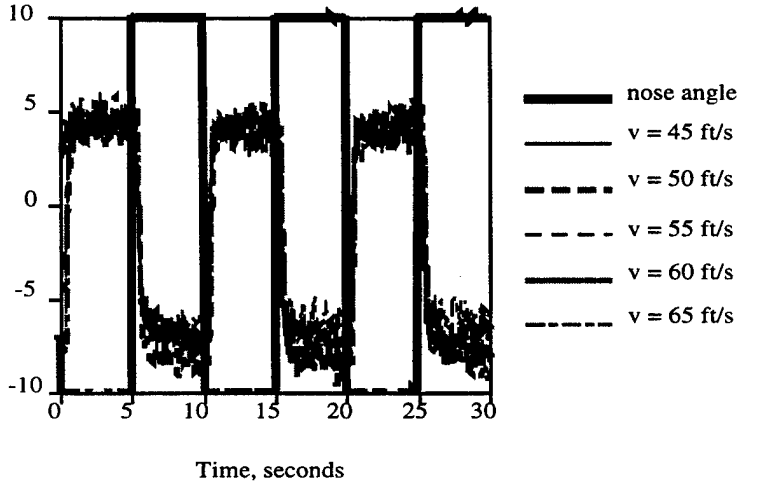

Figure B19: Rolling Moment Coefficient Response to Square Wave Motion at 0.1 Hz at 40 deg. angle of attack. Axis is nose angle in deg. and Cm * 100

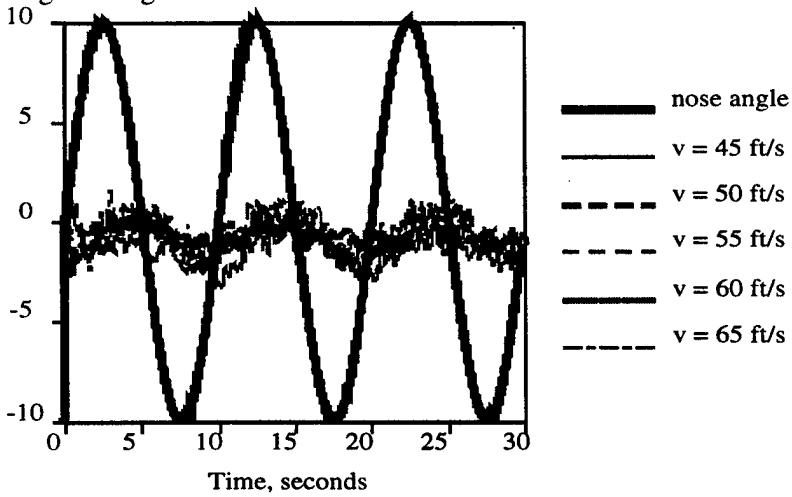

Figure B20: Rolling Moment Coefficient Response to Sine Wave Motion at 0.1 Hz at 35 deg. angle of attack. Axis is nose angle in deg. and Cm * 100

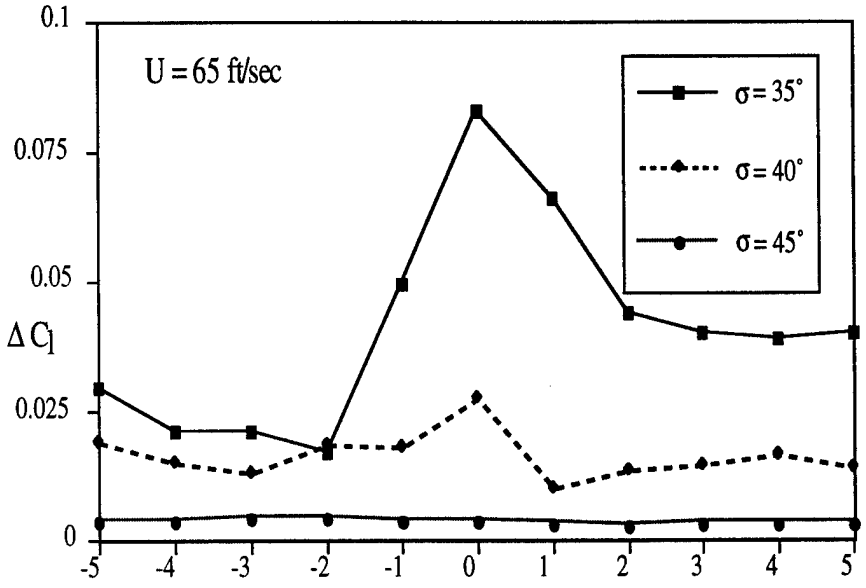

Figure B21: Average ΔC_l Induced by Square Wave Nose Excitation of 0.1 Hz

Examining the average roll moment induced by square wave nose oscillations for various sting angles in the Harper Tunnel (Fig. B21) indicates that the average roll moment is a function both of bank angle and angle of attack. One can see that increasing the sting angle will create a decrease in roll moment magnitude. In addition, the highest roll moment is created at zero bank angle, but the moment is surprisingly not symmetric with bank.

This asymmetry in roll moment response with bank angle has also been seen in the dynamic nose excitation cases. The time history of roll moment and pressure responses to square wave nose motion at 35 deg. sting angle in the Harper Tunnel for +/- 4 deg. bank attitude (Fig. B22) shows that the pressure responses for the two tests are approximately the same. However, there are significant differences in the initial peak responses, noise levels, and amplitudes of the roll moment responses. These differences in roll moment behavior despite the similar pressure responses seem to indicate that differences exist in the way the wing and forebody vortices interact at various bank angles.

Free-Roll Experiments: Wing Rock Excitation and Suppression

Finally, in order to simply introduce the inertia and dynamic attitude effects that occur in creating roll moments at high angle of attack, some results from the free-to-roll experiments are presented in Fig. B23 and B24. The data prove that the moving stagnation point can be used as an effective actuator in creating predictable changes in bank attitude. In addition, the stagnation point actuator can eliminate and instigate wing rock.

Fig. B25(a) from Ref. B27 shows the result of applying a 0.2 Hz square wave SPA excitation of 10 deg. amplitude at 40 deg. sting angle, at a flow speed of 16.76 m/s (55 fps) in the larger Harper Wind Tunnel. There is some natural asymmetry, so that the effect of a deflection to the right is different from that of a deflection to the left. We see that nose deflection to the right (positive) causes a response which is relatively free of oscillations. However, deflection to the left induces a mildly oscillatory roll response which damps out quickly. Fig. B25(b) shows what happens when the flow speed is increased to 19.81m/s (65 fps). The oscillatory response is much greater in amplitude, and persists over 3 or 4 cycles before being damped out. Nose deflection instantly stops the oscillation. In Fig. B25(c), the flow speed is raised further, to 22.86 m/s (75 fps). Now we see that full wing rock is caused by merely deflecting the nosetip to the left, and remains as a fully undamped oscillation until the nose is moved towards the right, which instantly stops the oscillation. When the sting angle is increased to 45 deg., the wing rock effect is greatly reduced, as shown in Fig. B25 d and e from Ref. 4. Notice the last part of Fig. B25(e), where nothing happens when the nose is deflected. This is part of a long-time-scale phenomenon which has to-date defied explanation.

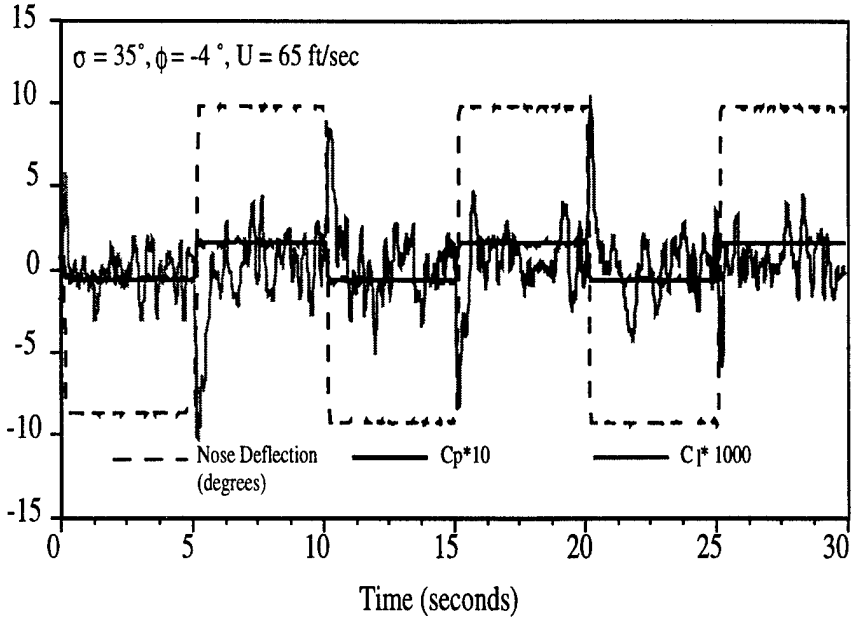

Figure B22a: Time History of ΔC_p and C_l Induced by Nose Excitation of 0.1 Hz at σ=35°, ϕ= -4°

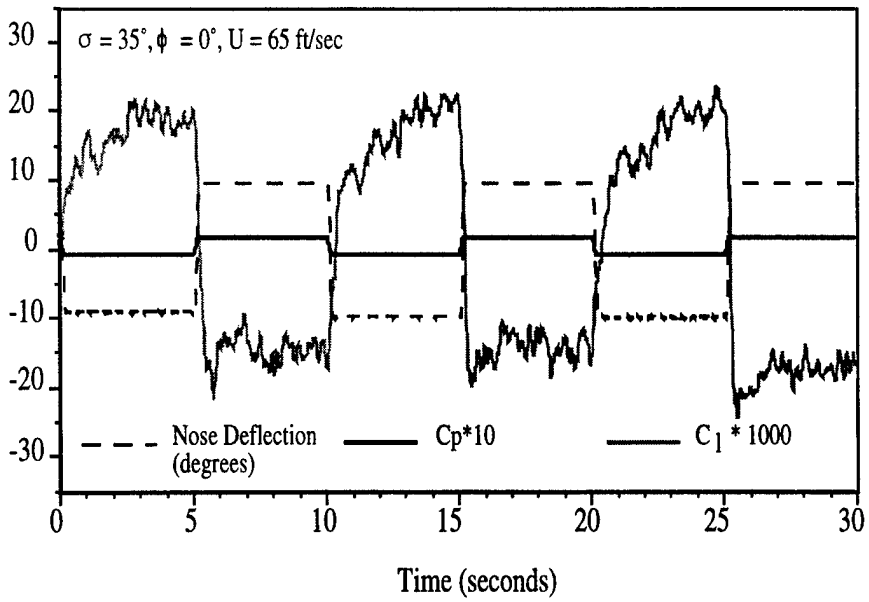

Figure B22b: Time History of ΔC_p and C_l Induced by Nose Excitation of 0.1 Hz at σ=35°, ϕ= +4°

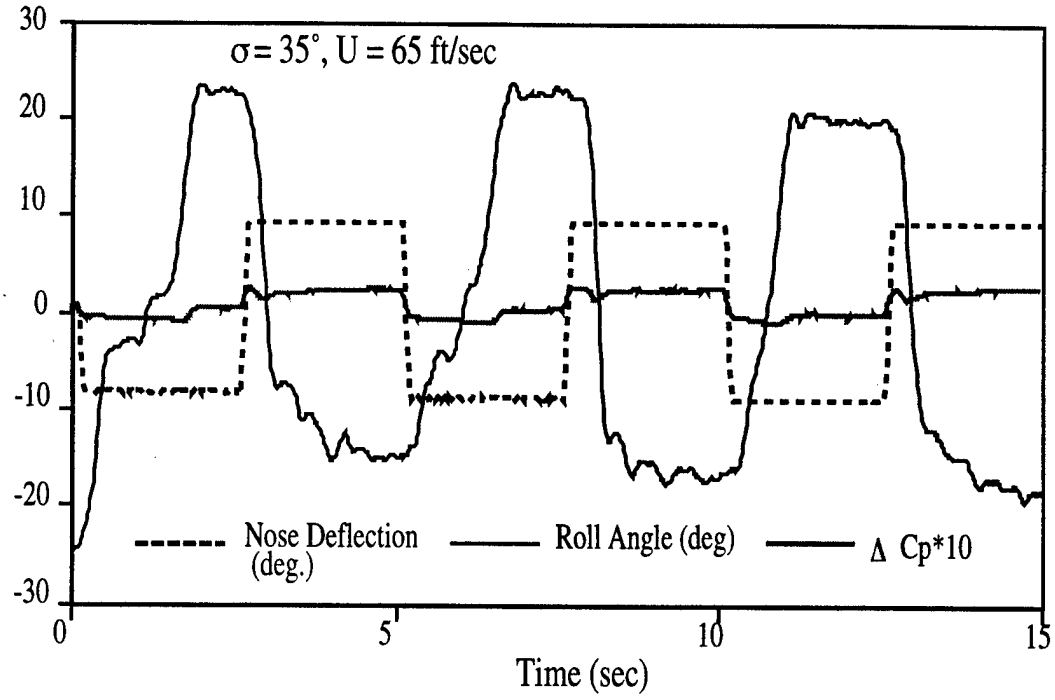

Figure B23: Free-to-Roll Roll Attractor Switching Induced by Nose Movement

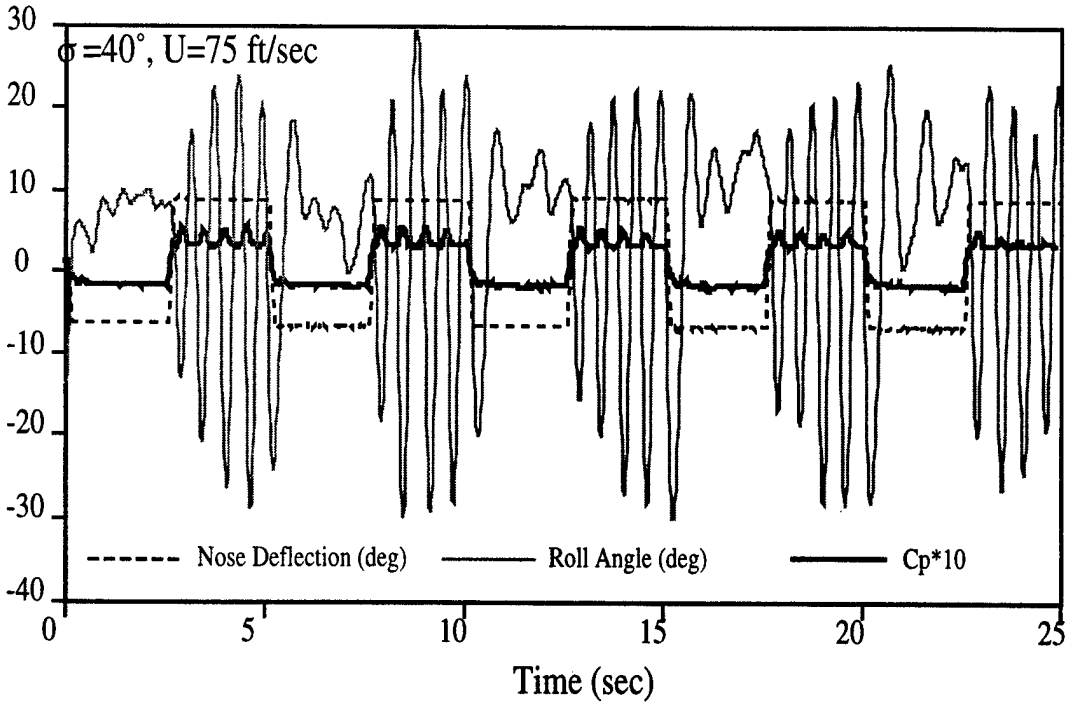

Figure B24: Initiation and Elimination of Wing Rock via Nose Deflection

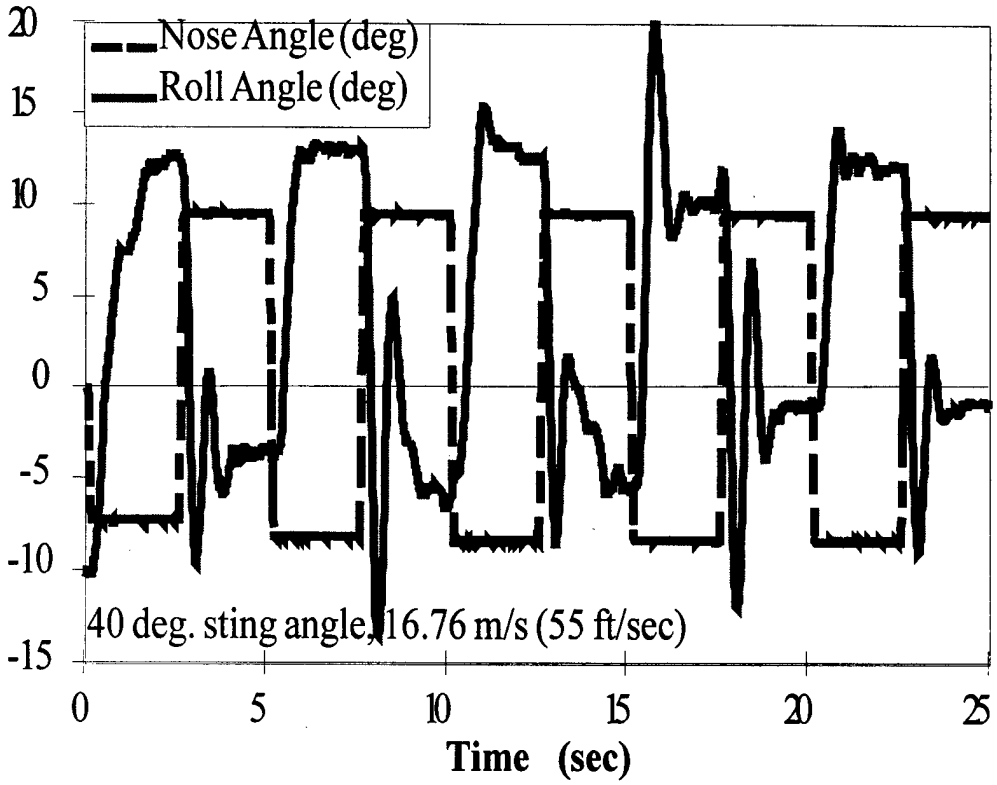

Figure B25a: Free-to-Roll Time History at 40 deg. sting angle and 16.76 m/s

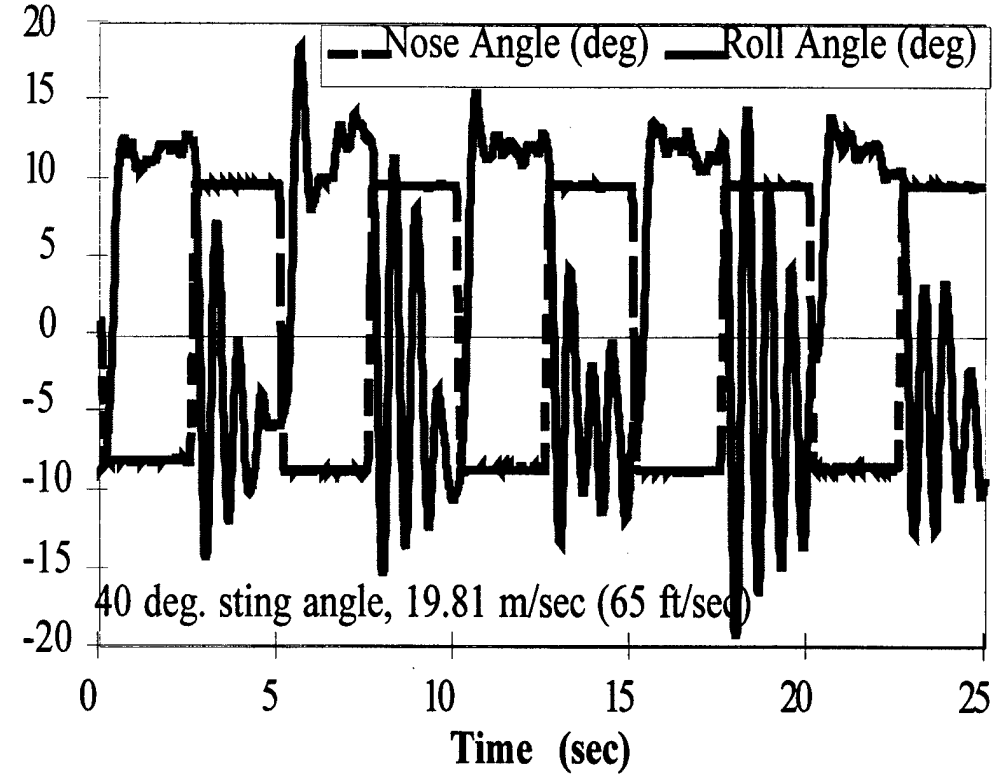

Figure B25b: Free-to-Roll Time History at 40 deg. sting angle and 19.81 m/s

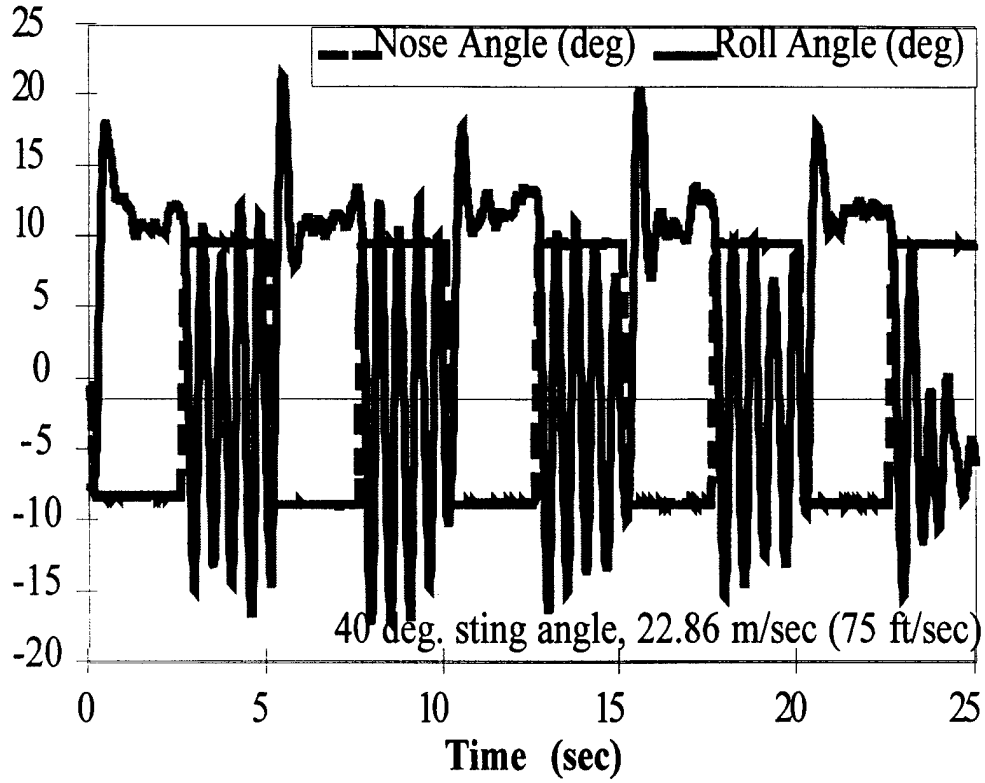

Figure B25c: Free-to-Roll Time History at 40 deg. sting angle and 22.86 m/s

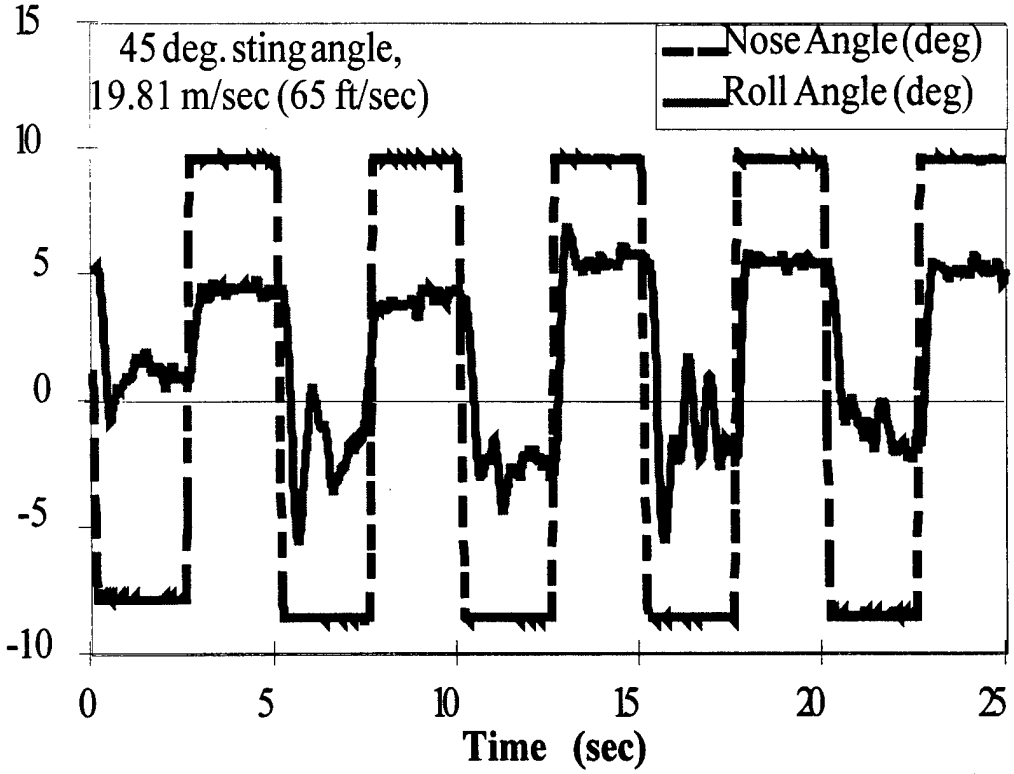

Figure B25d: Free-to-Roll Time History at 45 deg. sting angle and 19.81 m/s

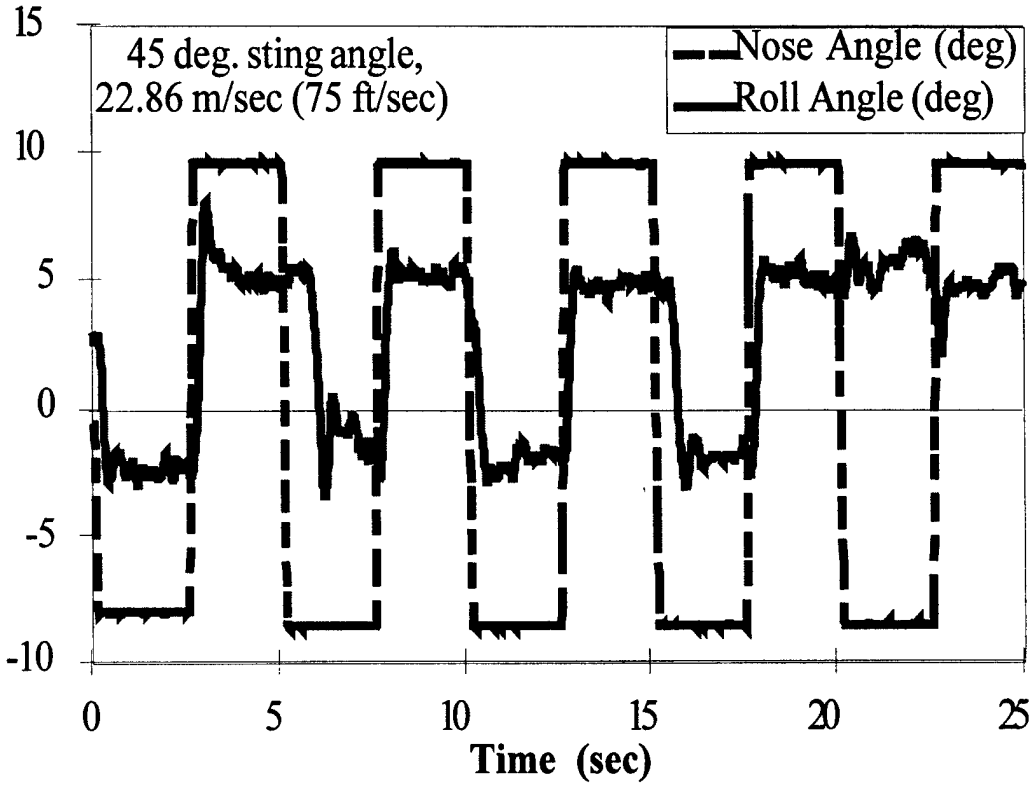

Figure B25e: Free-to-Roll Time History at 45 deg. sting angle and 22.86 m/s

Effectiveness in Creating Pressure Differentials

Displacing the nose stagnation point creates a series of flow phenomena which initiate a differential in pressure distribution across the forebody. From aerodynamic theory, one expects that displacing the nosetip stagnation point will cause the forebody vortex on the side to which the nose is moved to remain attached and unburst for a longer distance than the vortex core on the opposite side of the body. This allows the favored vortex core to grow in strength beyond that of the opposite core. In turn, this tighter vortex core will create a greater suction force on the surface upon which it is attached. The result is a vortex induced pressure difference across the forebody. Therefore, the surface pressure differential should serve as a metric of forebody vortex asymmetry.

To explore the effectiveness of creating forebody pressure differentials using the stagnation point actuator, let us examine the data of the Low Speed Wind Tunnel experiments. Figures B26 and B27 presents the pressure difference and roll moment response to sine wave and square wave nose oscillations for 35 deg. sting angle and 13.6 m/s freestream speed. Examination of the plots reveals that the pressure differential response is well correlated to the nose excitation. However, the roll moment response is quite complicated and only moderately correlated to the nose excitation.

Close examination of the data from the Harper Wind Tunnel experiments relating the average pressure differentials created at the forebody to nose motion indicate that the response is a function both of roll angle and incidence angle. Figure B28 presents the average pressure differential induced by 0.1 Hz square wave nose oscillation for various sting angles and bank angles. Notice that the highest pressure differential occurs at zero bank angle and that the pressure differential is not symmetric for finite roll angles. In addition, the lowest pressure differences created are for conditions at 35 deg. sting angle. Yet, from Fig. B21 we see that these are the conditions which create the greatest roll moment responses. This situation differs from the 45 deg. sting angle case, in that the high incidence condition produces the lowest roll moment, but not the lowest pressure differentials.

Time Scale Phenomena

Examining the data from each of the experiments reveals that the complex phenomena involved with high angle of attack vortex flow occur at a number of different time scales. In a conventional subsonic potential flow situation, one might expect that the effect of moving the stagnation point would be transported at the freestream convection speed. This would result in a convection time lag based on the distance from nosetip to wing leading edge at speeds used in the moment and pressure experiments of around 0.02

seconds. However, the data show that this accounts for only one physical feature of the current flow problem. Reexamination of Fig. B26 and B27 indicates that the pressure differential responds to nose excitation almost instantaneously.

The roll moment data discloses other time related features of the flow. The average time for the roll moment to respond to nose excitation at 35 deg. incidence is shown in Fig. B29 to be about 0.2 sec. However, as shown previously in Fig. B18, there is a longer time scale phenomenon in the sub-moderate incidence range in which the roll moment returns to almost zero, supposedly due to wing vortex interaction. Examining the average roll moment response time further shows that the roll moment response time is a function of sting angle. The quickest response time occurs for the high incidence range. The slowest response time occurs in the intermediate incidence range. In addition, one sees that the effects of velocity on the average time lag in roll moment response are minimal and inconsistent.

By studying Fig. B30 one sees that the roll moment time lag is also a function of bank angle. Further, that function of bank angle is asymmetric with the quickest response times occurring for -1 deg. bank angle.

Modeling Efforts

Because the nature of the flow problem is so complex and includes several time scale phenomena, we see great value in developing empirical control formulae, perhaps developed in piecewise linear fashion, to describe and predict the aerodynamic rolling moment. Eventually these must be linked to a better representation of the aerodynamics and fluid dynamics of the problem, which are theoretically available from nonlinear vortex lattice codes and Navier-Stokes codes: all indications are that these "first-principles-based prediction" options will become available to us only after our empirical control laws start working.

Therefore, we have proceeded to develop empirical transfer functions from the time series of roll moment and pressure differential data. The procedure is based on a Fast Fourier Transform code which calculates the cross-spectrum and auto-spectra of the nose deflection and either roll moment or pressure differential. The transfer function is then the cross-spectrum divided by the auto-spectrum of the input signal (nose deflection).

The results reveal some interesting patterns. The test case shown in Fig. B31 at sting angle of 35 degrees, with zero roll angle, tunnel speed of 45 fps, and a nose deflection waveform described by a square wave at 0.1Hz was used to compute the transfer function of the roll moment and pressure differential systems. The autospectra are shown in Fig. B32 to consist primarily of energy in 6 or 7 frequency bands, around the odd

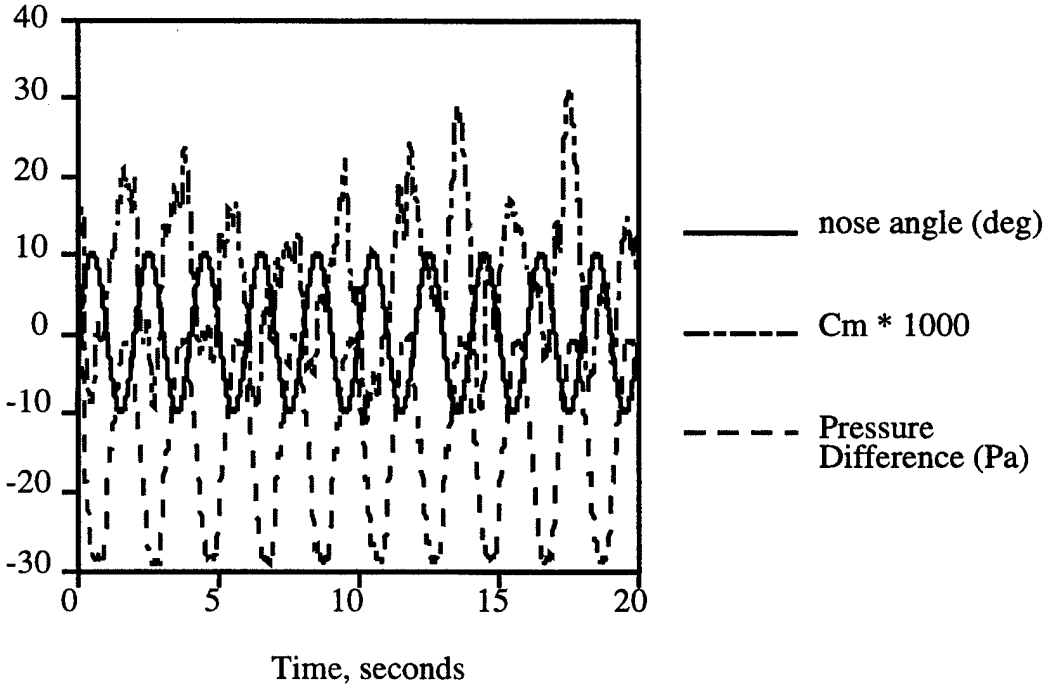

Figure B26: Pressure Difference and Moment Response to Sine Wave Nose Excitation at 0.5 Hz, 35 deg. Angle of Attack, and 13.6 m/s Freestream Velocity

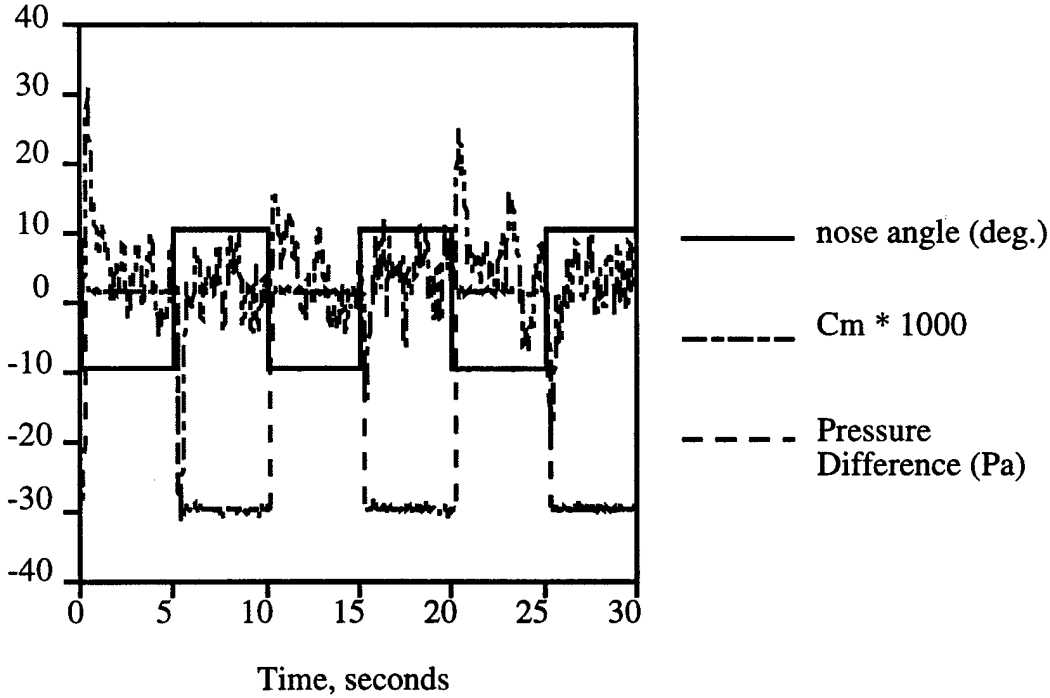

Figure B27: Pressure Difference and Moment Response to Square Wave Nose Excitation at 0.1 Hz, 35 deg. Angle of Attack, and 13.6 m/s Freestream Velocity

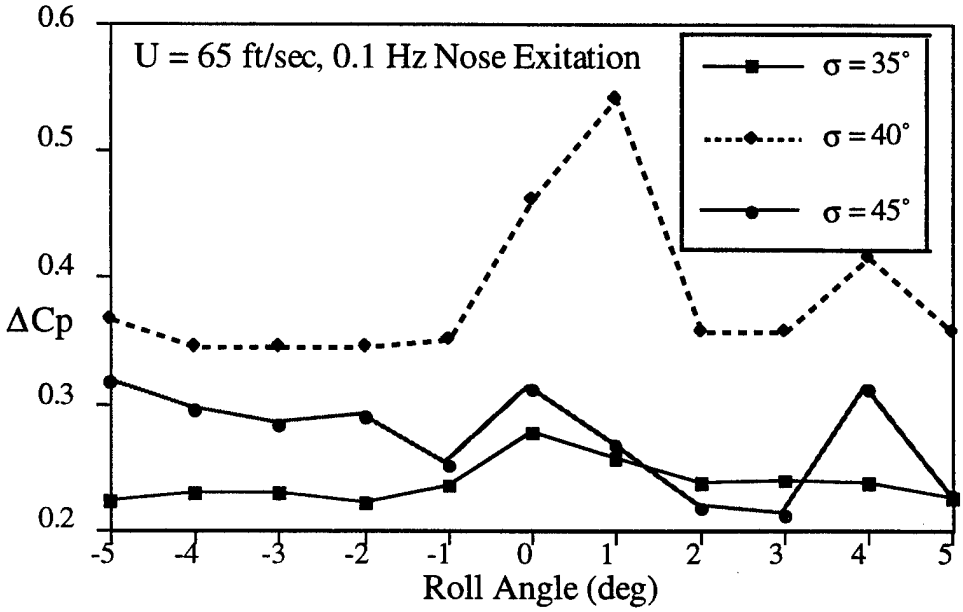

Figure B28: Average ΔC_p Induced by Square Wave Nose Excitation of 0.1 Hz

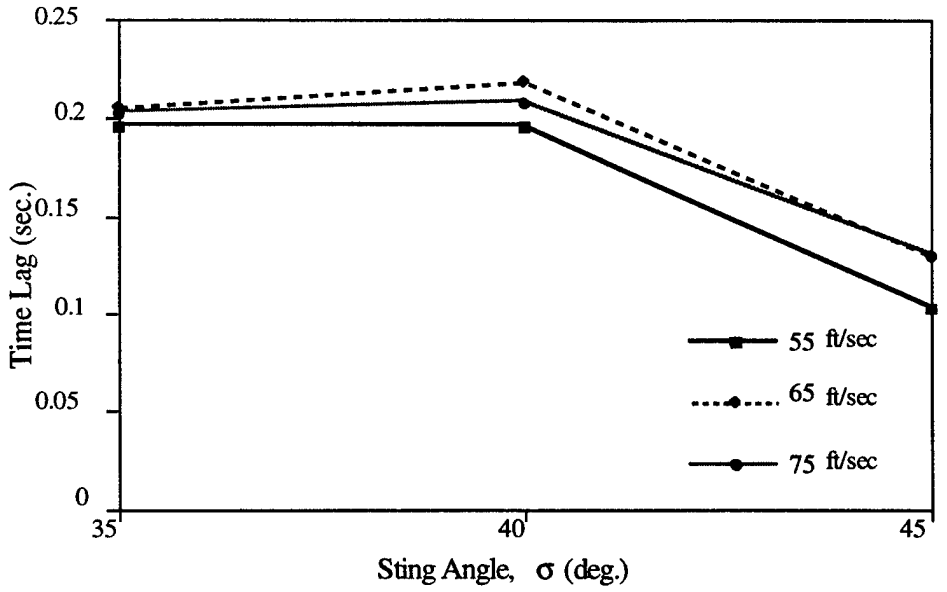

Figure B29: Rolling Moment Time Lag Variation with Sting Angle, 0.1 Hz Nose Excitation

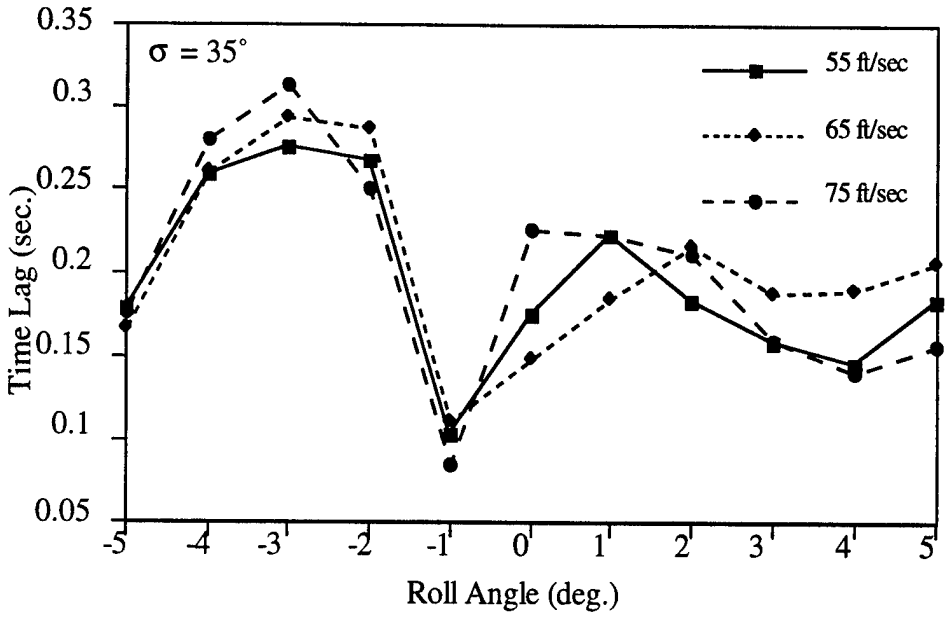

Figure B30: Rolling Moment Time Lag Variation with Roll Angle, 0.1 Hz Nose Excitation

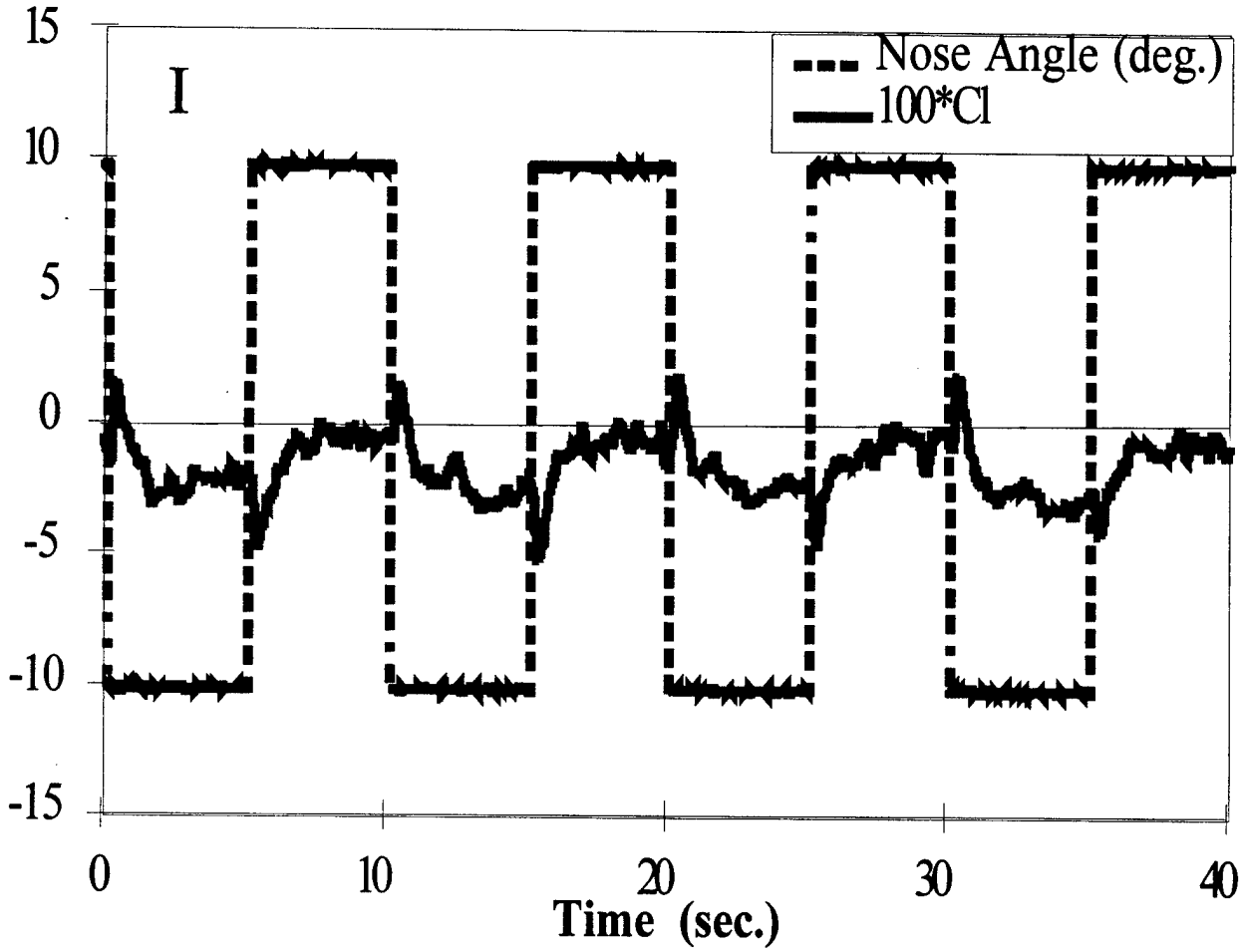

Figure B31(a): Time history of roll moment coefficient response to square wave nose deflection at 45 fps, 35 deg. angle of attack, 0 de. roll for 0.1Hz nose deflection.

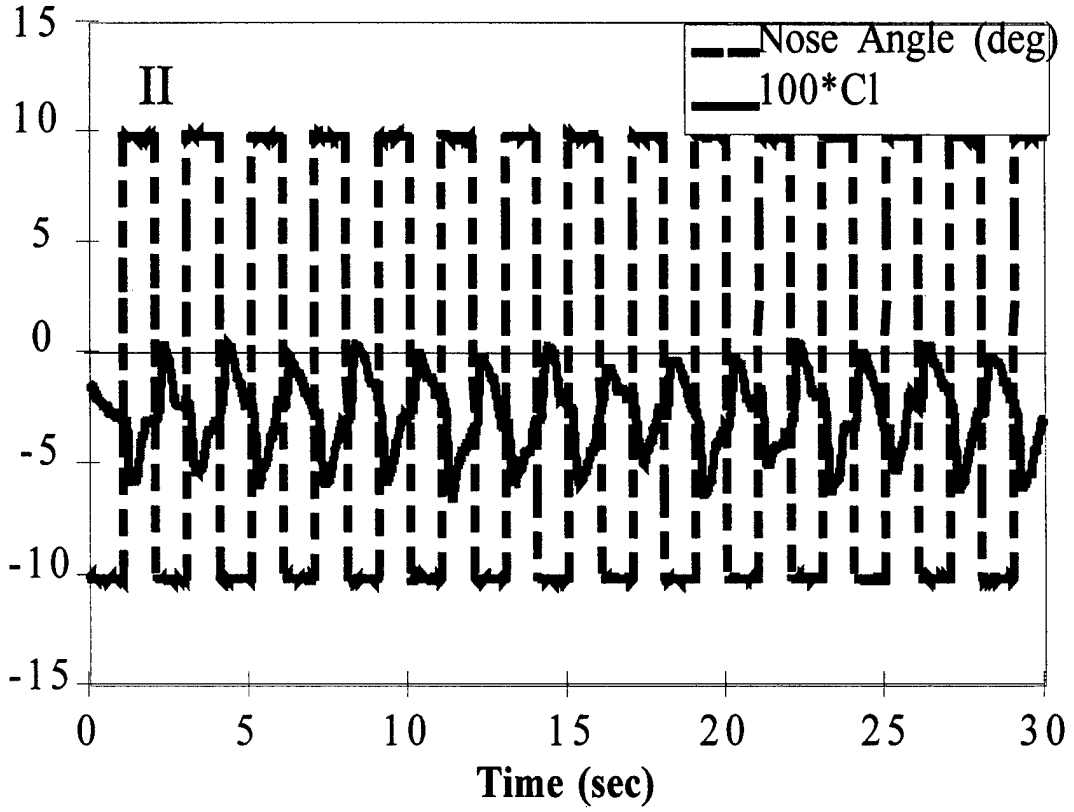

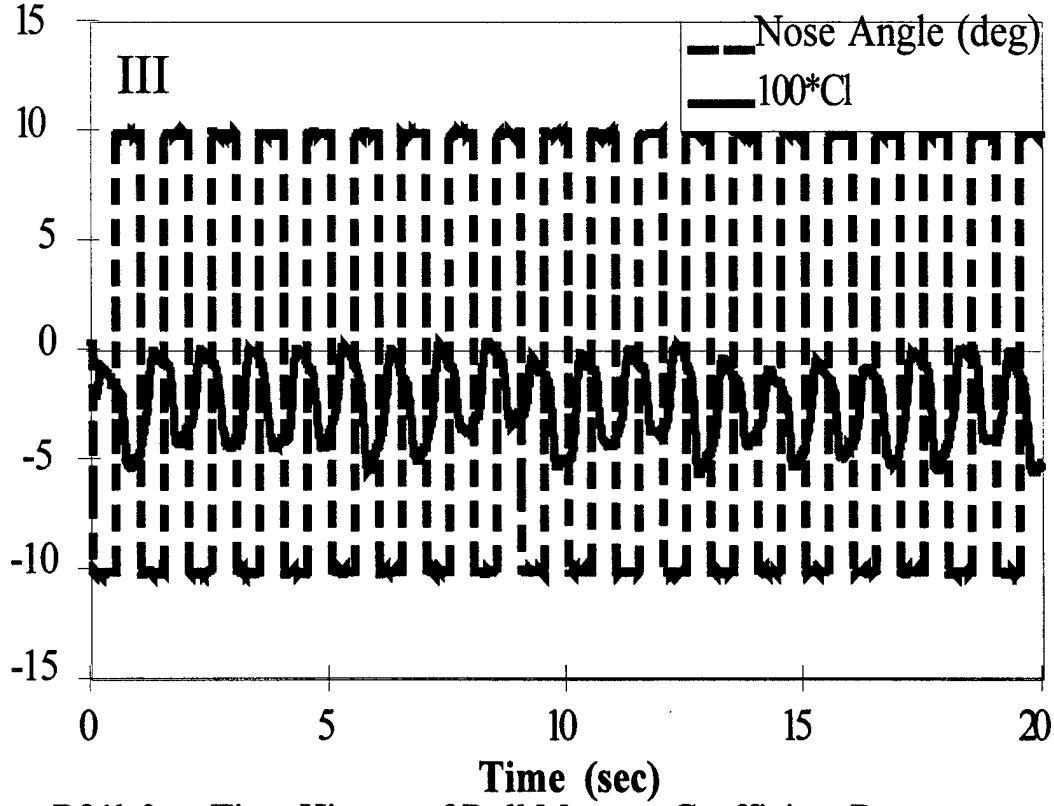

Figure B31b&c: Time History of Roll Moment Coefficient Response to Square Wave Nose Deflection at 45 ft/sec, 35 deg. angle of attack, and 0 deg. roll angle for : b) 0.5 Hz and c) 1.0Hz nose deflection

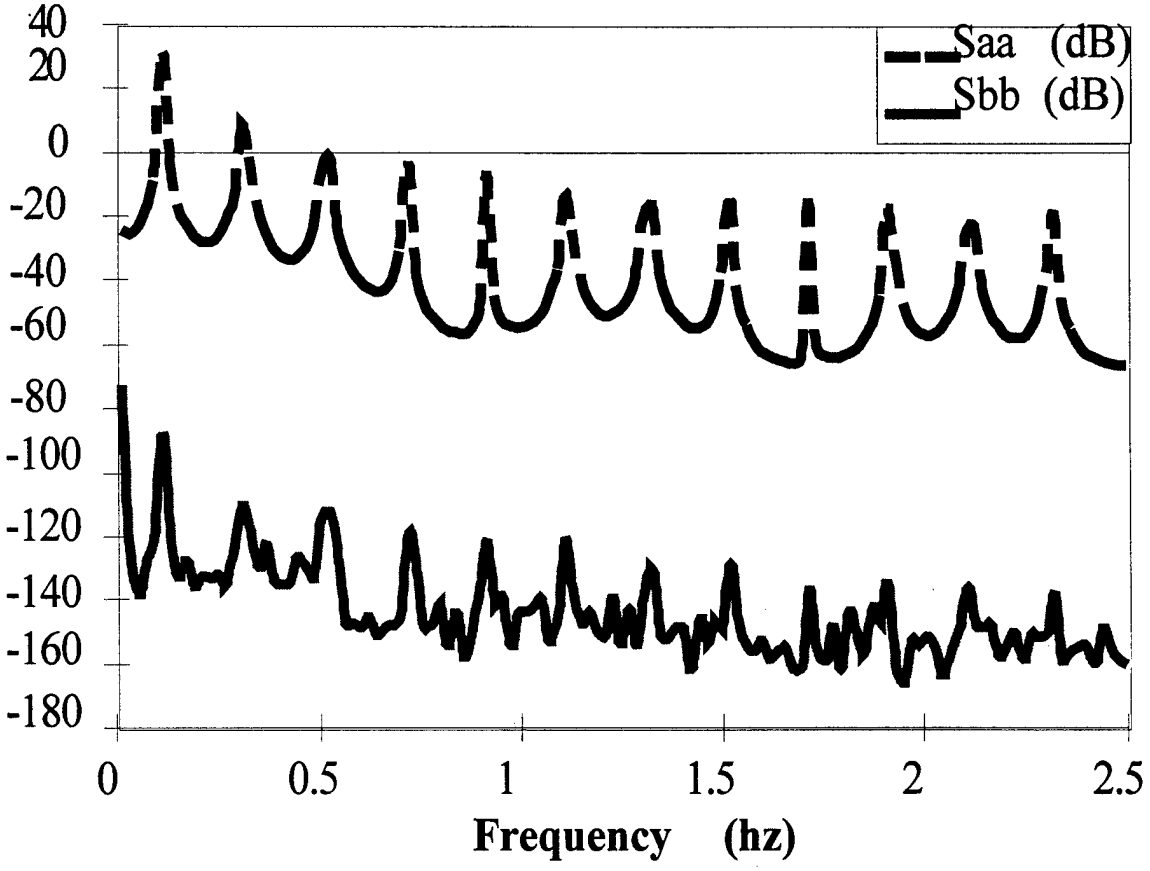

Figure B32: Autospectra of Nose Deflection and Roll Moment Coefficient Signals

harmonics of the square wave frequency. The coherence function shown in Fig. B33 is above 0.85 at the centers of these frequency bands, showing that the roll response is linear over the frequency content of the nose excitation. The corresponding transfer function magnitude is also shown in Fig. B33: the magnitude is flat over the frequency range where the signal has energy. The phase of the transfer function (Fig. B34) increases with frequency, but is not linear.

Next, we repeated the above process with nose excitation data acquired at the same test condition with 0.5 Hz and 1.0 Hz square wave frequencies (Fig. B31). The transfer function behavior was similar, and the values of the transfer function obtained at given frequencies for different excitation frequencies were the same: the transfer function did not change with excitation frequency. From the 0.5 Hz and 1.0 Hz cases, it was possible to construct the transfer function up to 10 Hz.

A surprising result occurred when the 3 speeds were compared: the time traces essentially repeated with very little phase shift. This shows that the time scales involved in the response are much longer than the convective time scale, which is what changes when the flow speed changes. A corollary is that a general transfer function can be constructed, valid over a substantial speed range, but only for a given angle of attack and roll angle.

Repeating the analysis for the pressure differential signal revealed that the coherence was excellent over a wide range of frequency (Fig. B35), and the phase variation (Fig. B36) is perfectly linear, indicating a constant dead time. Again, as shown in Fig. B36, the phase did not change appreciably when the tunnel speed was changed by almost 50%: the lag computed from the slope of the phase plot is two orders of magnitude larger than the freestream convection time from the nose stagnation point to the pressure tap location.

From the above, it is seen that a simple transfer function model of moment response can be constructed for a given sting angle and roll angle. This is presented in Table 8 below from Ref. B27, for 35 deg. sting angle, 0 deg. roll angle, and tunnel speed of 45 fps.

In modeling the aircraft behavior, a variety of control parameters must be taken into consideration. It has been shown previously in this report that angle of attack and bank angle create distinct roll moment states that must be carefully modeled. In addition, we have seen that the nose oscillation frequency is a determining factor in roll moment creation and that several time scales play a major role in the aircraft behavior. There are unique inertia and dynamic roll attitude effects that also play a major role in determining the aircraft roll response at high incidence angles. These features as well should be captured in the control law.

While the overall aerodynamic system is quite complicated, all the data seem to indicate that a control system can be designed using a series of piecewise linear models to

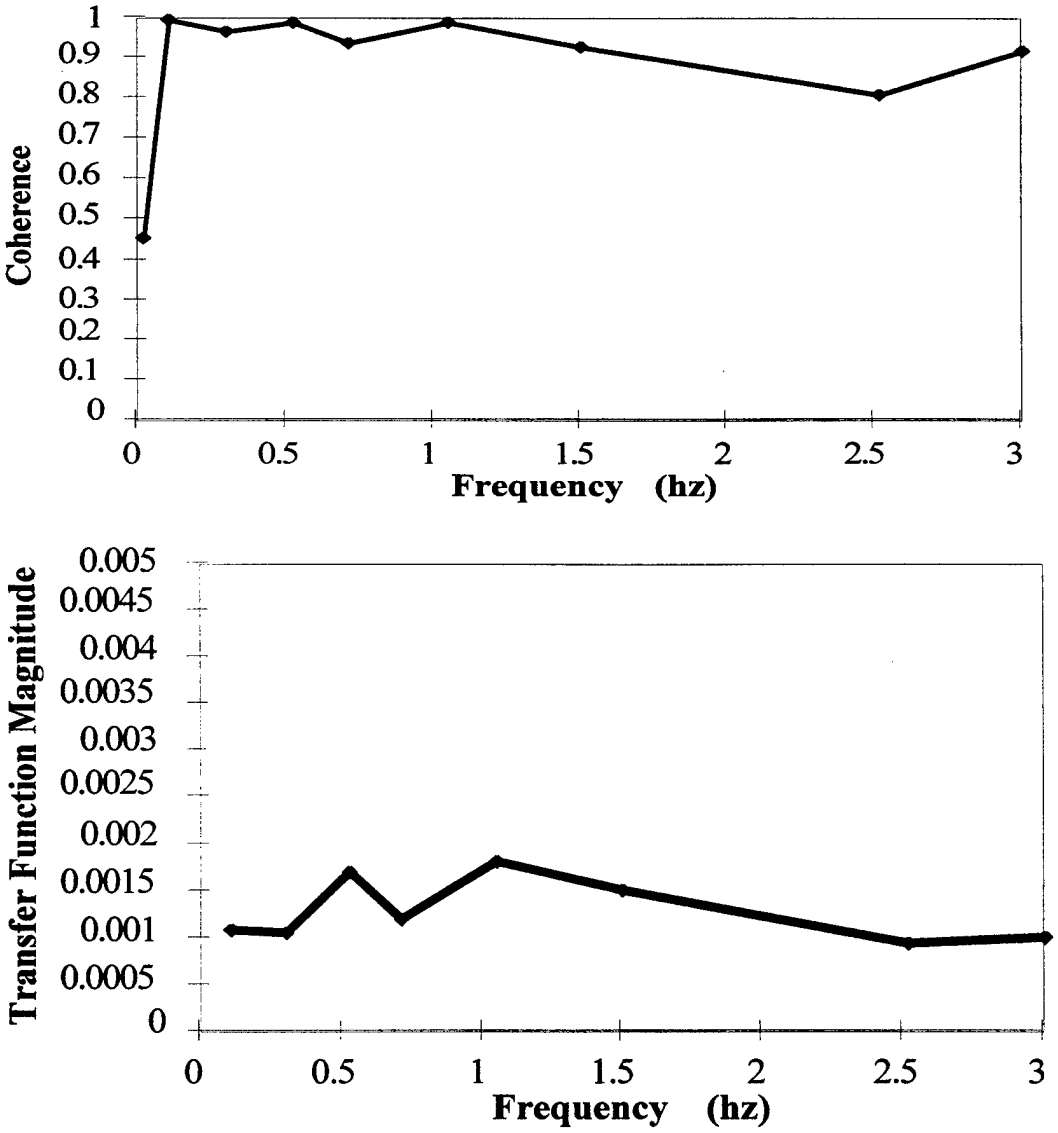

Figure B33: Transfer Function Coherence and Magnitude of Nose - Roll Moment Coefficient System

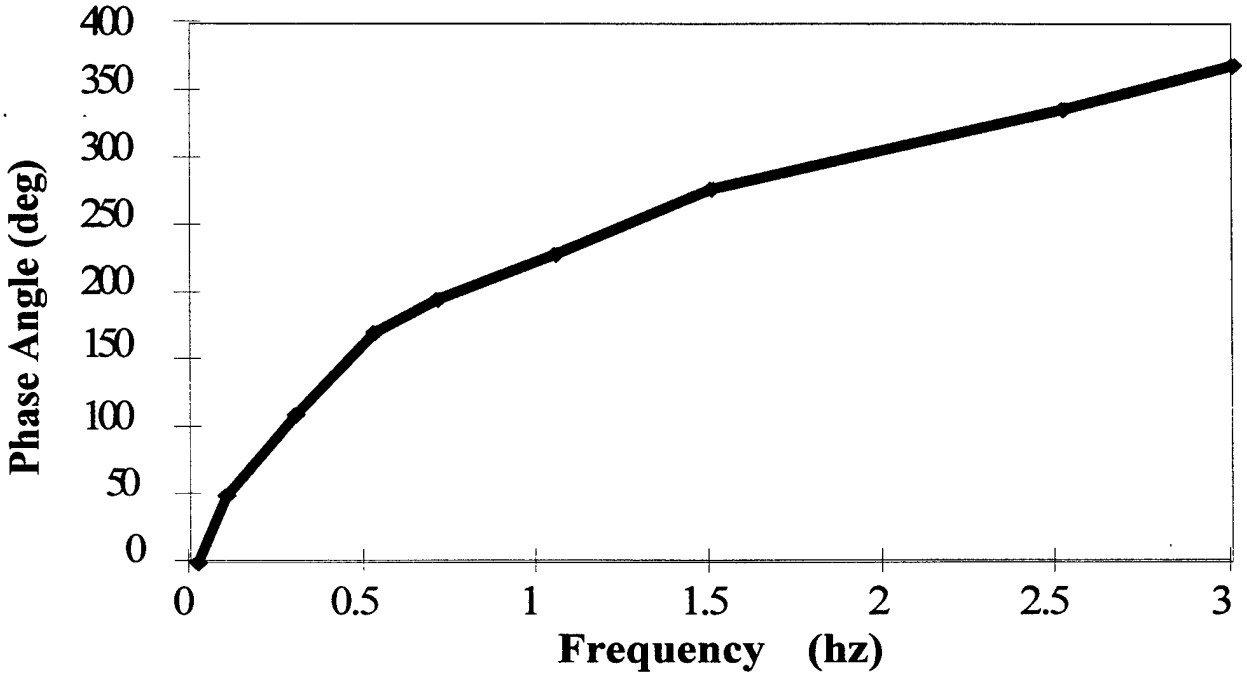

Figure B34: Transfer Function Phase Angle of Nose - Roll Moment Coefficient System

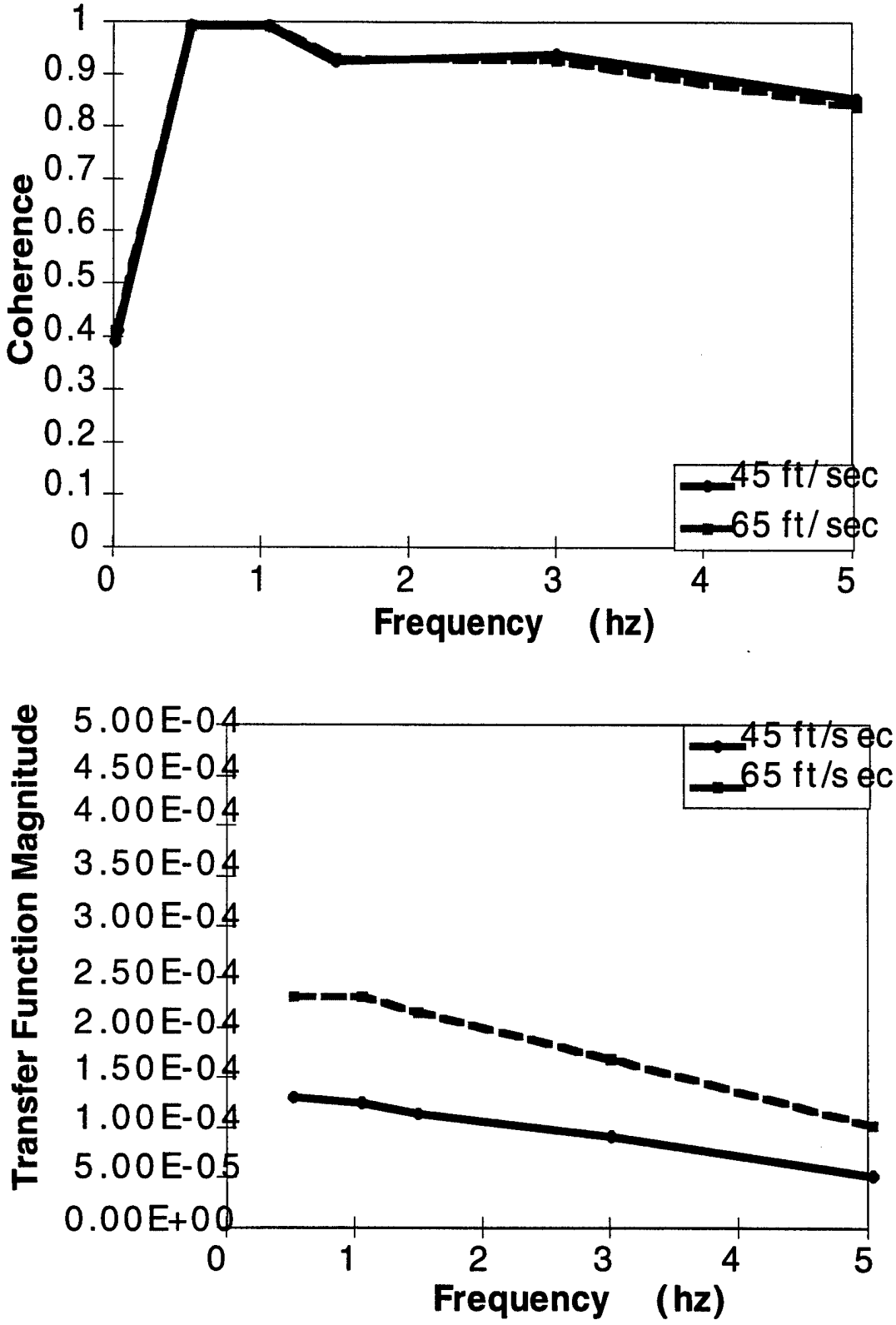

Figure B35: Transfer Function Coherence and Magnitude of Nose - Pressure Differential Coefficient System

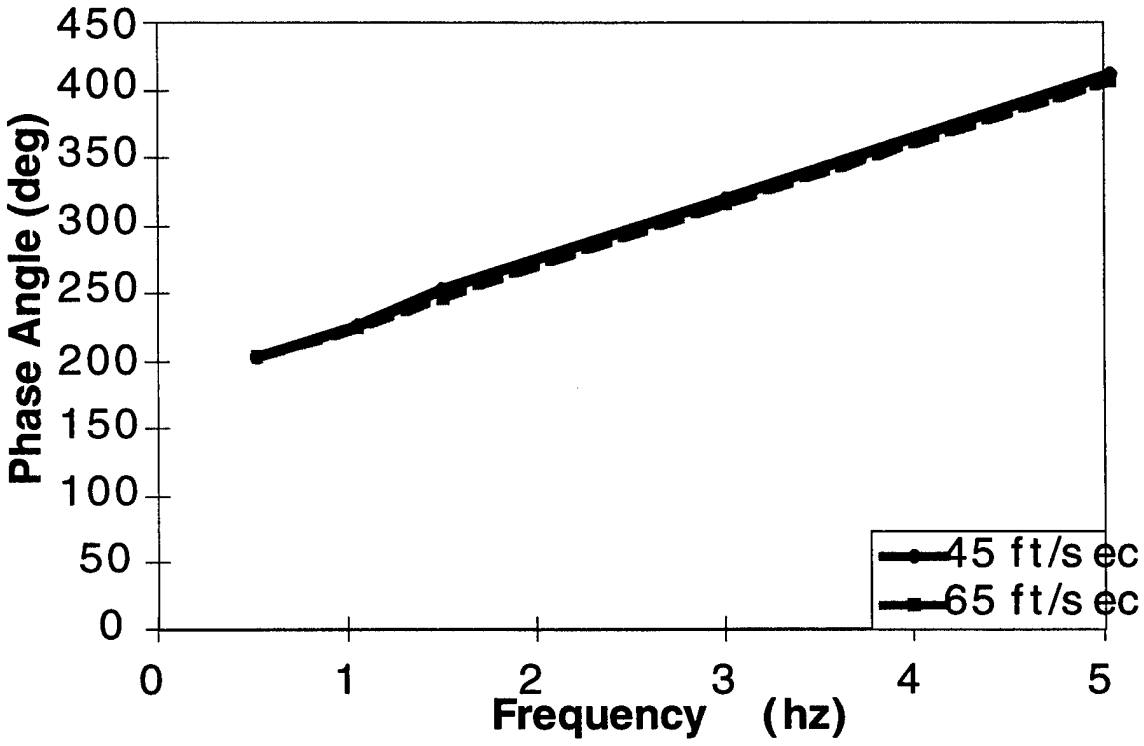

Figure B36: Transfer Function Phase Angle of Nose - Pressure Differential Coefficient System

describe the aircraft motion within each family of roll moment behavior. Efforts toward this goal continue at this time.

Table 8: Transfer Function Magnitude and Phase Angle for Frequencies of Highest Coherence

Frequency (hz)	Magnitude	Phase Angle (deg)
.02	.101	0
.107	.00109	50.52
.303	.00106	110.15
.527	.0017	171.18
.713	.00121	195.96
1.055	.00181	228.37
1.504	.00151	277.6
2.52	.000947	337.43
3.008	.00102	369.41

IV. REFERENCES

A1: Magill, J.C., Komerath, N.M., "Wind-Driven Dynamic Manipulator for Wind Tunnels". Experimental Techniques, Vol. 19, No. 1,Jan.-Feb. '95, p. 27-30.

A2: Magill, J.C., Komerath, N.M., "Wind Driven Dynamic Manipulator for a Wind Tunnel". U.S. Patent 5,345,818, September 1994.

A3: Magill, J.C., "Identification and Control of Wind Driven Dynamic Manipulators for Wind Tunnels". PhD Thesis, School of Electrical Engineering, Georgia Institute of Technology, September 1995.

A4: Orlik-Ruckemann,K.J. "*Aerodynamics of Manoeuvring Aircraft*", 1992 Turnbull Lecture, Canadian Aeronautics and Space Journal, Vol. 38, No. 3, Sept 92, 106-112.

A5: Gad-el-Hak, M., Ho, C-H., "Unsteady Flow Around an Ogive Cylinder". J. Aircraft, Vol. 23, No. 6, p. 520-528.

A6: Gad-el-Hak, M., Ho, C-H., "The Pitching Delta Wing", AIAA Journal, Vol. 23, No. 11, Nov. '85, p. 1661-1665.

A7: McKernan, J.F., Payne, F.M., Nelson, R.C., "Vortex Breakdown Measurements on a 10 Deg Sweepback Delta Wing". Journal of Aircraft, Vol. 25, No. 11, Nov. '88, p. 991-992

A8: LeMay, S.P., Batill, S.M., Nelson, R.C., "Vortex Dynamics on a Pitching Delta Wing". Journal of Aircraft, Vol. 27, No. 2, Feb. '90, p. 131-138.

A9: Soltani, M.R., Bragg, M.B., and Brandon, J.M., "Measurements on a Oscillating 70-Deg. Delta Wing in Subsonic Flow". Journal of Aircraft, Vol. 27, No. 3, March 1990, p. 211 - 217.

A10: Orlik-Ruckemann, K.J., (Editor): "Rotary Balance Testing for Aircraft Dynamics". Report of the AGARD Fluid Dynamic Panel Working Group 11. AGARD-AR-265, 1990.

A11: Blake, W., "Validation of the Rotary Balance Technique for Predicting Pitch Damping". AIAA 93-3619, Atmospheric Flight Mechanics Conference, August 1993.

A12: Buchanan, T.D., W.A. Crosby, "Captive Trajectory System Test Planning for AEDC Supersonic Wind Tunnel (A) and Hypersonic Wind Tunnels (B) and (C)", AEDC-TR-83-40, Dec 1983.

A13: Miller, L.S., Gile, B.E., "Effects of Blowing on Delta Wing Vortices During Dynamic Pitching". Journal of Aircraft, Vol. 30, No. 3, May-June 1993, p. 334-339.

A14: McCroskey, W.J., "Unsteady Airfoils". Annual Review of Fluid Mechanics, Vol. 14, 1982, p. 285-311.

A15: Francis, M.S., Keese, J.E., "Airfoil Dynamic Stall Performance with Large-Amplitude Motions". AIAA Journal, Vol. 23, No. 11, 1985, p. 1653-1659.

A16: Jumper, E.J., Schreck, S.J., Dimmick, R.L., "Lift-Curve Characteristics for an Airfoil Pitching at Constant Rate". Journal of Aircraft, Vol. 24, No. 10, 1987, p. 680-687.

A17: Carr, L.W., "Progress in Analysis and Prediction of Dynamic Stall", Journal of Aircraft, Vol. 25, No. 1, Jan. 1988, p. 6-17.

A18: Lorber, P.F., and Carta, F.O., "Airfoil Dynamic Stall at Constant Pitch Rate and High Reynolds Number". Journal of Aircraft, Vol. 25, No. 6, 1988, p. 548-556.

A19: Koochesfahani, M.M., Smiljanovski, V., "Initial Acceleration Effects on Flow Evolution Around Airfoils Pitching to High Angles of Attack". AIAA Journal, Vol.31, No.8, p. 1529 - 1531.

A20: Hebbar, S.K., Platzer, M.F., Cavazos, O.V., "Pitch Rate/Sideslip Effects on Leading-Edge Extension Vortices of an F/A-18 Aircraft Model". J.Aircraft, Vol. 29, No.4, p.720-723.

A21: Simpson, R., et al., "*Design And Development Of A Dynamic Pitch-Plunge Model Mount*", AIAA-89-0048, 27th Aerospace Sciences Meeting, Jan 9-12 1989, Reno, NV.

A22: Magill, J.C., Komerath, N.M., Dorsey, J., "An Experimental Evaluation of Controllers for Wind Driven Manipulators". AIAA Paper 95-3502, Atmospheric Flight Mechanics Conference, Baltimore, MD, August 1995.

A23: Magill, John C., Komerath, N.M., Dorsey, J.F., "Experimental Evaluation of an Adaptive Controller for a Wind Driven Pitch Manipulator". Journal of Guidance, Dynamics and Control, March-April '96 .

A24: Magill, J.C., Darden, L.A., Komerath, N.M., "Visualization of Flow Interactions During High-Rate Maneuvers". AIAA Paper 94-0669, Jan. 94.

A25: Magill, John C., Darden, L.A., Komerath, N.M., "Flow Visualization During Multiple-Axis Motions Using a Wind-Driven Manipulator". Journal of Aircraft, Vol. 33, No. 1, January-February 1996, p. 163-170.

A26: Magill, J.C., Darden, L.A., Komerath, N.M., Dorsey, J.F., "Measurement of Aircraft Stability Parameters in the Wind Tunnel Using a Wind Driven Manipulator". AIAA 94-3457, Atmospheric Flight Mechanics Conference, Scottsdale, Arizona, August 1994.

A27: Ames, R.G., Magill, J.C., Komerath, N.M., "Design and Testing of a 3-d.o.f. Wind-Driven Manipulator". AIAA Paper 96-0581, 34th Aerospace Sciences Meeting, January 1996.

B1. Ericsson, L.E., "Sources of High Alpha Vortex Asymmetry at Zero Sideslip", Journal of Aircraft, Vol. 29, No. 6, Nov.-Dec., 1992, 1086-1090.

B2. Zillac, G., Degani, D., and Tobak, M., "Asymmetric Vortices on a Slender Body of Revolution", AIAA 90-0388, Jan., 1990.

B3. Moskovitz, C., Hall, R., and Dejarnette, F., "Experimental Investigation of a New Device to Control the Asymmetric Flowfield on Forebodies at Large Angles of Attack", AIAA 90-0068, Jan., 1990.

B4. Ericsson, L.E. and Reding, J.P., "Asymmetric Vortex Shedding from Bodies of Revolution", Tactical Missile Aerodynamics, Vol. 104, 243-296.

B5. Jenkins, J.E. and Hanff, E.S., "Highlights of the IAR/WL Delta Wing Program, Proceedings of Workshop III: Delta Wings, Unsteady Aerodynamics and Modeling", Baltimore, Aug., 1995.

B6. Brandon, J.M. and Nguyen, L. T., "Experimental Study of Effects of Forebody Geometry on High Angle-of-Attack Stability," Journal of Aircraft, Vol. 25, No. 7, July 1988, 591- 597.

B7. Hall, R., "Influence of Forebody Cross-Sectional Shape on Wing Vortex-Burst Location," Journal of Aircraft, Vol. 24, No. 9, 1987, 645-652.

B8. Jobe, C.E., Hsia, A.H., Jenkins, J.E., and Addington, G.A., "Critical States and Flow Topology on a 65° Delta Wing", AIAA 94-3479, Aug., 1994.

B9. Peterson, K.G., Darden, L.A., and Komerath, N.M., "Dynamic Roll Control Experiments Using a Moveable Nosetip", AIAA 96-0789, Jan., 1996.

B10. Ericsson, L.E., "Flow Physics of Critical States for Rolling Delta Wings", Journal of Aircraft, Vol. 32, No. 3, May - June, 1995, 603 - 610.

B11. Murri, D.G., Shah, G.H., DiCarlo, D.J., and Trilling, T.W., "Actuated Forebody Strake Controls for the F18 High Alpha Research Vehicle", Journal of Aircraft, Vol. 32, No. 3, May - June, 1995, 555 - 562.

B12. Ng, T.T. and Malcolm, G.N., "Aerodynamic Control Using Forebody Blowing and Suction", AIAA 91-0619, Jan., 1991.

B13. Cornelius, K.C., Pandit, N., Osborn, R.F., and Guyton, R.W., "Experimental Study of Pneumatic Control of Forebody Vortices at High Alpha", Journal of Aircraft, Vol. 31, No. 1, Jan. - Feb., 1994, 49-56.

B14. Miller, L.S. and Gile, B.E., "Effects of Blowing on Delta Wing Vortices During Dynamic Pitching", Journal of Aircraft, Vol.30, No.3, May - June, 1993, 334-339.

B15. Alexander, M.G. and Meyn, L.A., "Wind Tunnel Results of Pneumatic Forebody Vortex Control using Rectangular Slots on a Chined Forebody", AIAA 94-1854, June, 1994.

B16. Celik, Z.Z., Pedreiro, N., and Roberts, L., "Dynamic Roll and Yaw Control by Tangential Forebody Blowing", AIAA 94-1853, June, 1994.

B17. Malcolm, G.N. and Skow, A.M., "Enhanced Controllability Through Vortex Manipulation on Fighter Aircraft at High Angles of Attack", AIAA 86-2277-CP, August, 1986.

B18. Murri, D.G. and Rao, D.M., "Exploratory Studies of Actuated Forebody Strakes for Yaw Control at High Angles of Attack", AIAA 87-2557-CP, August, 1987.

B19. Ng, T.T. and Malcolm, G.N., "Aerodynamic Control Using Forebody Strakes", AIAA 91-0618, Jan., 1991.

B20. Malcolm, G.N., "Forebody Vortex Control". In "Special Course on Aircraft Dynamics at High Angles of Attack: Experiments and Modeling", AGARD Report 776, March, 1991, 6-1 to 6-40.

B21. Suárez, C.J., Malcolm, G.N., and Ng, T.T., "Forebody Vortex Control with Miniature, Rotatable Nose-Boom Strakes", AIAA 92-0022, Jan., 1992.

B22. Komerath, N.M., Liou, S-G., DeBry, B., and Lenakos, J., "Measurements Of The Unsteady Vortex Flow Over A Wing-Body At Angle Of Attack", AIAA 92-2729, June, 1992.

B23. Komerath, N.M., Darden, L.A., Peterson, K.G., Magill, J.C., "Stagnation Point Vortex Controller". U.S. Patent Pending.

B24. Darden, L.A., Komerath, N.M., "Vortical Flow Control Using a Moveable Stagnation Point", Bulletin of the American Physical Society, Vol. 39, No. 9, November, 1994.

B25. Darden, L.A. and Komerath, N.M., "Forebody Vortex Control at High Incidence Using a Moveable Stagnation Point", AIAA 95-1775, June, 1995.

B26. Darden, L.A., Peterson, K.G., and Komerath, N.M., "Vortex Control Using a Moveable Nose with Pressure Feedback", AIAA 95-3468, Aug., 1995.

B27. Darden, L.A., Peterson, K.G., and Komerath, N.M., "Roll control Using a Stagnation Point Actuator", AIAA 96-2498, June, 1996.

V. PERSONNEL, INVENTIONS AND PUBLICATIONS

Personnel

Narayanan Menon Komerath is a Professor in the School of Aerospace Engineering.

John Carl Magill received a PhD in the School of Electrical Engineering, on the Wind -Driven Manipulator project. His thesis advisors were Prof. John Dorsey of the School of Electrical Engineering and Prof. Komerath of the School of Aerospace Engineering.

Leigh Ann Darden received the M.S. in Aerospace Engineering, and has completed her PhD Thesis Proposal in Aerospace Engineering, working on the Stagnation Point Actuator. She is now doing the analysis and experiments needed before writing her thesis.

Kevin Gordon Peterson received the M.S. in Aerospace Engineering, working on the SPA project.

David Dishman received the M.S. in Aerospace Engineering, working on the SPA project.

Richard Ames completed an undergraduate Special Problem on the 3 d.o.f. Wind Driven Manipulator, and is now working towards an M.S. in Aerospace Engineering.

Inventions

1. Magill, J.C., and Komerath, N.M., "Wind-Driven Dynamic Manipulator for a Wind Tunnel". United States Patent 5345818, September 1994.
2. . Komerath, N.M., Darden, L.A., Peterson, K.G., Magill, J.C., "Stagnation Point Vortex Controller". United States Patent Pending.

Theses

1. Magill, J.C., "Identification and Control of Wind Driven Dynamic Model Manipulators for Wind Tunnels", Ph.D. Thesis, Georgia Institute of Technology, September, 1995.
2. Peterson, K.G., "Rolling Moments and Aerodynamic Time Scales for a Model with a Moving Nose Stagnation Point", Ph.D. Thesis, Georgia Institute of Technology, March, 1996.

Journal Papers

1.Magill, J.C., Komerath, N.M., "Wind-Driven Dynamic Manipulator for Wind Tunnels". Experimental Techniques, Vol. 19, No. 1, Jan.-Feb. '95, p. 27-30.

2. Magill, John C., Darden, L.A., Komerath, N.M., "Flow Visualization During Multiple-Axis Motions Using a Wind-Driven Manipulator". Journal of Aircraft, Vol. 33, No. 1, January-February 1996, p. 163-170.

3. Magill, John C., Komerath, N.M., Dorsey, J.F., "Experimental Evaluation of an Adaptive Controller for a Wind Driven Pitch Manipulator". Journal of Guidance, Control and Dynamics, Vol. 19, No. 3, May-June 1996 , p. 671-679.

Conference Papers

1. Komerath, N.M., "Aerodynamics of Coupled-Axis Maneuvers". Proceedings of the AFOSR Workshop on High Lift Concepts, Colorado Springs, Co, October 1993.

2. Magill, J.C., Darden, L.A., Komerath, N.M., "Visualization of Flow Interactions During High-Rate Maneuvers". AIAA Paper 94-0669, Aerospace Sciences Meeting, Reno, Nevada, Jan. 94.

3. Magill, J.C., L.A. Darden, N.M. Komerath, and J.F. Dorsey, "Measurement of Aircraft Stability Parameters in the Wind Tunnel Using a Wind Driven Manipulator", AIAA Paper 94-3457, AIAA Atmospheric Flight Mechanics Conference, Scottsdale, Arizona, August 1994.

4. Magill, J.C., Komerath, N.M., Dorsey, J.F., "Dynamics and Control of Wind Driven Manipulators". AIAA Paper 94-3657, Proceedings of the Guidance, Navigation and Control Conference, Scottsdale, AZ August 1994.

5. Darden, L.A., Komerath, N.M., "Vortical Flow Control Using a Moveable Stagnation Point". Session AC5, Bulletin of the American Physical Society, Vol., 39, No. 9, p. 1844, November 1994.

6. Darden, L.A., "Asymmetric Vortex Control on an Aircraft at High Incidence Using a Moveable Stagnaton Point", AIAA Southeastern Regional Student Conference, Atlanta, April 1995.

7. Darden, L.A., Magill, J.C., Komerath, N.M., "Forebody Vortex Control at High Incidence Using Moveable Nose Stagnation Point". AIAA Paper 95-1775, 13th Applied Aerodynamics Conference, San Diego, CA, June 1995.

8. Komerath, N.M., Magill, J.C., "Dynamic Testing in Wind Tunnels Using the Wind-Driven Manipulator". ICIASF '95 Record, Proceedings of the International Congress on Instrumentation in Aerospace Simulation Facilities, Dayton, OH, July 1995,p.25.1 - 25.7. IEEE95-CH34827- 95/0000-25.1

9. Darden, L.A., Peterson, K.G., Komerath, N.M., "Vortex Control Using a Moveable Nose with Pressure Feedback". AIAA Paper 95-3468, Proceedings of the Atmospheric Flight Mechanics Conference, Baltimore, MD, August 1995, p. 393-403.
10. Magill, J.C., Komerath, N.M., "An Experimental Evaluation of Controllers for Wind Driven Manipulators". AIAA Paper 95-3502, Guidance, Navigation and Control Conference, Baltimore, August 1995.
11. Ames, R.G., Magill, J.C., Komerath, N.M., "Design and Testing of a 3-D.O.F. Wind-Driven Manipulator". AIAA Paper 96-0581, 34th Aerospace Sciences Meeting, Reno, NV, January 1996.
12. Peterson, K.G., Darden, L.A., Komerath, N.M., "Dynamic Roll Control Using a Moveable Nosetip". AIAA Paper 96-0789, 34th Aerospace Sciences Meeting, Reno, NV, January 1996.
13. Darden, L.A., Komerath, N.M., Peterson, K.G., "Roll Control Using a Stagnation Point Actuator". AIAA Paper 96-2498, 14th AIAA Applied Aerodynamics Conference, New Orleans, LA, June 1996.